DESIGN AND SYNTHESIS OF MONOSACCHARIDE FUNCTIONALIZED CONJUGATED POLYMERS, POLYROTAXANES AND OLIGOMERS FOR BIOLOGICAL APPLICATIONS

A THESIS SUBMITTED TO
THE GRADUATE SCHOOL OF ENGINEERING AND SCIENCE
OF BILKENT UNIVERSITY
IN PARTIAL FULFILLMENT OF THE REQUIREMENTS FOR
THE DEGREE OF
MASTER OF SCIENCE
IN
CHEMISTRY

By
Esra Deniz Soner
September, 2015

DESIGN AND SYNTHESIS OF MONOSACCHARIDE FUNCTIONALIZED CONJUGATED POLYMERS, POLYROTAXANES AND OLIGOMERS FOR BIOLOGICAL APPLICATIONS

By

Esra Deniz Soner

September 2015

We certify that we have read this thesis and that in our opinion it is fully adequate, in scope and in quality, as a thesis for the degree of Master of Science.

_____

Assoc. Prof. Dönüş Tuncel

_____

Prof. Dr. Engin Umut Akkaya

_____

Assist. Prof. İrem Erel-Göktepe

Approved for the Graduate School of Engineering and Science:

_____

Prof. Dr. Levent Onural

Director of the Graduate School

ABSTRACT

DESIGN AND SYNTHESIS OF MONOSACCHARIDE FUNCTIONALIZED CONJUGATED POLYMERS, POLYROTAXANES AND OLIGOMERS FOR BIOLOGICAL APPLICATIONS

Esra Deniz Soner

M.Sc. in Chemistry

Advisor: Assoc. Prof. Dr. Dönüş Tuncel

September, 2015

In this work, the design, synthesis and characterization of fluorescent, water-soluble, multivalent glycoconjugates for their potential applications in active-targetted cellular theranostics through receptor-mediated endocytosis are presented. Gluco-functionalized thiophene monomers are utilized for the pre-functionalized Suzuki coupling polymerization of glycopolythiophenes and glycopolythiophenerotaxanes. The pre-functionalized glycopolythiophenerotaxane synthesis route was designed to provide *in situ* complexation between boronic ester thiophene monomer and water-soluble macrocycle cucurbit[7]uril, for the Suzuki coupling with the glycothiophene monomer in water.

Red emitting oligomers carrying azide groups were utilized for the synthesis of post-functionalized glycoconjugate oligomers.

These functionalizations were carried through 1,3-dipolar cycloaddition (click reaction) between azide groups and alkyne-functionalized monosaccharides (mannose or glucose).

Structural and photophysical properties of glycopolythiophenes were investigated through ^{1}H-NMR, UV-VIS, and Fluorescence Spectroscopy. Monomers in synthetic steps were analysed through ^{1}H-NMR, IR, and ^{13}C-NMR. Structural, photophysical and morphological properties of red oligomers were investigated through ^{1}H-NMR, HRMS-TOF, DLS, SEM.

Keywords: Conjugated polymers, Glycoconjugate, Cucurbituril, Polyrotaxane, Click reaction.

ÖZET

BİYOLOJİK UYGULAMALARA YÖNELİK MONOSAKKARİT FONKSİYONLU KONJUGE POLİMER, POLİROTAKSAN VE OLİGOMERLERİN TASARIM VE SENTEZİ

Esra Deniz Soner
Kimya Bölümü Yüksek Lisans Tezi
Tez Danışmanı: Doç. Dr. Dönüş Tuncel
Eylül, 2015

Bu çalışmada reseptör aracılığıyla endositoz yoluyla aktif-hedeflenmiş hücre teranöstiği uygulamalarına olanaklı floresan, suda çözünebilen, çoklu- glikokonjugelerin tasarım, sentez ve karakterizasyonu sunulmaktadır. Gluko-fonksiyonel tiyofen monomerleri, Suzuki eşlenme polimerizasyonu öncesinde fonksiyonelleştirilmiş glikopolitiyofen ve glikopolitiyofen rotaksanları yapımında kullanılmıştır. Önceden fonksiyonelleştirilmiş glikopolitiyofen rotaksanının sentez yöntemi, boronik ester ve suda-çözünen bir makroçember olan kükürbituril-7 arasında, glikotiyofen monomeriyle suda Suzuki eşlenmesi *yerinde* kompleksleşme sağlamak amacıyla tasarlandı.

Azit grubu taşıyan kırmızı ışıyan oligomerler, sonradan fonksiyonelleştirme sentezi ile glikokonjuge oligomer yapımında kullanıldı.

Bu fonksiyonelleştirmeler azit grupları ve alkin-fonksiyonel monosakkaritler (mannoz veya glikoz) arasında 1,3-dipolar sikloekleme (çıtçıt reaksiyonu) ile yürütüldü.

Glikotiyofenlerin yapısal ve fotofiziksel özellikleri ^{1}H-NMR, UV-vis ve Floresans Spektroskopisi kullanılarak incelendi. Sentez adımlarında kullanılan monomerler ^{1}H-NMR, IR, ve ^{13}C-NMR kullanılarak incelendi. Kırmızı oligomerlerin yapısal, fotofiziksel ve morfolojik özellikleri ^{1}H-NMR, HRMS-TOF, DLS ve SEM kullanılarak incelendi.

Anahtar sözcükler: Konjuge polimerler, Glikokonjuge, Kükürbituril, Polirotaksan, Çıtçıt reaksiyonu.

Acknowledgement

I would like to express my appreciation to Assoc. Prof. Dr. Dönüş Tuncel, for first ingraining the love of organic chemistry in me through her lectures, then for her dedication to the lab, her enthusiasm for trying new things, her valuable feedback and her supervision in my research. I am sincerely thankful to the examining committee members, Prof. Dr. Engin Umut Akkaya and Assist. Prof. İrem Erel-Göktepe for their valuable time and feedback. I thank TUBITAK (project no: 112T058) for the financial support.

I am grateful to former or present -all my labmates Muazzam İdris, Özlem Ünal, Alp Özgün, Dr. Rehan Khan, Dr. Josheed PK, Hamidou Keita, Obadah Albahra, Emre Köken, Sinem Gürbüz, Ahmet Koç and Dr. Maasoomeh Bazzar (aka. Masi) for their constant help and support. I thank Masi again for synthesizing the beautiful oligomer. I would also like to express my gratitude to former UNAM member Dr.Ashif Shaikh for his practical advice in carbohydrate chemistry. I am especially grateful to Hamidou for his inspirational peaceful mindset and subtle awesomeness, and Obadah for his innate kindness, exquisite companionship and matchless generosity.

I would like to express my heartfelt gratitude to friends with whom I was able to share a mutual understanding, especially for having my chemistry BFFs Cansu Kaya and Aykut Aydın with me through this journey. I am deeply grateful to have Jan Sayılgan's support along the way; sharing the *meta* perception of things. I have been very lucky to have this campus as my neighborhood, I'm grateful for the peace it has given me throughout my studies, with its beautiful flora and wildlife.

I owe the deepest gratitude to my everloving and endlessly supporting family; my grandma who unites the big family, my aunt who always knows how to sort things out, my sister who made every step in life feel easier by leading the way, my father and my mother who filled me with love of nature, arts and ideas.

I dedicate this thesis to my beloved nephew Halil, the newest member of our family, who fills our hearts with joy.

TABLE OF CONTENTS

Abbreviations

^{1}H-NMR	Proton-Nuclear Magnetic Resonance spectroscopy
^{13}C-NMR	Carbon-Nuclear Magnetic Resonance spectroscopy
FTIR	Fourier Transform Infrared spectroscopy
HRMS-TOF	High Resolution Mass Spectrum Time of Flight
UV-Vis	Ultraviolet-Visible spectroscopy
PL	Fluorescence spectroscopy
DLS	Dynamic Light Scattering
SEM	Scanning Electron Microscope
PA	*trans*-Polyacetylene
PPP	Poly(*p*-phenylene)
PF	Polyfluorene
PPV	Poly(*p*-phenylenevinylene)
PP	Polypyrrole
PT	Polythiophene
PDV	Polydiphenylenevinylene
CD	Cyclodextrin
$CDCl_3$	Deuterated Chloroform
D_2O	Deuterated water
d-DMSO	Deuterated dimethylsulfoxide
DMSO	Dimethylsulfoxide
DMF	Dimethylformamide
THF	Tetrahydrofuran
CP	Conjugated Polymers
NPs	Nanoparticles
CPNs	Conjugated Polymer Nanoparticles
BT	Benzothiadiazole
PEG	Polyethylene glycol
CB	Cucurbitur[n]uril
M1	2-(2,5-dibromothiophen-3-yl)ethanol
M2	2,5-dibromo-3-(2-bromoethyl)thiophene
M3	3-(2-azidoethyl)-2,5-dibromothiophene
S1	1,2,3,4,6-Penta-O-acetyl-D-glucopyranose

S2 2,3,4,6-Tetra-O-acetyl-O-prop-1-yl-ß- D-glucopyranoside

S3 1,2,3,4,6-Penta-O-acetyl-D-mannopyranose

S4 2,3,4,6-Tetra-O-acetyl-O-prop-1-yl- ? - D-mannopyranoside

M4 (2,5-dibromothiophen-3-yl)ethyl)-prop-1,2,3-triazol-4-yl-tetra-O-acetyl ß-D-glucopyranoside

M5 2,5-thiophenediboronic ester

M6 Cucurbit[7]uril

P1 Poly[(3- triazol-ß-D-glucopyranosyl-thiophene)-co-(2,5-thiophene)]

P2 Poly[(3- triazol-ß-D-glucopyranosyl-thiophene)-co-(2,5-thiophene)] with Cucurbit[7]uril

OA 4,7-bis((E)-2-(9,9-bis(3-azidopropyl)-9H-fluoren-2-yl)vinyl)benzo[c][1,2,5]thiadiazole

O1 4,7-bis((E)-2-(9,9-bis(3- triazol- tetra-O-acetyl- α– D- mannopyranosyl)-9H-fluoren-2-yl)vinyl)benzo[c][1,2,5]thiadiazole

O2 4,7-bis((E)-2-(9,9-bis(3- triazol- α – D- mannospyranosyl)-9H-fluoren-2-yl)vinyl)benzo[c][1,2,5]thiadiazole

O3 4,7-bis((E)-2-(9,9-bis(di-(3- triazol- tetra-O-acetyl- α – D-mannopyranosyl))- (di-(3-azidopropyl))-9H-fluoren-2-yl)vinyl)benzo[c][1,2,5]thiadiazole

List of Figures

List of Schemes

List of Tables

Chapter 1 INTRODUCTION

1.1 Conjugated Polymers

Conjugated polymers are synthetic organic materials with electroluminescent and photoluminescent properties. Conjugation refers to the backbone of the molecular structure where there is a system of alternating single and multiple bonds. This system results in the delocalization of π-electrons along the chain to establish energy stabilization throughout the overlapping p-orbitals. The properties of such systems were first being discovered in late 70's. In 1977 Alan G. MacDiarmid, Alan J. Heeger and Hideki Shirakawa were the ones to discover the drastic change in the conductive properties of polyacetylene (PA) upon doping.[1] Soon later, the Nobel Prize in Chemistry 2000 was awarded jointly for these three scientists "for the discovery and development of conductive polymers".[2] Besides the simple alternating double bond structure of PA, structures with aromatic cycles on the backbone (i.e. PPP, PF), with both double bonds and aromatic cycles (i.e. PPV), and with heteroatom containing aromatic cycles (i.e. PP, PT) are some common conjugated polymer structures then reported.[3] Figure 1.1 shows some common conjugated polymer structures.

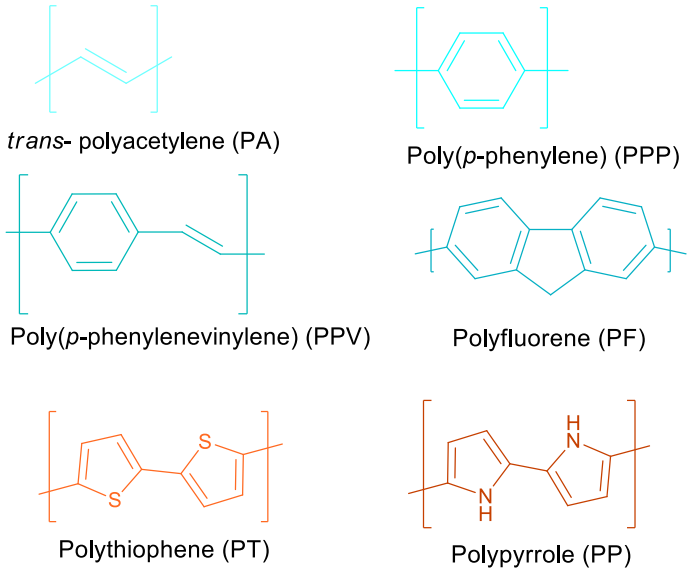

Figure 1.1. Common conjugated polymer structures.

These polymers were shown to be applied in many interesting fields of optoelectronics, such as in organic light-emitting diodes (screen displays) [4], solar cells (photovoltaics) [5], and electronic circuits.[6] Performance enhancements rapidly progress for optoelectronics, in which the use of conjugated polymers are well-established by now. Additionally, conjugated

systems have found applications through their photoluminescent properties in other fields, like chemosensing [7], biosensing [8], and biomedicine.[9,10]

How these applications are all possible for conjugated polymers lies in their unique electronic properties. Molecular orbital diagrams for such well defined molecules indicate whether the material can conduct electricity, as well as the types of relaxations it can undergo when its electrons are excited by light. The energy difference between the highest occupied molecular orbital (HOMO) and lowest unoccupied molecular orbital (LUMO) is called the band gap. These orbitals are also referred to as π-level (or S_o), and π*-level (or S_1), respectively. The electrical conductivity of such materials increase as the band gap decreases; the typical band gap for these materials being in the range of 1.5 eV to 4 eV.[11] Also, electron excitations can occur upon photon absorption at these molecular energy levels, and these excitations can relax back to the groundstate through several paths. If the energy is released as photon emission from the lowest singlet excited state, it is called fluorescence. If the electrons first cross to a triplet state, then photon emission occurs as electrons return to singlet ground state from this triplet state which is lower energy than the lowest singlet excited state, it is called phosphorescence. Conjugated polymers exhibit fluorescence.

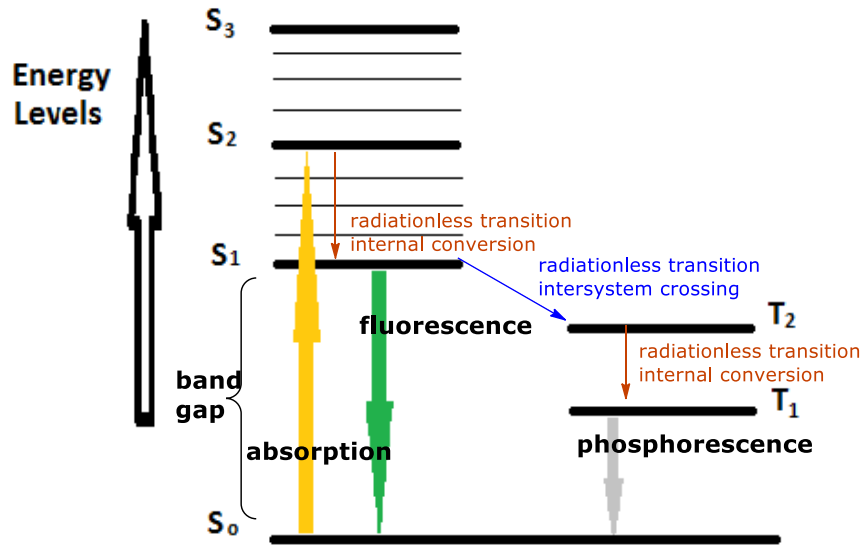

Figure 1.2. A simplified Jablonski Diagram for photoluminescent phenomena.

The fluorescence of conjugated polymers can be altered through the monomers involved for color tuning. The energy of the emitted photon is directly determined by the band gap energy (Figure 1.2). The band gap is primarily governed by the extend of conjugation; as the number

of repeating units increase, more electrons are delocalized, lower the energy gap.[12] Also, copolymer designs of alternating electron donating and withdrawing groups affect the band gap of the molecule. For example, benzothiadiazole (BT) is a commonly used electron acceptor monomer with a low LUMO, which can be conjugated with an electron donating monomer with a high HOMO energy level such as a fluorene unit to produce oligomers or polymers with small band gap energies and a broad absorption. Similar band gap engineering is shown in Figure 1.3a, comparing the colors of two fluorene co-polymers, and Figure 1.3b gives common monomers and corresponding colors of resulting copolymers.

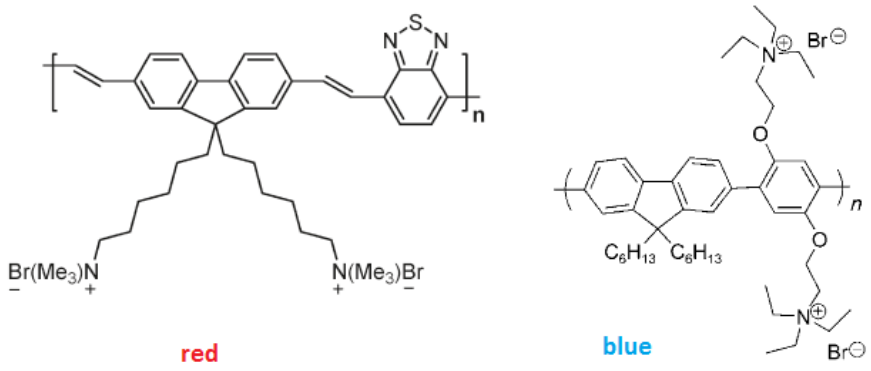

Figure 1.3a. Similar fluorene-based structures and color of emissions in water (ref [13] and [14] respectively).

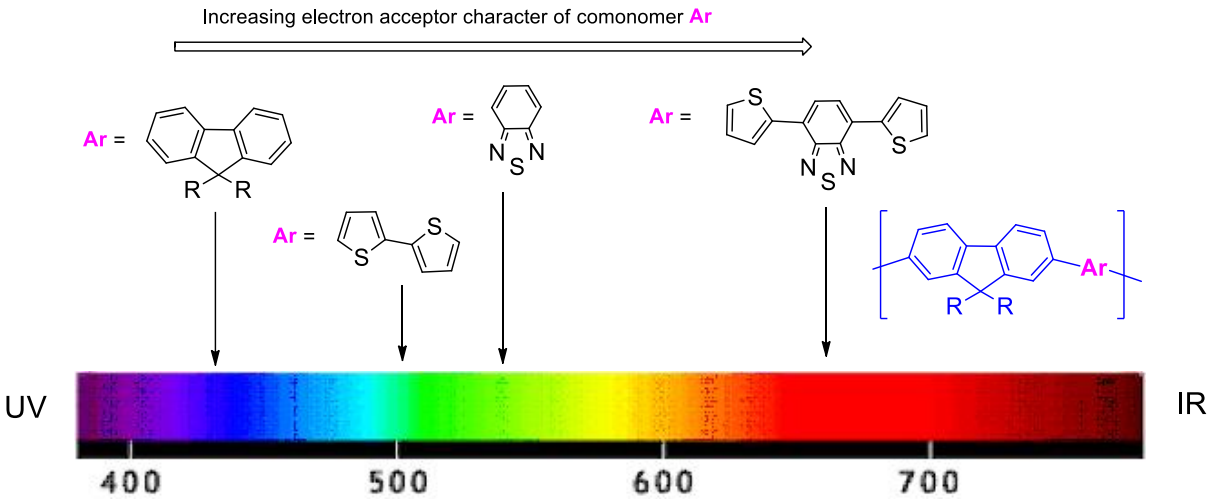

Figure 1.3b Bandgap engineered fluorene-based LEDs of colors blue, green, yellow, red. ref [15]

Besides the factors determined by the band gap through the backbone, pendant groups (side chain functionalities) can also affect the photoluminescence. Large bulky groups can indirectly improve fluorescence by reducing aggregation induced quenching, and with polar

groups, conjugation may be enhanced or disrupted through changing the planarity of the backbone by forcing the molecule into a specific conformation depending on its interactions with the solution.[16] Effects of electron donating or accepting side chains are also investigated. The end-groups of the monomers can be designed for the synthesis of these polymers using facile palladium catalyzed C-C bond forming cross-coupling reactions in solution. Palladium catalyzed cross-coupling is a commonly used technique of polymerization in the field, due to high efficiency, and the flexibility they provide in terms of monomer combination, reaction media, and due to the fact that they do not require a special experimental set-up as in the electrochemical techniques. The Nobel Prize in Chemistry in 2010 was awarded to Richard F. Heck, Ei-ichi Negishi and Akira Suzuki who developed unique and advantageous variations of such Pd-catalysis. [17]

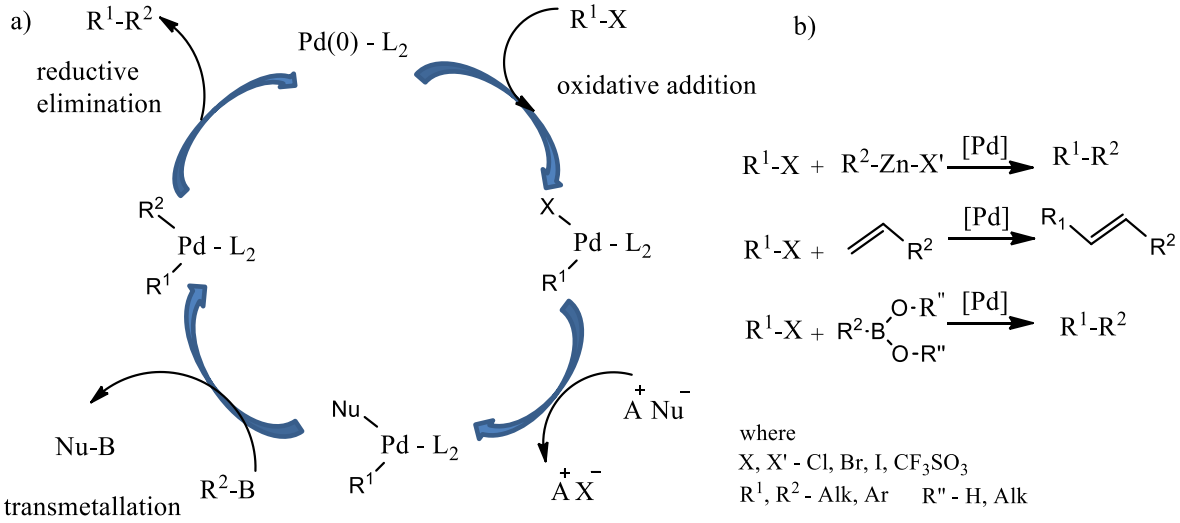

Figure 1.4. A schematic summary including a) General catalytic cycle for Pd-catalyzed cross-coupling reactions. b) Simplified reaction schemes for Negishi, Heck, and Suzuki reactions, respectively.

In fact, the main advantage of these three reactions (Figure 1.4) over other Pd-catalyzed techniques is that no other transition metal or heavy metallic moiety is needed [18], Suzuki coupling being the most prominent since it can be carried out in aqueous solutions, as well as being tolerant to different organoborane functionalities and environmentally friendly.[19] In Suzuki, the Pd-catalyzed cross coupling takes place between the organoboronic species and the aryl halide, and this C-C bond forms in the presence of a base.[20] For conjugated polymers, Suzuki reaction is exceptionally important for *in situ* or one-pot synthesis of water-soluble products.

1.1.1. Polythiophenes

Polythiophenes (PTs) are one of the conjugated polymers (Figure 1.1) to find a wide range of synthetic approaches [21a,b] and applications.[22] Polythiophenes have highest charge carrier mobilities reported for conjugated polymers.[3] They are also good candidates for biological applications since they are biocompatible [23], and their absorbance range is beyond the harmful UVB region. Various water-soluble thiophene species have been synthesized and reported in literature, to find various biological applications.[9] Biocompatibility of these conjugated polymers can easily be improved through functionalizing the side chains. Although the most reported, and possibly the simplest method for PT synthesis is chemical oxidation polymerization, it is useful only when regioregularity and/or solubility is of no importance, and one type of monomer is used for the polymerization (Figure 1.5a).

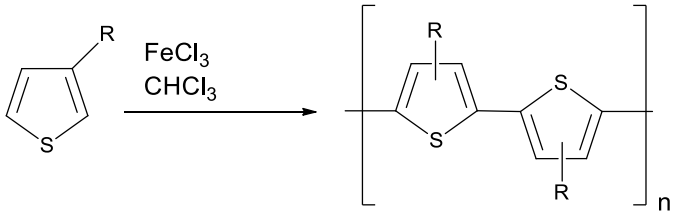

Figure 1.5a PT synthesis using chemical oxidation polymerization.

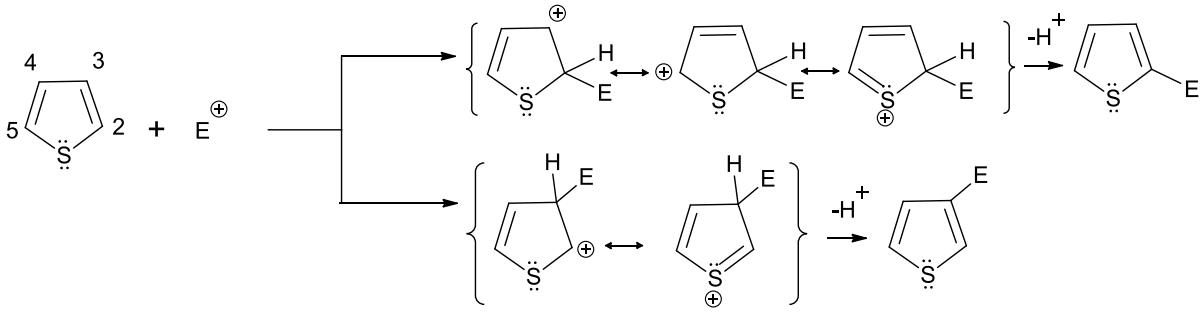

Figure 1.5b Thiophene carbon sites and heterocyclic resonance towards an electrophilic attack

The heterocyclic chemistry of thiophene favors site-selective functionalization. C2 and C5 are highly susceptible to an electrophilic attack, and this α-selectivity is due to the higher charge delocalization stabilizing the intermediate of C2 attack compared to C3 attack (Figure 1.5b). Commercial thiophene reagents for polymer applications have C2 and C5 sites available for desired substitutions for head–tail (2,5'), head–head (2,2'), or tail–tail (5,5') coupling. 3-Alkylthiophene is the most used thiophene monomer. Since it is not a symmetrical molecule, there are three relative orientations available. Head-head

or tail-tail couplings lead to regio-irregular PTs due to steric effects of the 3-substituent that leads to a backbone twist, and loss of conjugation.[21a] Head-tail coupling PTs are regioregular. This can be controlled through the choice of end-groups and polymerization.[21b] For Pd-catalyzed cross-coupling reactions, the end-groups can be designed as shown in Figure 1.4. Co-polymers can also be achieved through end-group design.

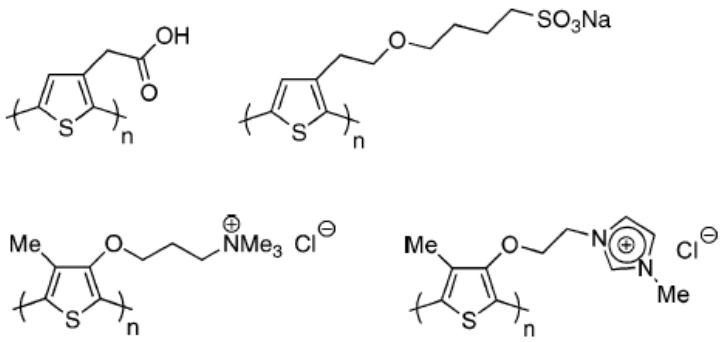

Figure 1.6. Polythiophenes with various ionic functionalities, ref [7]

Polythiophenes can thus be side-chain functionalized either pre-polymerization or post-polymerization. In the literature, the monomer designs usually consist of pre-polymerization attachment of a spacer followed by a post-polymerization functional group addition. For PEG-based water soluble designs the spacer *is* the functionality.[24] Some ionic functional groups to achieve water solubility reported include carboxylic acids [26], amino acids [27], sulfonates [28], amines [25], imidazolium [29] moieties.(Figure 1.6) Spacer length is important for side chain stability, since conjugation of the backbone can end up extended through elimination if possible during polymerization for pre- functionalization.

Side chains can be functionalized using different approaches, mainly through substitution-type reactions with halide or better leaving groups, however this may not be preferred in the possibility of an adverse side reaction, or problems of stability in harsh reaction conditions. One of the most reported alternative is a 1,4-cycloaddition reaction, often referred as the “click reaction”. 1,4-substituted click reaction occurs easily in mild conditions between an azide and an terminal alkyne to form 1,2,3-triazoles in the presence of Cu(I) catalyst (Figure1.7). This reaction was used to functionalize [30] or cross link [31] various conjugated polymers. One recent example is shown in Figure 1.8

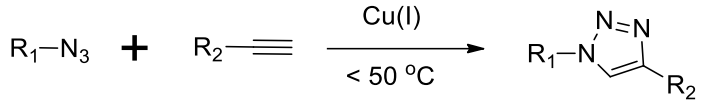

Figure 1.7. Copper-catalysed 1,4-cycloaddition.

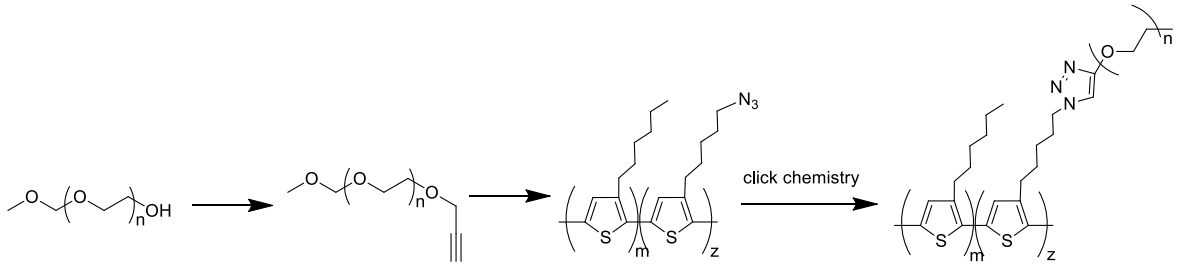

Figure 1.8. PT functionalization using click chemistry. [32]

Along with the advantages of synthetic feasibility and low toxicity, various applications have been monopolized specifically by PTs due to the unique regio-photochemistry they can provide. When the backbone can be forced into a more planar conformation from a non-planar one, it results in a significant red-shift in absorbance (Figure 1.9). Using these properties, water soluble polythiophenes have been designed and applied as sensing probes for detection of DNA (Figure 1.10) and fibrillar proteins like ß-amyloid [33b] through conformational changes. Although long polymeric chains of thiophene are usually preferred in applications of conformation monitoring, it is also a choice for biomedical applications. Fluorescent oligomers have been designed with similar monomers too.

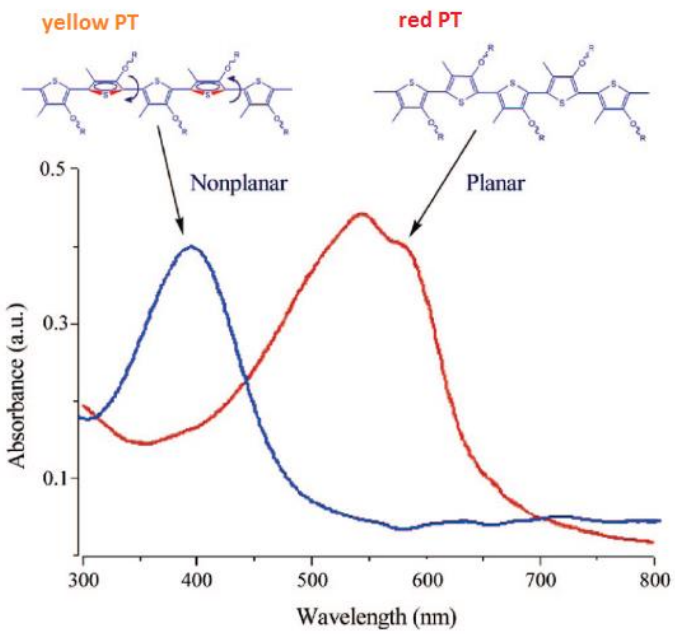

Figure 1.9. Conformations and corresponding absorption of a polythiophene. Reproduced with permission from ref. [33c], Copyright © 2008 American Chemical Society

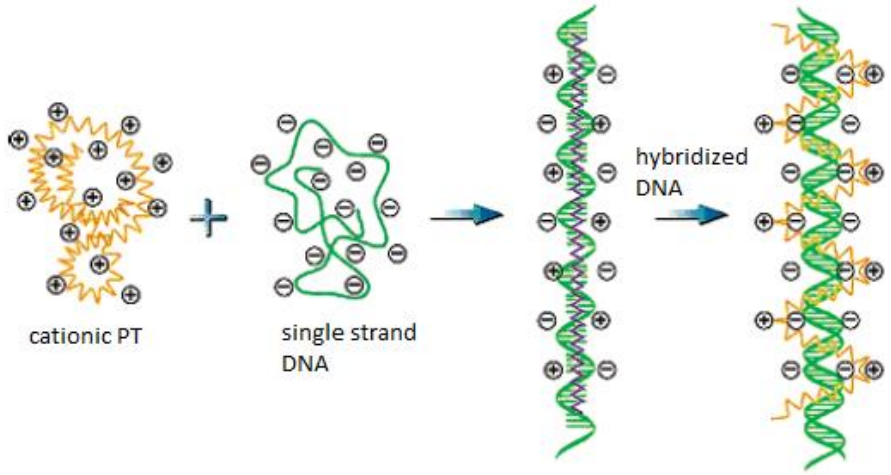

Figure 1.10 Hybridized DNA sensing cationic PT. Reproduced with permission from ref [33a], Copyright © 2005 Wiley-VCH Verlag GmbH & Co. KGaA, Weinheim

1.1.2 Oligomers

Oligomers that have convergent molecular properties with that of polymers have been of great interest especially in terms of synthesis; due to synthetic reproducibility, and the ease of establishing uniformity, having higher control over end-groups and molecular weight. The structure-property relationships of oligomers have been long investigated also to better understand longer conjugated materials.[34] Oligomers may have advantage over polymers depending on the intended application; oligomers may be preferred over their analogous polymers which are poorly soluble or intractable, which is especially important in photovoltaic device fabrication.[35] Especially symmetrical donor-acceptor-donor (D-A-D) type conjugated oligomers have been studied for solar cell and field effect transistors.[36]

Monodisperse amphiphilic π-conjugated oligomers have been designed for imaging too. Oligomers with fluorescence colours spanning the entire visible spectrum have been made amphiphilic to form water solubile, extremely stable self-assembled particles in water (Figure 1.11) With the use of oligomeric moieties that self-assemble, it gives the possibility co-assemble multi-targeting agents for biological imaging.[37]

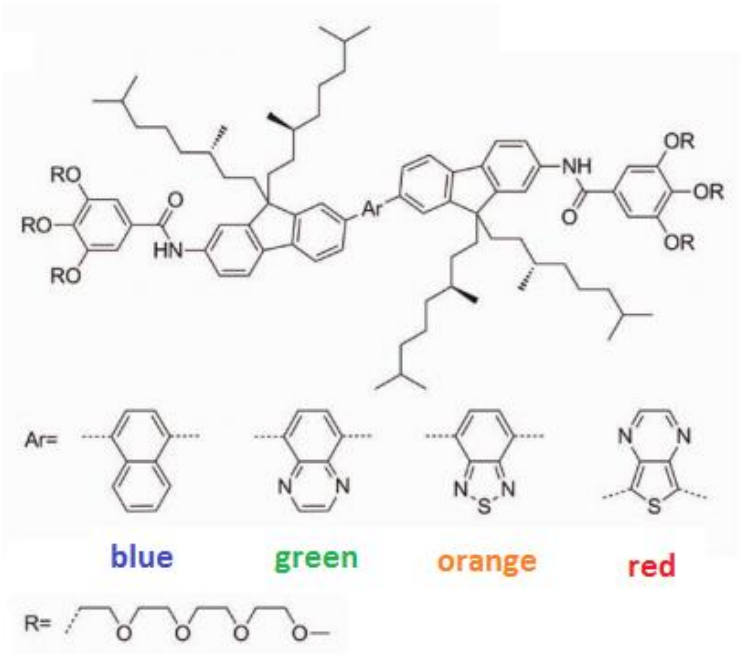

Figure 1.11 Fluorescent amphiphilic oligomers. [37]

Oligomers were made far-red near-infrared (NIR) emitting for light emitting diodes [38] through bandgap engineering. Establishing efficient photoluminescence in NIR-

region is also very important for biological applications. NIR fluorescent probes have been widely used because NIR light has the ability to deep-penetrate in tissue, and also preferable in cellular level because it causes minimal cellular autofluorescence in imaging.[39] The ultimate goal is to achieve NIR-emitting bio-active or –compatible oligomers to form nanoparticles.

1.2. Polyrotaxanes and Cucurbituril

Cucurbiturils (CB) are bulky and symmetrical pumpkin shaped macrocyclic oligomers formed from glycoluril units (n= 5,6,7,8 or 10) linked through methylene bridges.[40] These CB homologues all consist of portals decorated with polar carbonyl groups that enable strong dipole-dipole or ion-dipole interactions with the environment, and a hydrophobic cavity, but they all have different physical properties than one another. CBs are prepared from the acid-catalyzed condensation polymerization of glycoluril with formaldehyde.[42]

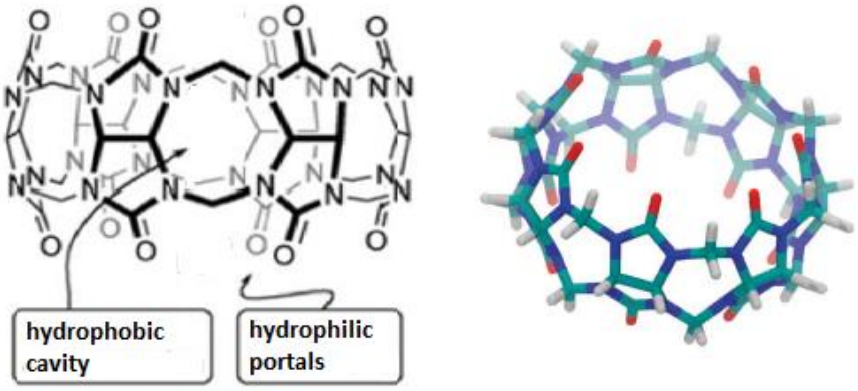

Figure 1.12 Molecular structures of CB6 and CB7, ref [41a] modified and [41b] reproduced, respectively.

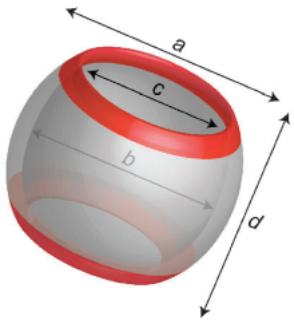

	Labels	CB5	CB6	CB7	CB8	CB10
Outer diameter /Å	a	13.1	14.4	16.0	17.5	20.0
Cavity diameter /Å	b	4.4	5.8	7.3	8.8	11.7
Portal diameter /Å	c	2.4	3.9	5.4	6.9	10.0
Height /Å	d	9.1	9.1	9.1	9.1	9.1

Table 1.1 Size parameters for the major CBn species. Reproduced from Ref [41b]

Most important difference between the physical properties is the solubility. The homologues are thus seperated from the reaction mixture using solubility differences, using acid, methanol and water.[43] Efficient solubility in water is crucial for any application that aims to benefit from these amphiphilic structures, which only the unique structural parameters of CB5 and CB7 (Table 1.1) was discovered to provide. CB7 is used since CB5 is too small in size and its abundance in a reaction mixture. CB7 also has very low toxicity and is safe even *in vivo*.[44]

Cucurbiturils have found interesting applications in supramolecular polymerization [45], charge-transfer complexes [46], molecular switches [47], responsive drug release systems [48], reaction catalysis [49], surface functionalizations of nanoparticles [50] and 2D platforms.[51]

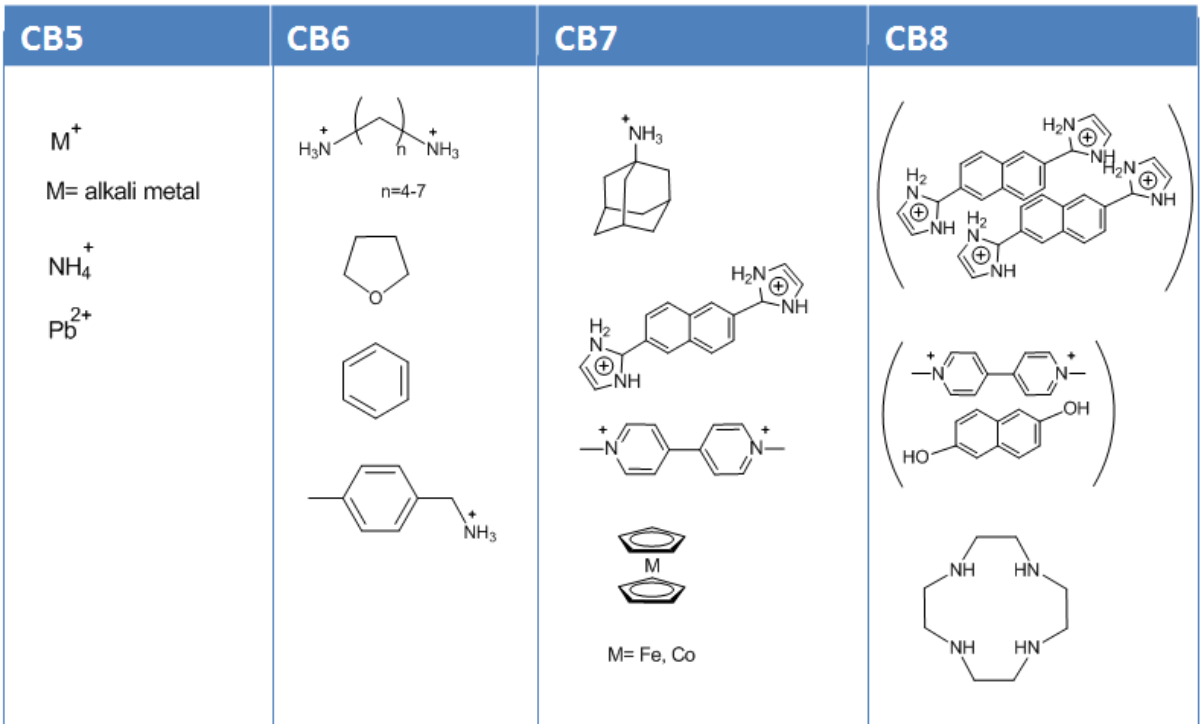

Figure 1.13 Common guests for CB homologues. Reproduced from ref. [52]

Typical guests for CB hosts (Figure 1.13) are often used as moieties for side chains or backbones of larger molecular designs, to have strong interaction with the encapsulating macrocycle. These large molecules may either have bulky stoppers to avoid "slipping" of the macrocycle or not. The general name for this type of architecture is called "rotaxanes". If it lacks stoppers, it is called a "pseudorotaxane".

If the whole structure consists of the rotaxane as a repeating unit, this polymeric form is referred to as “polyrotaxane”. Rotaxanes are often used as pH-responsive [53] and photo-responsive [54] systems.

For conjugated molecules, macrocycles can enhance electrical or photophysical stability of the backbone. Macrocycles can insulate delocalized electrons from reactive species. With insulation, unfavorable intermolecular interactions like aggregation that can result in quenching, polarizability changes that can occur through solvation, or conformational changes can be avoided. Due to this, conjugated rotaxane species are often called “insulated molecular wires”. The field of insulated molecular wire designs, however, is dominated by another macrocycle called cyclodextrin (CD) species, a commercially available bio-product. Polyrotaxanes of poly-*para*phenylene (PPP) (Figure 1.14), polyfluorene (PF) and polydiphenylenevinylene (PDV) (Table 1.2) backbones threaded through macrocycles with Suzuki coupling in aqueous solutions were synthesized.

Polymer backbone	Diboronic inclusion monomer	Diiodide monomer	End-group monomer
PPP	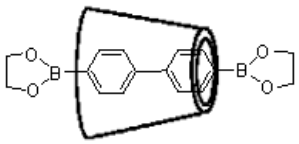	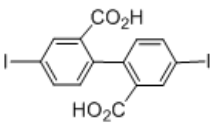	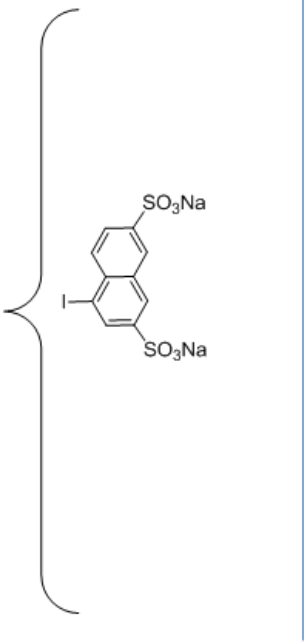
PF	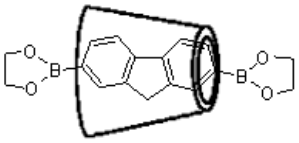	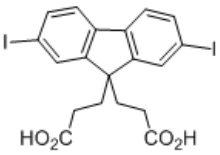	
PDV	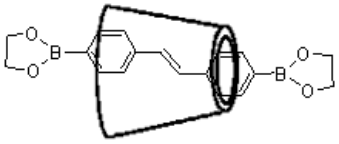	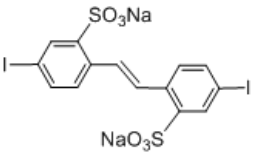	

Table 1.2 Monomers for Suzuki coupled conjugated polyrotaxanes based on macrocycle β-Cyclodextrin [55]

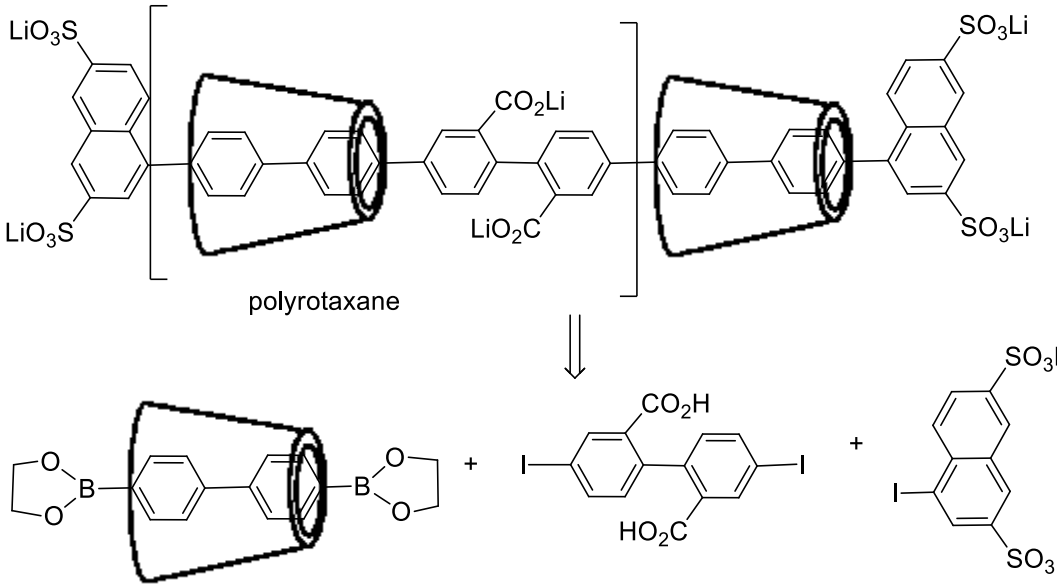

Figure 1.14 PPP Conjugated polyrotaxane [55]

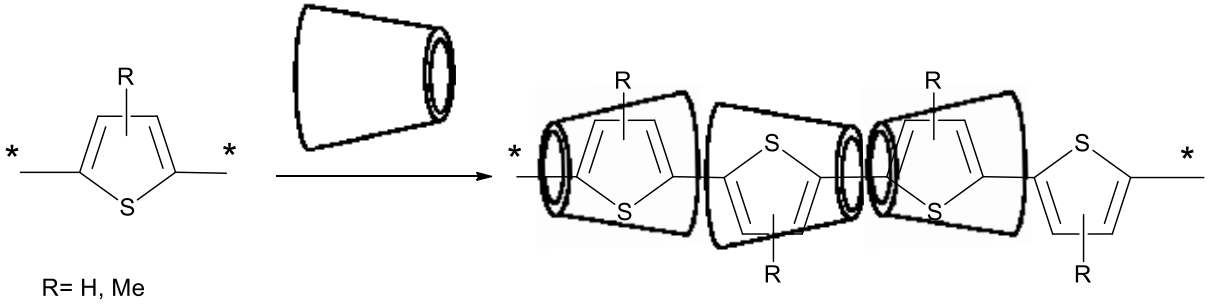

Figure 1.15 Post-polymerization pseudopolyrotaxane having PT backbone [56]

The use of CBn as the macrocycle for such conjugated polyrotaxanes, however, is uncommon. Farcas et al. recently reported [57] a fully conjugated polyrotaxane PF-BT•CB7 that consists of a fluorene – bithiophene backbone threaded with CB7 (Figure 1.16), however the encapsulation was solely done for insulation, and the polymer is not a water-soluble species. In their comprehensive 2007 review of insulated molecular wires, Anderson and Frampton [58] stated that growing interest in CB7 and CB8 and their strong affinities for aromatic guests makes them suspect that these macrocycles soon will make an important contribution to the field. Still, many reported CB-based rotaxane species [59] do not feature long π- conjugated systems.

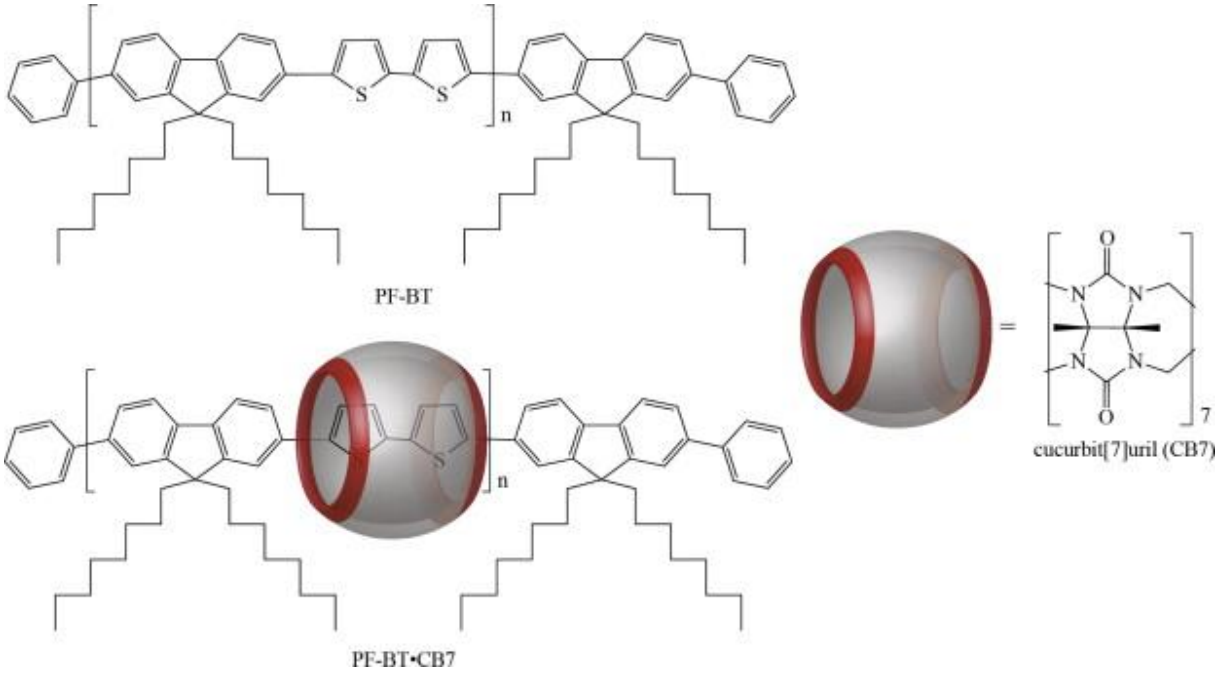

Figure 1.16 Chemical structures of PF-BT and PF-BT•CB7 Reproduced with permission from ref [57], Copyright © 2014 Elsevier Ltd.

Besides these "main chain" polyrotaxanes and pseudopolyrotaxanes, conjugated backbones with "side chain" pseudorotaxane designs that are chemically responsive can be made use of. A recent example [60] is a red-emitting oligomer capped with CB7 to achieve pH-responsiveness (Figure 1.17)

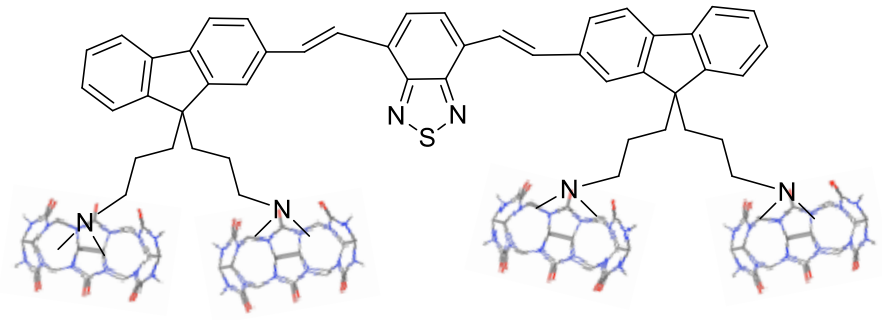

Figure 1.17 Side chain- CB7 pseudorotaxane of red conjugated oligomer, ref [60]

1.3. Nanoparticles of Conjugated Materials

Due to their aromatic backbones, conjugated polymers are partially hydrophobic although they may have water-soluble side chains. With highly-hydrophilic or amphiphilic components on the side chains, conjugated polymers effectively self-assemble to form nanoparticles in aqueous media (Figure 1.18).

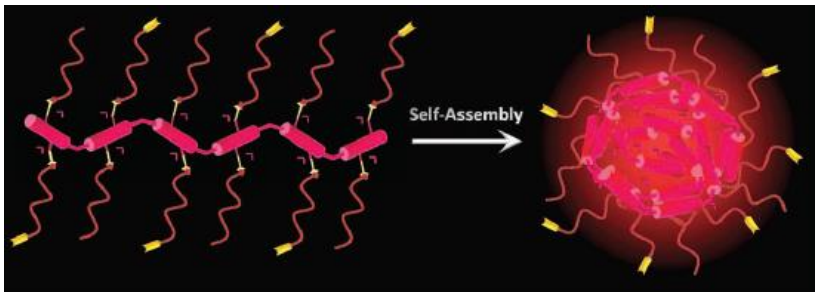

Figure 1.18 Amphiphilic nanoparticle formation, reproduced with permission from ref [61]. Copyright © 2011 WILEY-VCH Verlag GmbH & Co. KGaA, Weinheim

Slightly soluble polymers and oligomers can easily be made water-dispersible by forming nanoparticles through namely miniemulsion or nanoprecipitation methods (Figure 1.19). In miniemulsion method a surfactant in aqueous solution is introduced to the polymer solution which the solvent is water-immiscible. This method has the disadvantage of the need to use another reagent to stabilize the particle. In nanoprecipitation method, a water miscible solvent (i.e. THF, DMSO, DMF etc.) that can dissolve the materials at hand is used, and the solution is slowly added onto water and ultrasonicated to avoid aggregation and to induce dispersion, then after obtaining a homogeneous solution the solvent is removed.[62] Spherical nanoparticles form in order to minimize surface contact in water. One can get smaller particles with nanoprecipitation, compared to miniemulsion.

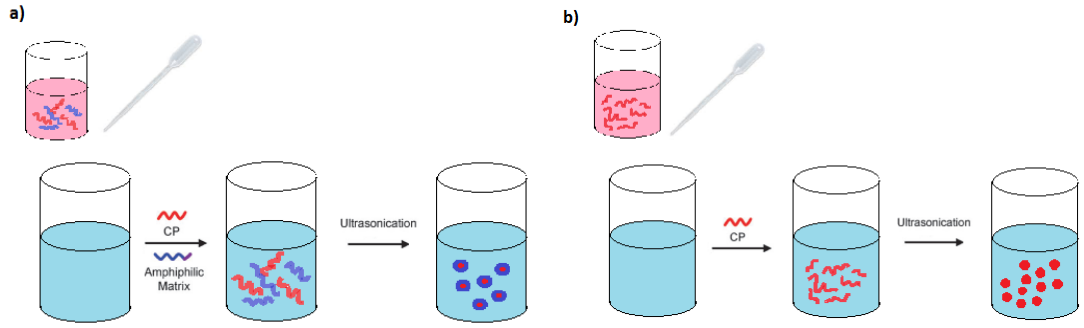

Figure 1.19 Nano-precipitation method using a) an additional amphiphilic matrix b) intrinsically amphiphilic CP

Conjugated nanoparticles have been a favorable choice for easy device fabrication in light emitting diode displays, solar cells, as well as bio-imaging probes, bio-sensing agents and nanomedical systems.[63]

1.4. Biomedical Applications of Conjugated Materials

Conjugated polymers have been of great interest in biomedical field since the 80s when they were shown to be compatible with cells and tissues *in vitro* and *in vivo* [64,61] Since then they have found applications of cell labeling, *in vivo* imaging and tracking [65], biomolecular sensing, and drug delivery.[66,67] Figure 1.20 shows major areas of use of CPNs in biomedical field. Conjugated polymers have been shown to detect small biomedically significant molecules like ATP, GSH, or biologically restricted amounts of metal ions [68] malfunctions in DNA methylation, single nucleotide polymorphisms, and protein misfoldings.[69]

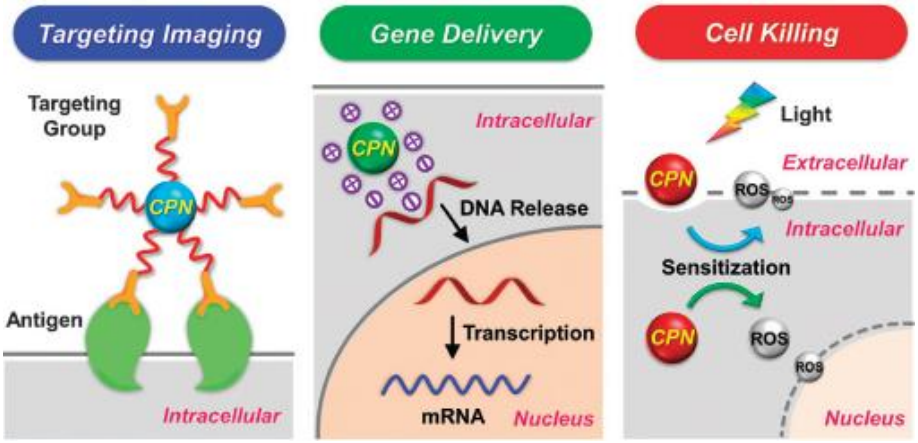

Figure 1.20 Schematic representation of CPNs in biological applications. Reproduced with permission from ref [62], © The Royal Society of Chemistry 2013

Conjugated bare nanoparticles achieve high photostability and low cytotoxicity, and efficient permeability to cellular cytoplasm. In bioimaging, organic dyes and fluorescent proteins are used often, but they show to rapid photobleaching which is a major drawback. Besides these materials frequently used in biology, quantum dots are a synthetic alternative to CPNs but are quite cytotoxic due to their heavy-metal cores, thus they need extensive shealth. Conjugated polymers have good light-harvesting and signal amplification properties, high fluorescence brightness and photostability, as well as

innately having much lower cytotoxicity, thus are more suitable for live cell imaging.[70]

Some charged conjugated polymers are reported for intracellular imaging biomolecules without particle formation or a bioconjugation. Polyelectrolyte thiophenes (PTs) shown as probes for both *ex vivo* and *in vivo* specific staining of protein aggregates related to Alzheimer's disease and their preliminary fibrils aggregates [71] Cationic polymers easily bind to cell surfaces through electrostatic attractions as a result of the anionic phosphate groups of the phosphoipids but cellular uptake is hard to control due to strong nonspecific electrostatic interactions. However, cationic PPVs were reported to monitor cell apoptosis [72] using the fact that cellular membranes of apoptotic cells have higher permeability and have higher charge compared to healthy cells because apoptosis causes exposure of negatively-charged phosphatidylserine, in addition to their inherent negative charge.

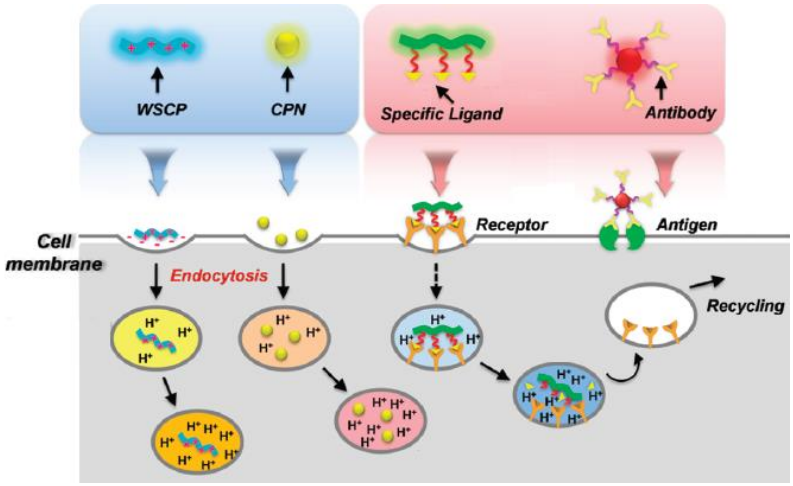

Figure 1.21 Pinocytic cellular internatization pathways of linear or nanoparticular polymers,simplified and reproduced from ref. [9]

For cell internalization, there are two major mechanisms of endocytosis, meaning how cells take up particles and macromolecules, and these are phagocytosis and pinocytosis. Large particles within micrometer-range are only internalized by phagocytic cells, such as macrophages, neutrophils, or dendritic cells, thus pinocytosis may be more relevant. Pinocytic cellular internalization of polymers is schematically shown in Figure 1.21. Pinocytic (fluid-phase) uptake and can occur through either receptor-mediated endocytosis (RME) or an initial non-specific adsorption to cell membrane. Thus size is very important for nanoparticle-based biomedical purposes. It is argued that 40–50 nm being the optimal size range for *in vitro* uptake due to the trade off between multivalent

surface membrane wrapping occurs versus the drawback of size increase, however 10–100 nm is a generally accepted range of NPs for *in vivo* applications due to issues of clearance and biodistribution.[73]

For treatment of tumorous cancer tissues, however, setting the particle size on the larger end of this spectrum is beneficial. The reason lies in the difference in vasculature compared to normal tissues. The vasculature of tumors (Figure 1.22) appear inherently leaky, generally having larger vessel diameters, higher vascular density, and enhanced permeability. In addition to this, the lymphatic drainage of macromolecules is impared in these tissues.[74] So considering these two effects, nanoparticles accumulate in the tumor interstitial space, and are not cleared out properly. The overall effect is referred to as "EPR effect", meaning 'enhanced permeability and retention'.

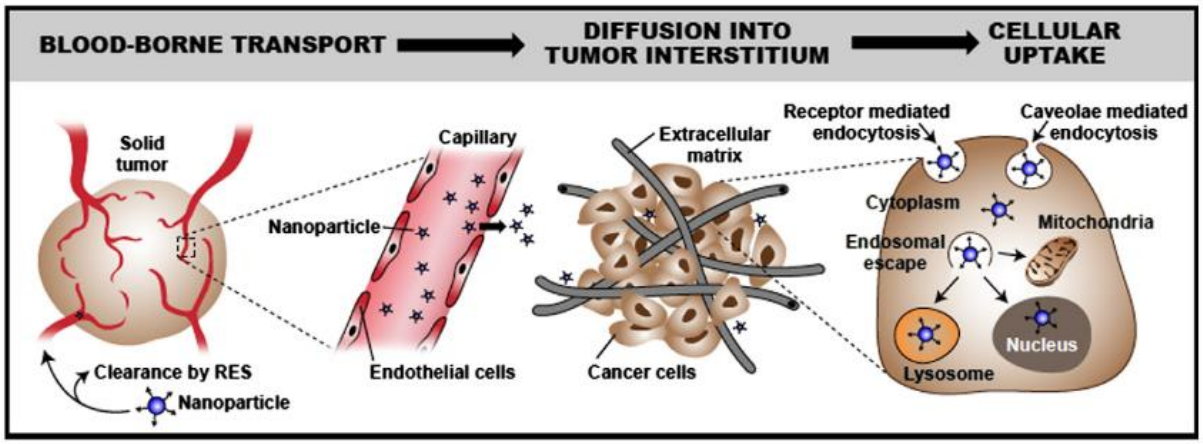

Figure 1.22 Transportation mechanism of nanoparticles to tumor microenvironment, Reproduced with permission from ref [74],© 2014 Elsevier B.V.

Conjugated polymer can be used to encapsulate photosensitizer or drugs for cell therapy. A photosensitizer, such as porphyrin, is often reported to be attached to have it in close proximity to the light harvesting conjugated polymer backbone for efficient energy transfer from to photosensitizer for photodynamic cancer cell therapy. Polythiophene – porphyrin dyad is often used for this purpose, for killing cancer or microbial cells.[75]

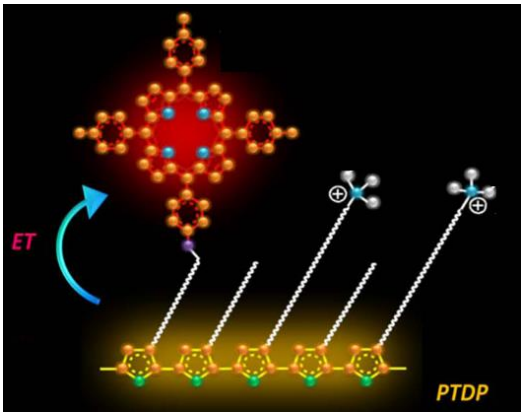

Figure 1.23 Polythiophene – porphyrin dyad for photodynamic therapy. simplified and reproduced from ref [75].

Similar to covalent attachment, energy transfer through short-range interactions may be designed using complex formation upon strong interactions between opposite charged molecules and it provides useful for a charged cargo. Cationic polymers have been reported as vectors for gene delivery, since they form complexes with DNA or RNAs [9] However, high positive charge of nanocarriers results in undesired levels of cytotoxicity, and often additional hydrophobic moieties have been incorporated into side chains to improve the cytocompatibility. A simpler design often may be achieved through milder ion-dipole interactions, or bioconjugates. For example, nanoparticles were prepared from an oligonucleotide carrier π- conjugated oligomer (Figure 1.24).

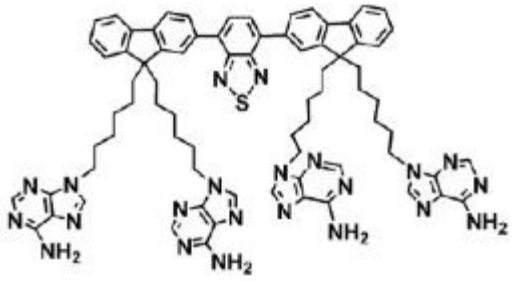

Figure 1.24 An oligonucleotide carrier π- conjugated oligomer [76].

Not all approaches may favor particles. Since spherical nanoparticle formation itself occurs to minimize surface contact with water, the surface is fairly inactive. Surface functionality becomes especially important for biological interactions. Post-functionalization approaches are applied to decorate nanoparticle surfaces after the particle is formed out of a polymer, however an extremely mild chemistry is needed because otherwise results in the disruption of the size and structural features of the generated particle.[61]

Water soluble conjugated polymers may be favored for the famous Ringsdorf model for drug delivery by polymers introduced in mid 70's where a polymer would be used as an anchor for a targeting, a solubilising and a drug moiety, which is attached by a cleavable linker.[77] Targetting can be achieved by attaching bioconjugate recognition groups to the side. An often used functionality is folic acid (FA) because FA-receptors are overexpressed in many cancer cell lines. FA-substituted PPE, for example, was reported for imaging an oral carcinoma cell type through receptor mediated uptake.[78]
Cellular imaging and/or therapy are done using other bioconjugates, such as cell-specific oligopeptides [79] , antibodies [80] or carbohydrates.[81]

1.4.1. Glycoconjugates for Active-Targetting

Carbohydrates have gained attention as targeting ligands due to their ease of production, low molecular weight and high abundance in nature.[73] There are a variety of carbohydrate ligands that target carbohydrate-binding proteins (called "lectins"). Lectin is a general name for proteins having affinity to carbohydrates, and if they reside on a cell membrane they're referred to as "membrane lectins". There are membrane lectins specific for types of cells that are differentially expressed, thus carbohydrates provide suitable ligands for nanocarrier designs, for cell-selective drug delivery.
Although the interaction between a lectin and the complementary carbohydrate is often weak, it may be greatly enhanced through multivalency. This phenomenon has become known as the "cluster glycoside effect".[82] Multivalent glycoconjugates have found nanomedical applications ranging from bacterial anti-adhesins and sensors, drug delivery particles, imaging agents, to immune-inducer vaccines.[83] Multivalent carbohydrate ligands have been used to provide receptor mediated endocytosis frequently in literature, with dendritic [83], linear[84] or core-shell particle[82] anchors.

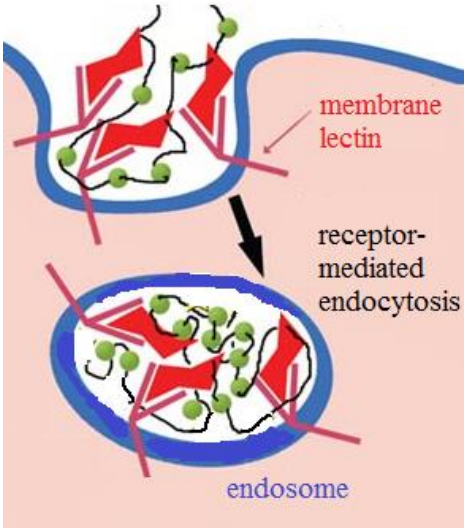

Figure 1.25 Receptor-mediated endocytosis of a glycoconjugate through "cluster glycoside effect", modified from ref [85]

Although oligosaccharide functionalities dominate biological targetting applications, these multivalent functionalized particles can mimic the multiple carbohydrate-protein interactions used by cells, viruses, or bacterial toxins with multivalent monosaccharide functionalities.[86]

The biocompatibility, solubility, and active endocytosis properties make glycoconjugates a desirable choice for nanomedicine. In glycopolymers, the carbohydrate moieties can be used as both the targeting and the solubilising part. According to Veronese et al. there are approximately 20 drugs (on the market or in clinical trials) based on this model.[87]

1.4.1.2. Monosaccharides as Pendant Groups

Glycoside chemistry

Hexoses (sugars of 6 carbons) are the most abundant monosaccharides in nature, thus the general term "monosaccharide" is often used to mean hexose. Monosaccharides are simplest carbohydrates with unique stereochemical properties. They are found in equilibrium with their acyclic and two cyclic forms (Figure 1.27) in nature, but upon glycoside formation on the "anomeric site" their conformation can be directed to a certain "anomeric form", as in the case of activated acetylated glucoside and mannoside and an alcohol substituent (Figure 1.28). The R group can be alkane, alkene or alkyne. Borontrifluoride reagent is a typical activator for this reaction.[88] The glycosides are often designed as groups of azide, halide or sulfide for further reactions.

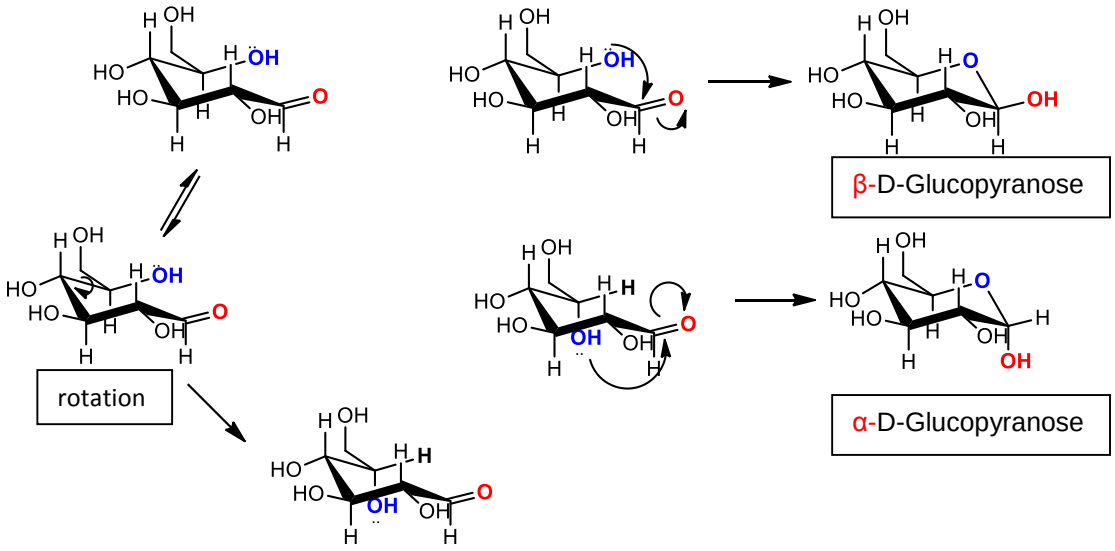

Figure 1.26 Equilibrium and anomeric forms of glucose.

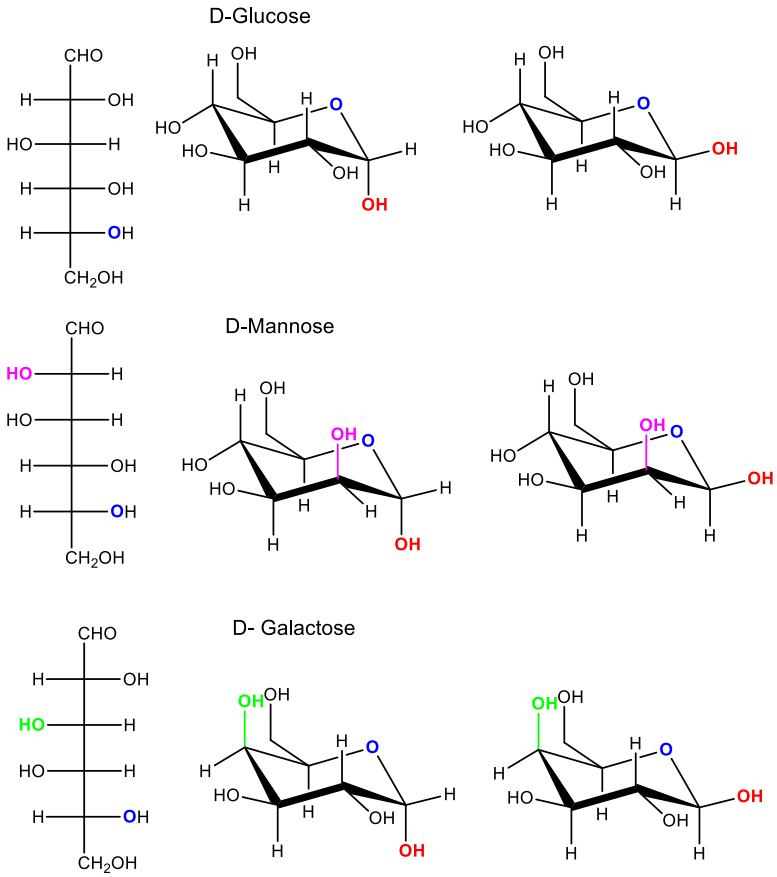

Figure 1.27 Cyclic and acyclic forms of glucose and its stereoisomers mannose and galactose.

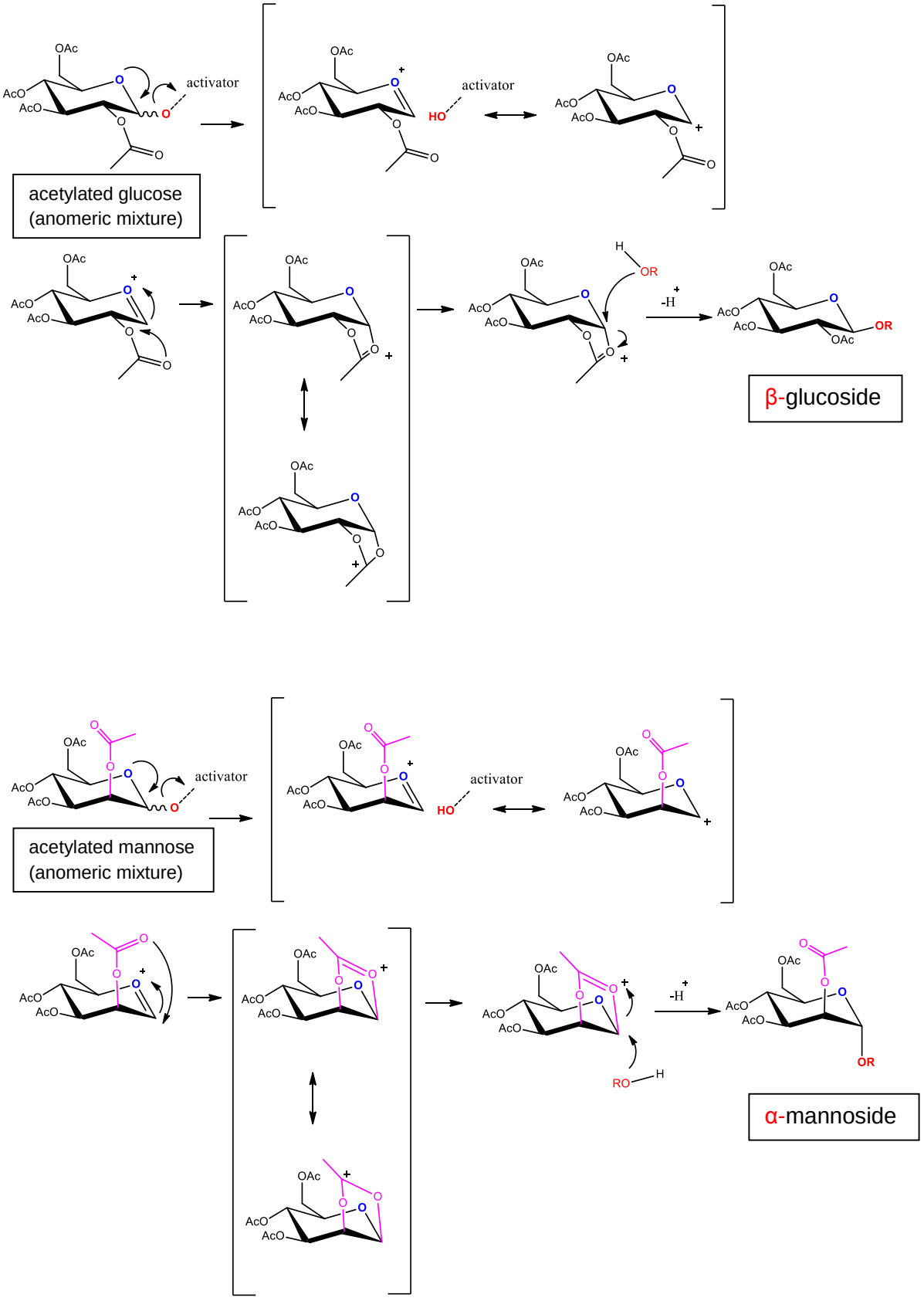

Figure 1.28 Anomer-selective activated glucoside and mannoside formation with an alcohol substituent.

The choice of monosaccharide, however, apparently has many factors to consider, such as its anomeric site being either α- or ß- [89], stereoisomerism [90], [91], or another attachment site (C2, C3, C4, C5) for the functional group [92], [93], [94], [95]. Anomeric functionalized mannoside[96], glucoside[97] and galactosides[98] are often reported as targeting moieties. Monosaccharides all have found a variety of purposes. However, most of the human cell types have cancer-related differentiations as mannose and galactose receptor over-expression.

Glucose

In vitro imaging using vero cells [99] and human cervical cancer cells [100] were done with glucosides. *In vitro* anti-inflammation studies with red blood cells [101] The inhibition of tetrameric PA-IL lectin from pathogenic *P. aeruginosa* [102] and affinity towards LOLI, a non-toxic *Lathyrus ochrus* lectin [103] was shown for sensing. LOLI is a possible candidate for a glucose-responsive drug release design, as in ref [104]. Also "GLUT1", a receptor that facilitates the transport of glucose in mammalian cells, is overexpressed in many tumors [105] and naturally highly expressed in the blood–brain barrier.[106] GLUT1 is also a receptor used by the HTLV virus (spherical, 100 nm diam.) to gain entry into target cells.[105]

Mannose

There are many mannose-functional conjugated materials (oligomer or polymer) reported only for the use of sensing the lectin Con A.[107-110] Concanavalin A (Con A), a multivalent lectin of jack bean plant *C. ensiformis*, is often used as a safe study model, less toxic than other lectins such as ricin, *Boulium* and *E. Coli* toxins [107] Besides aggregation-induced luminescence sensing (Figure 1.29), confirmation is achieved for particles through a range of competitive and non-competitive binding assays, namely haemagglutination inhibition (HIA), ELLA and ITC.[83,111] with bacterial lectins like *E. coli* FimH, and virulence factors PA-IL and PA-IIL of *P. aeruginosa*. ConA is the most widely used lectin in biosensing studies, and it's reported to have a strong affinity to mannose, but also binds α-glucose and not ß-glucose.[111] Mannose-functionalized conjugated polymers were synthesized and used for aggregation-induced detection of *E.coli*.[112-114]

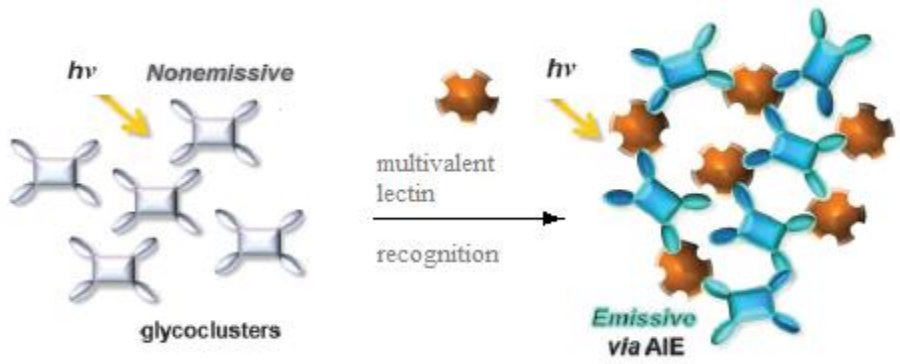

Figure 1.29 Direct detection of lectins with "turn on"luminescent probes, modified from ref [83]

Other glycopolymers have also been applied to advanced applications of cancer therapy. [81,115] Targeting C-type lectin receptors on cells has been shown to induce immunity against melanomas tumors *in vivo* [116]. Mannose targeting is done for MMR on macrophages, and DC-SIGN on dendritic cells, to mimick high mannose glycoprotein of HIV-1 gp120 and other pathogenic microorganisms that have similar interactions with these cells [83]. Mannose receptor on macrophages and liver endothelial cells produce opportunities for cell-specific gene delivery.[96] Mannose is reported to be a dendritic cell antigen that activates cytotoxic T cells for antitumor vaccine efficacy. Mannose-grafted nanocarriers were reported for this purpose and showed increased cellular uptake.[117] A quick summary of mammalian lectins and their ligand stereoisomers can be found in Table 1.3.

Receptor	Cell type or expression	Organ or tissue	Ligand	Function
Asialoglycoprotein receptors	Hepatocytes	Liver	Galactosyl residues	Targeted drug or gene delivery
Mannose receptors (C-type lectin receptor)	Endothelial cells and Kupffer cells	Liver	mannose residues	Receptor-mediated rapid endocytosis
	Macrophages	liver, spleen, brain, bone marrow and lungs	Terminal mannose groups	Phagocytosis; Internalization by macrophages, treatment of disease localized in macrophages like Gaucher disease
	Dendritic cells	Spleen, lymph nodes, blood	Complex with terminal mannose groups	Targeted DNA delivery to trigger cellular immunity; pathogen recognition; vaccination
Galactosyl receptor	Hepatic endothelial and Kupffer cells	Liver	galactose Residues	Endocytosis
Lectin-like receptors	Malignant cells	Tumor	galactose, lactose, mannose, fucose, 3-Aminopropyl glycosides of Sialyl-Lewisx	Drugs targeting to malignant tissue

Table 1.3 Summary of mammalian lectin receptors. ref [118]

Galactose

Hepatocytes (liver cells) are known to express the galactoside-binding asialoglycoprotein receptor (ASGPR) on their surface; on binding, the galactoside-conjugate is internalised by the cell.[119] However, it has been reported in the review article by Pawar et al, that galactose and mannose could both recognize the asialoglycoprotein receptor.[120]

The conjugated glycopolymers

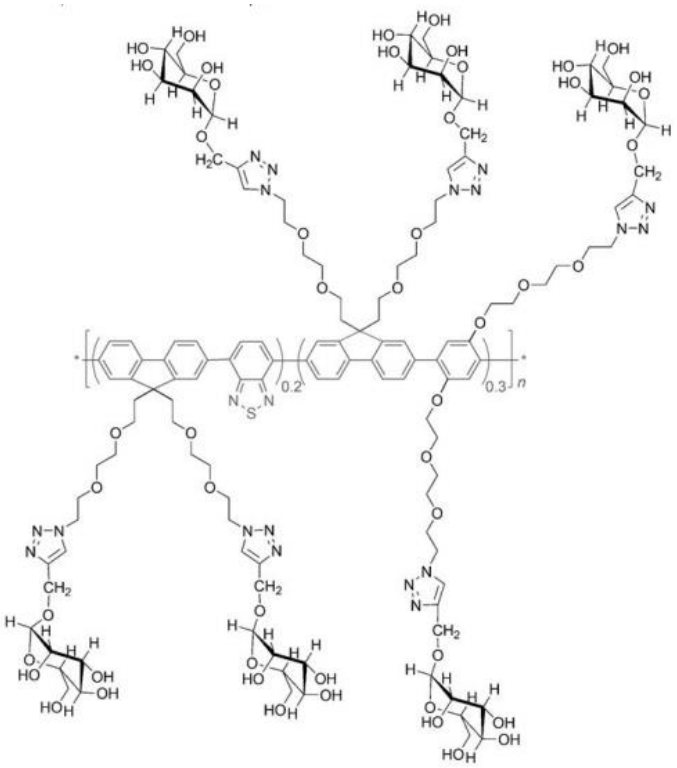

Figure 1.30 Benzothiadiazole-fluorene- based conjugated glycopolymer for Con A sensing. Ref [107]

Aggregation-induced fluorescence (see Figure 1.29) is used typically for Con A sensing with post-functionalized conjugated polymers. It has been shown that benzothiadiazole-fluorene- based conjugated glycopolymer (Figure 1.30) had a drastic fluorescence intensity increase at the 555nm-peak upon aggregation.[107] Liu et al. reported a neutral water-soluble oligomer similar to this polymer with four α-mannose side chains (Figure 1.31). The design for light-up detection of ConA and *E. coli* was achieved through an energy transfer pair with a mannose-substituted conjugated polyelectrolyte [121].

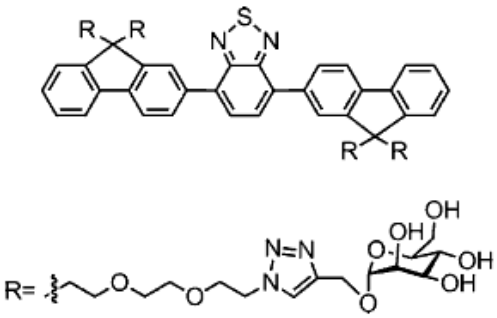

Figure 1.31 Mannose-functionalized oligomer for ConA and *E. coli* detection. ref. [121]

Glycopolythiophenes have been reported in the last few years, as in Figure 1.32, for the same purpose.[110] This homo-glycopolythiophene shows similar increase in intensity in its 460nm-fluorescence peak. β-glucoside analogue of this glycopolymer was shown to displays no binding ability to Con A, and was used as a control.

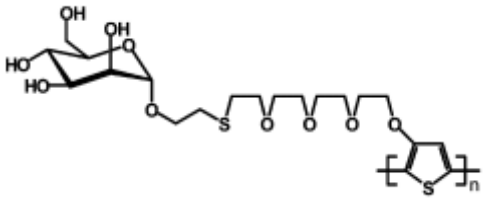

Figure 1.32 Mannose-functionalized homo polythiophene for Con A sensing. Ref [110]

In 2010, Han et al. reported a fluorescent polymer with galactose pendant groups for Ca^{2+}-induced fluorescence quenching studies. This polymer was prefunctionalized and Suzuki coupling was carried out in THF (Figure 1.33).

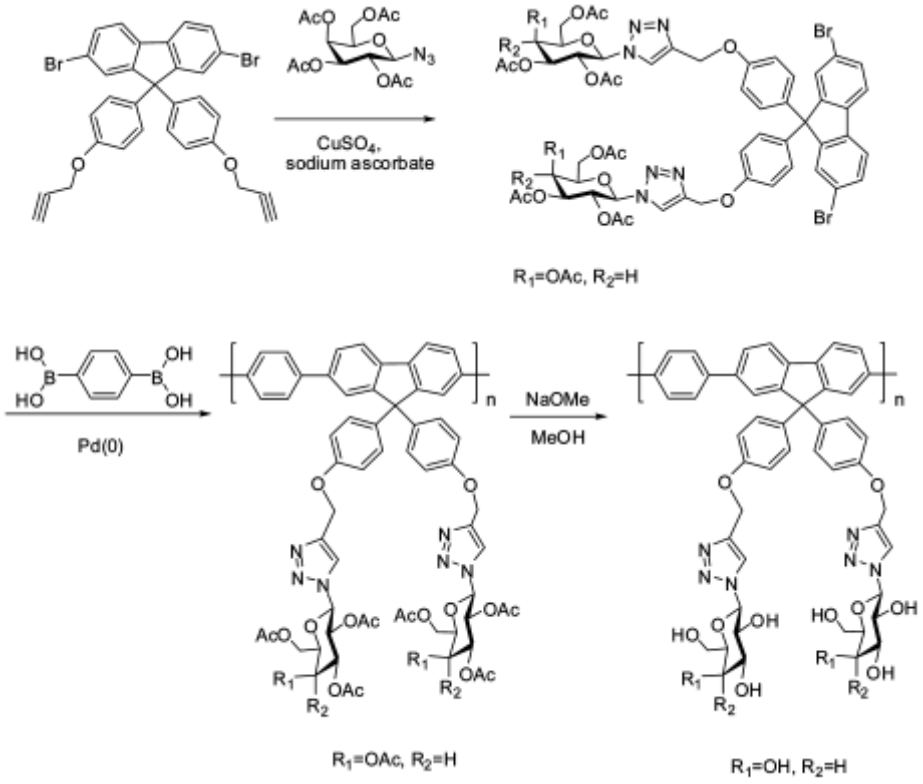

Figure 1.33 Pre-functionalized galactoside-functionalized monomer for Suzuki Coupling. ref [122]

1.5. Aim of the Thesis

Initially, an *in situ* cucurbituril threadded polyrotaxane in water was designed using Suzuki coupling reaction with a cationic thiophene monomer. The idea for the synthesis discussed in the first part of this thesis was elaborated on as a solution to an occuring problem. The 3-substituted water-soluble cationic thiophene monomer went through undesired elimination in the reaction conditions due to the favored extention of conjugation. For this, a more stable alternative and application-wise favorable pre-functionalized monomer without the risk of elimination was proposed instead. Glucose functionality was proposed as an sugar prototype, as an alternative to both trimethylamine and triethyleneglycol functionalities. A thiophene monomer was designed through cycloaddition of an alkyne glucopyranoside moiety for Suzuki polymerization with an encapsulated boronic ester. A new synthesis route for a novel polyrotaxane design was investigated.

For the second part, similar alkyne functional mannoside was synthesized for post-functionalization of a red-emitting conjugated oligomer.

Water-soluble monosaccharide functionalized conjugated polymers, polyrotaxanes and oligomers as fluorescent, water-soluble, multivalent glycoconjugates were thus synthesized, designed for possible bioactive and biocompatible purposes, and may provide better alternative to specific cell applications compared to the nonspecific-binding cationic or PEG moieties.

Chapter 2 EXPERIMENTAL

2.1 Materials

All reagents and solvents used were commercial grade, and were used without further purification unless stated. All column chromatography purifications were done using silica gel (Kieselgel 60, 0.063 – 0.200 nm) and were monitored by thin layer chromatography silica gel plates (Kieselgel 60 F254, 1mm) under shortwave UV lamp (254nm).

2.2 Instrumentation

2.2.1. ^{1}H-NMR and ^{13}C-NMR Spectroscopy

For the characterization of all molecular structures, nuclear magnetic resonance were measured and recorded with Bruker Avance DPX-400 MHz spectrometer. All measurements were taken in deuterated solvents. All chemical shifts were given relative to the internal standart tetramethylsilane.

2.2.2. UV-VIS Spectroscopy

UV-Vis absorbance spectra for optical characterization were recorded by Cary 300 UV-vis Double Beam Spectrometer equipped with Xenon-lamp as the light source. UV-Vis absorbance of sample solutions were measured within the range of 200-800nm, using quartz cuvettes with 1cm width. Solvents are chosen according to the sample and stated for each characterization.

2.2.3. Photoluminescence Spectroscopy

Photoluminescence spectra for optical characterization were recorded by Cary Eclipse Varian Spectrometer equipped with Xenon-lamp as the light source. Photoluminescence of sample solutions were measured within the range of 200-800nm, using quartz cuvettes with 1cm width. Samples were excited at their respective excitation wavelength, and initial wavelength for the measurement range was set 10nm higher. Solvents are chosen according to the sample and stated for each characterization.

2.2.4. FT-IR Spectroscopy

For the characterization of chemical functional groups on the monomers, Fourier Transform Infrared spectra were measured and recorded with Bruker Tensor 27 spectrometer equipped with a DLATGS detector with a resolution upto $1cm^{-1}$. All measurements were taken by dropping chloroform solutions onto KBr plates and drying in the oven to evaporate solvent

and moisture, unless otherwise stated. KBr plates were prepared by grinding IR grade KBr to a fine powder and were pressed into solid pellet disks. The data were recorded in the spectral range of 4000-400cm^{-1} for 64scans.

2.2.5. Flow-Syringe Pump

Oligomer nanoparticles were prepared using KD Scientific 270 (KDS 270) Constant Flow-Syringe Pump, in Infusion mode. Plastic syringe was inserted onto the equipment, and filled with ddH_2O. The flow rate ($mL{\cdot}h^{-1}$) was set electronically.

2.2.6. Mass Spectroscopy

The mass of oligomers were determined with Agilent 6224 High Resolution Mass Time-of-Flight (TOF) LC/MS with Electrospray Ionization.

2.2.7. Dynamic Light Scattering

The sizes of the oligomer nanoparticles were measured by DLS method using Zetasizer Nano-ZS instrument with 633nm laser beam, for 13 scans. The measurements were taken in 1mL of ddH_2O at room temperature, using disposable DLS cuvettes with 1cm width. The average particle diameters were calculated in the software via Marquardt method.

2.2.8. Scanning Electron Microscopy

The morphological characterizations of nanoparticles were done using scanning electron microscopy (SEM) Quanta 200 FEG.

2.3 Synthesis

2.3.1. Synthesis of 2-(2,5-dibromothiophen-3-yl)ethanol (M1)

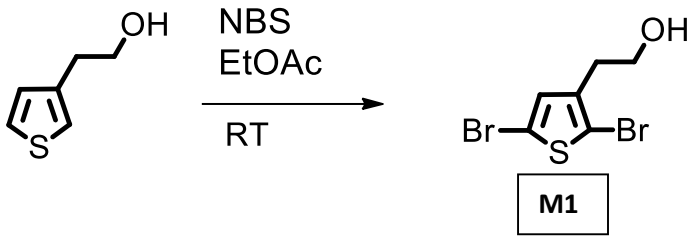

M1

Freezethaw was initially applied to 100mL EtOAc in a two neck round bottomed flask. 2-(3-thienyl)ethanol (3.00 g, 23.4 mmol) was completely dissolved in the freezethawed solvent. *N*-bromosuccinimide (NBS) (10.4 g, 58.5 mmol) was added to the solution and the flask was sonicated for 10 minutes in dark. Then it was stirred in dark, at RT, under nitrogen, overnight. The work-up was done to the reaction mixture by first water extraction. The organic layer was further extracted with brine, then subjected to suction filtration using silica gel. The solvent was evaporated under reduced pressure. Yellowish transparent viscous liquid product was obtained. TLC Rf= 0.13 using 9:1 (Hexane:EtOAc) mobile phase. Yield: 2.95 g, 45%. ^{1}H-NMR (400 MHz, $CDCl_3$, δ): 6.90 (s, 1H), 3.84 (t, 2H), 2.82 (t, 2H), 1.58 (s, 1H) ppm. FT-IR (KBr, pellet, $\nu_{max}(cm^{-1})$): 3300 cm^{-1} (O-H, s, b).

2.3.2. Synthesis of 2,5-dibromo-3-(2-bromoethyl)thiophene (M2)

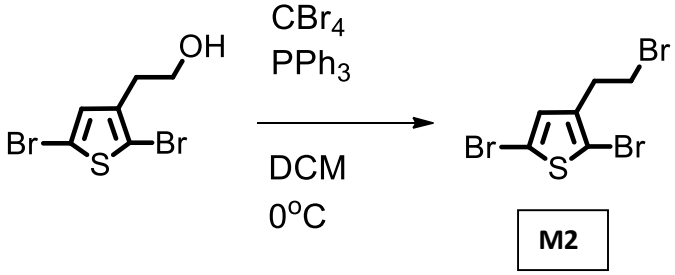

M2

DCM was distilled after adding CaH_2, then further dried by keeping with activated molecular sieves overnight. Dried DCM was degassed before the reaction. 2-(2,5-dibromothiophen-3-yl)ethanol (M1) (2.95 g, 10.4 mmol) and PPh_3 (6.55 g, 25.0mmol) were dissolved in 15mL DCM in a two neck round bottom flask. The solution is freezethawed two times, and fed nitrogen. CBr_4 (8.27 g, 25.0mmol) was seperately dissolved in 3mL degassed dry DCM, and added dropwise into the flask while it was kept at 0°C in ice bath. The reaction mixture was stirred for overnight under nitrogen. The work-up was done to the reaction mixture by first water extraction. The organic layer was further extracted with brine, then subjected to suction filtration using silica gel. The solution collected was concentrated by evaporating solvent

under reduced pressure then was dissolved in cyclohexane. A second suction filtration was done using silica gel. The solution collected was concentrated by evaporating solvent under reduced pressure again. Silica packed column chromatography was done using cyclohexane. Transparent liquid product was collected. Yield: 2.40g, 70%. TLC Rf= 0.75 using 9:1 (Hexane:EtOAc) mobile phase**.** ^{1}H-NMR (400 MHz, $CDCl_3$, δ): 6.88 (s, 1H), 3.52 (t, 2H), 3.12 (t, 2H) ppm.

2.3.3. Synthesis of 3-(2-azidoethyl)-2,5-dibromothiophene (M3)

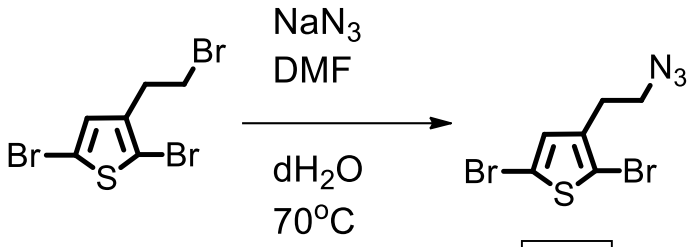

M3

DMF and ddH_2O were seperately degassed before the reaction. 2,5-dibromo-3-(2-bromoethyl)thiophene (M2) (2.40 g, 7.77mmol) was put into a two neck round bottom flask with DMF (5mL) and a reflux set-up was done. NaN_3 (0.59g, 10.1mmol) was dissolved in 3 mL degassed water. The mixture was heated to 70°C, stirred overnight. The DMF-water mixture was evaporated using vacuum distillation set-up under high vacuum using the Schlenk line. The reaction mixture was subjected to water:chloroform extraction. The organic layer was collected and the solvent was evaporated under reduced pressure. Orange tinted transparent liquid product was collected. Yield: 1.84g, 86%. TLC Rf= 0.69 using 9:1 (Hexane:EtOAc) mobile phase. ^{1}H-NMR (400 MHz, $CDCl_3$, δ): 6.87 (s,1H), 3.48 (t,2H), 2.84 (t,2H) ppm. FT-IR (KBr, pellet, $\nu_{max}(cm^{-1})$): 2100 cm^{-1} (N=N, s).

2.3.4. Synthesis of 1,2,3,4,6-Penta-O-acetyl-D-glucopyranose (S1)

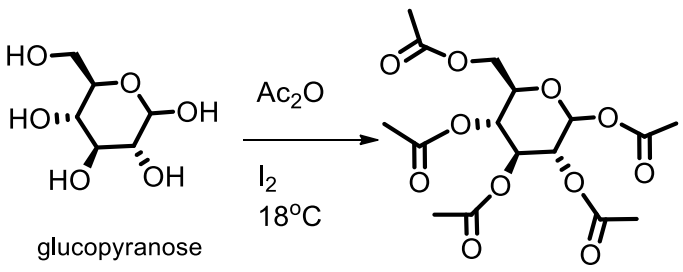

S1

Iodine crystals (0.13g, 0.50mmol) were completely dissolved in Ac_2O (50mL) in 250mL one neck round bottom flask. The flask was then placed in a cool water bath (18°C). D-glucopyranose (10.1g, 56.1mmol) was added to the solution portionwise while stirring. The solution was stirred for 2 hours. The work-up was done to the reaction mixture by first pouring it into 100mL solution of ice-cold saturated aqueous solution of sodium thiosulfate in a 800mL beaker while vigorously stirring. After complete addition and mixing, sodium bicarbonate is added to the mixture slowly portionwise, until the violent bubbling disappears. 50mL of DCM was added to the mixture and stirred. The solution is then transferred to a 250mL separatory flask. A 50mL of saturated aqueous sodium bicarbonate solution was prepared separately and cooled beforehand. The organic layer was first extracted with the cool saturated bicarbonate solution, then three times with water. The organic layer was dried using sodium sulfate, then solvent was evaporated under reduced pressure. Yellowish transparent sticky viscous liquid product was first observed, then upon high vacuum drying, white crystals were obtained. Yield= 19.2g, 88% ^{1}H-NMR (400 MHz, $CDCl_3$, δ) for abundant β: 6.36 (d, 1H), 5.52- 5.49 (t, 1H), 5.19-5.11 (m, 2H), 4.30-4.27 (dd,1H), 4.14- 4.10 (m, 2H), 2.21 (s, 3H), 2.11 (s, 3H), 2.07 (s, 3H), 2.05 (s, 3H), 2.04 (s, 3H) ppm. FT-IR (KBr, pellet, $\nu_{max}(cm^{-1})$): 1750 cm^{-1} (C=O, s), 1250 cm^{-1} (C-O, s).

2.3.5. Synthesis of 2,3,4,6-Tetra-O-acetyl-O-prop-1-yl-β- D-glucopyranoside (S2)

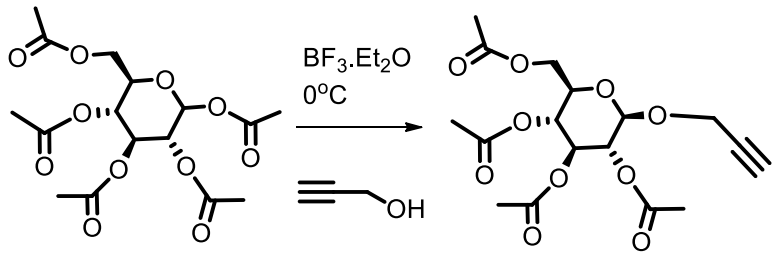

S2

DCM was distilled after adding CaH_2, then further dried by keeping with activated molecular sieves overnight. 1,2,3,4,6-Penta-O-acetyl-D-glucopyranose (S1) (10.7g, 27.4mmol) was dissolved in dried DCM in 100mL round bottomed flask. Propargyl alcohol (2.7mL) was added to the solution and flask was put in ice bath and cooled to 0°C. Sealed dropping funnel set-up was done. $BF_3.Et_2O$ (26.7mL) was put in the sealed dropping funnel. The set-up was fed with nitrogen for a short time then closed. $BF_3.Et_2O$ was dropped into the round bottom flask very slowly while vigorous stirring at 0°C, over a period of approx. 40 minutes, with a

corresponding rate of approx. 20s per drop. Once the addition is finished, the reaction mixture was stirred for 12h at RT. The work-up was done to the reaction mixture first diluting it by pouring it into 100mL DCM and stirring for 5 min. Water extraction was done 5 times, until visible residues of black cloudy suspension is cleared out. The solvent was evaporated under reduced pressure. Dark viscous liquid was first observed at this step, then further purification was done through crystallization using Et_2O at -4°C. White crystals form overnight. The Et_2O decanted was further subjected to crystallization, and this is repeated until no crystals were observed (approx. 3 times). The crystals were collected using suction filtration. NMR indicated mixture. Rfs in TLC were inseparably close. ^{1}H-NMR (400 MHz, $CDCl_3$, δ) for β-propargyl glucoside: 5.27 (t, 1H), 5.14-5.12 (t, 1H), 5.04 (t, 1H), 4.81 (d, 1H), 4.39 (d, 2H), 4.28 (dd, 1H), 4.19-4.13 (dd, 1H), 3.77 (d, 1H), 2.49 (s, 1H), 2.48 (s, 3H), 2.12 (s, 3H), 2.08 (s, 3H), 2.06 (s, 3H), 2.04 (s, 3H) ppm. . FT-IR (KBr, pellet, $\nu_{max}(cm^{-1})$): 3250 cm^{-1} (-C≡C-H).

2.3.6. Synthesis of 1,2,3,4,6-Penta-O-acetyl-D-mannopyranose (S3)

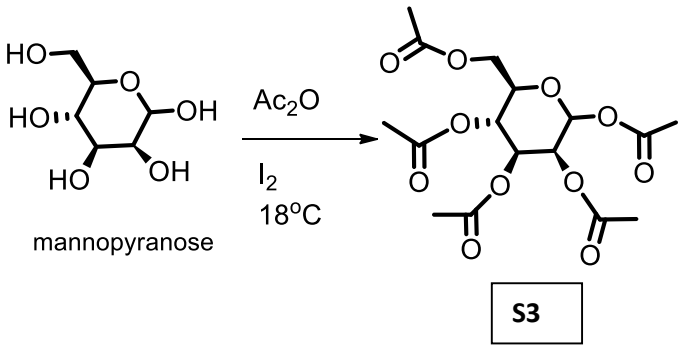

S3

The procedure of synthesis and workup of 1,2,3,4,6-Penta-O-acetyl-D-glucopyranose (see section 2.3.4) was applied to the stereoisomer D-mannose using the same amounts of reagents, and the same yield was obtained. ^{1}H-NMR (400 MHz, $CDCl_3$, δ): for α 6.11 (d, 1H), 5.38 (d, 1H), 5.29 (d, 1H), 5.18 (d, 1H), 4.33 (t, 2H), 3.83 (m, 1H), 2.13 (s, 3H), 2.11 (s, 3H), 2.08 (s, 3H), 2.04 (s, 3H), 2.03 (s, 3H) ppm. {for β, 5.89 (d, 1H), 5.51 (d, 1H), 5.32 (d, 1H), 5.14 (d, 1H), 4.29 (t, 2H), 4.10-4.07 (br, 1H), 2.25 (s, 3H), 2.23 (s, 3H), 2.21 (s, 3H), 2.20 (s, 3H), 2.19 (s, 3H) ppm.}

2.3.7. Synthesis of 2,3,4,6-Tetra-O-acetyl-O-prop-1-yl- α - D-mannopyranoside (S4)

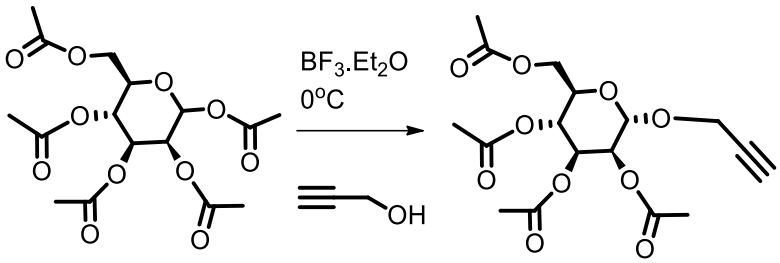

S4

The procedure of synthesis and workup of 2,3,4,6-Tetra-O-acetyl-O-prop-1-yl-β-D-glucopyranoside (see section 2.3.5) was applied to the stereoisomer 1,2,3,4,6-Penta-O-acetyl-D-mannopyranose (S3) using the same amounts of reagents. The crystallization was much more efficient for 2,3,4,6-Tetra-O-acetyl-O-prop-1-yl-α-D-mannopyranoside. Pure product was obtained, confirmed by NMR. Yield= 12.4g, 70%. ^{1}H-NMR (400 MHz, $CDCl_3$, δ): 5.36 (dd, 1H) , 5.35(dd, 1H), 5.30 (dd, 1H), 5.05 (d, 1H), 4.30 (m, 2H), 4.15(dd, 1H), 4.12 (dd, 1H), 4.06 (m, 1H), 2.50 (t, 1H), 2.18 (s, 3H), 2.12 (s, 3H), 2.06 (s, 3H), 2.01(s, 3H).

2.3.8. Synthesis of (2,5-dibromothiophen-3-yl)ethyl)-prop-1,2,3-triazol-4-yl-tetra-O-acetyl β-D-glucopyranoside (M4)

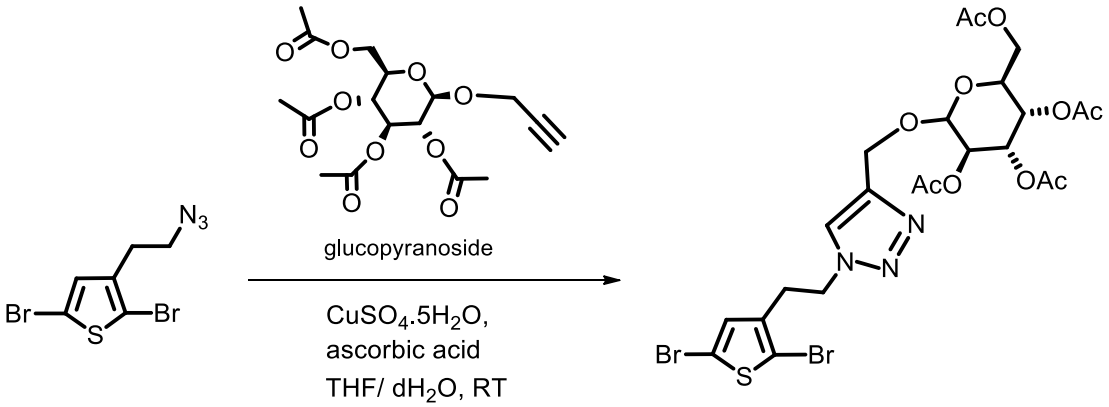

M4

THF and ddH_2O were seperately degassed before the reaction. 3-(2-azidoethyl)-2,5-dibromothiophene (M3) (1.8g, 5.8mmol) was put into a 25mL round bottom flask and dissolved in 10mL degassed THF. 2,3,4,6-Tetra-O-acetyl-O-prop-1-yl-β- D-glucopyranoside (S2) (2.9g, 7.6mmol) was added and stirred for 10 min until completely dissolved. Aqueous

solutions of $CuSO_4.5H_2O$ (0.15g, 0.58mmol) and sodium ascorbate (0.23g, 1.16mmol) were prepared seperately using 1mL degassed ddH2O each. First the $CuSO_4$ solution, then ascorbate solution was added into the reaction mixture slowly with a pipette, while stirring. The reaction was stirred at 50°C for 2 days. The workup was done by first evaporating the solvent in a one neck round bottom flask under reduced pressure, washed with water by decanting, then drying again. The crude material was dissolved in toluene. The solution was filtrated over silica using suction filtration. The collected solution was concentrated under reduced pressure, then silica packed column chromatography was done using 7:3 Hexane:EtOAc elution. The only spot active both under UV light and *p*-Anisaldehyde staining was checked in TLC. Unfunctionalized penta-acetylated glucopyranose species were eliminated. TLC Rf= 0.21(M4), Rf= 0.59 (S1) using 1:1 Hexane:EtOAc mobile phase. Pure white crystalline product was obtained. Yield: 2.0g, 50%. ^{1}H-NMR (400 MHz, $CDCl_3$, δ): 7.35 (s, 1H), 6.61 (s, 1H), 5.10 (t, 1H), 5.00 (t, 1H), 4.91 (t, 1H), 4.81- 4.71 (dd, 2H), 4.57(d, 1H), 4.44 (t, 2H), 4.16- 4.06 (dd, 2H), 3.67 (d, 1H), 3.05(t, 2H), 1.97 (s, 3H), 1.92 (s, 3H), 1.88 (s, 3H), 1.87(s, 3H) ppm. ^{13}C-NMR (100 MHz, $CDCl_3$, δ): 169.30, 169.17, 143.97, 137.40, 130.64, 123.08, 111.41, 110.23, 99.61, 72.67, 71.78, 71.13, 68.30, 61.75, 49.30, 30.28, 20.66, 20.57 ppm.

2.3.9. Synthesis of 2,5-thiophenediboronic ester (M5)

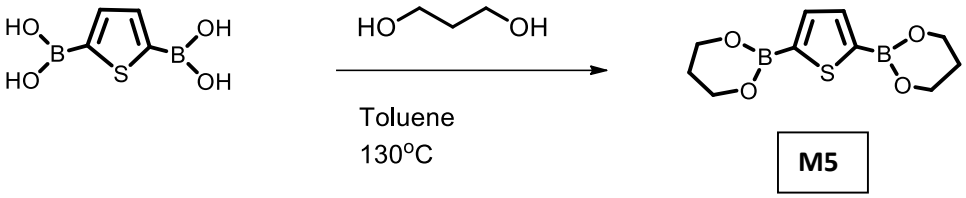

2g of 2,5-thiophenebiboronic acid (11.6 mmol) was dissolved in 25mL toluene in 50mL two-neck round bottom flask, and stirred for 10 minutes in room temperature. Then, 2mL of 1,3-propanediol (27.8 mmol) was added dropwise. The mixture was heated to 130°C and refluxed overnight. The solvent was then evaporated in a one neck round bottom flask under reduced pressure. Pinkish white crystalline residues were observed. Purification was done by washing with EtOH, then n-Hexane, using suction filtration. White crystalline product was obtained. Yield= 1.90 g, 65%. ^{1}H-NMR (400Hz, $CDCl_3$, 25 ^{o}C) δ: 7.57 (s,2H), 4.17 (t, 8H), 2.08 (m, 4H). ^{13}C-NMR (100Hz, $CDCl_3$, 25 ^{o}C) δ: 136.03, 62.10, 27.41 ppm

2.3.10. Synthesis of Cucurbit[7]uril (M6)

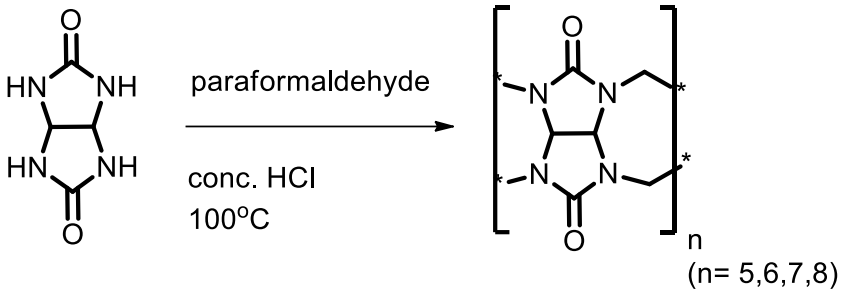

M6: n=7

Glycoluril (20.0g, 141mmol) and paraformaldehyde (11.8g, 19.6mmol) were put into 250mL two neck round bottom flask, and 45mL of conc. HCl was added. Initially the components formed a clump and did not disperse.The flask was put in pre-heated 100°C oil bath and refluxed by stirring overnight. Before the workup, the reaction mixture was kept still in RT to cool and slowly crystallize for 3 days. The work-up was done by first filtrating the acidic supernatant was decanted and filtrated using suction filtration. The clear supernatant was precipitated into 500mL MeOH in a beaker. White precipitate was collected using suction filtration, and redispersed in 500mL MeOH and filtrated again for two times. The white precipitate at this step consists mostly of CB5 and CB7 species. CB7 was further purified by dispersing the dried mixture in 150mL 20% aqueous glycerol solution in a 250mL one neck round bottom flask and refluxing for 2 hrs vigorously stirring and heating upto boiling (approx. 90°C). The hot solution was filtrated using suction filtration. The collected precipitate was redispersed in 500mL MeOH and filtrated again for three times to wash glycerol residues. The precipitate was filtrated and dried. Sephadex filtration was applied by loading sephadex gel, then the CB in minimum amount of water. NMR shows pure CB7. Yield: 1.28 g, 5.46%. ^{1}H-NMR (400 MHz, D_2O, δ): 5.73 (d, 14H), 5.45 (s, 14H), 4.18 (d, 14H) ppm.

2.3.11. Synthesis of poly[(3- triazol-β-D-glucopyranosyl-thiophene)-co-(2,5-thiophene)] (P1)

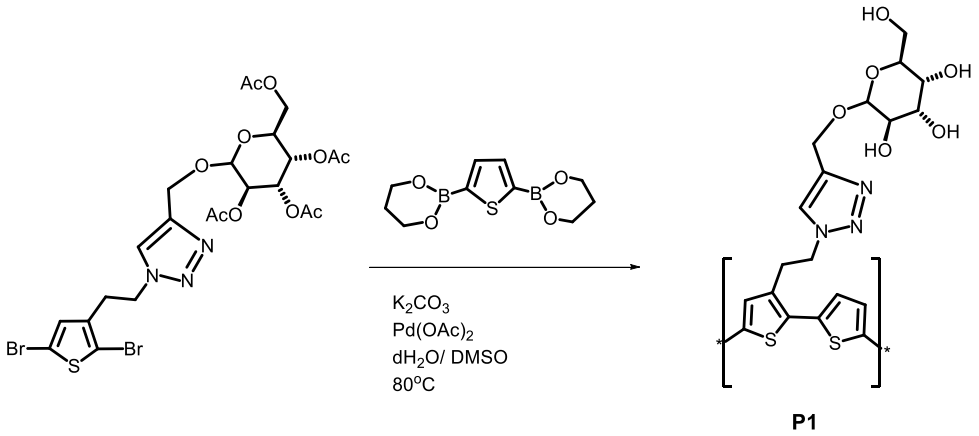

DMSO and dH_2O were seperately degassed before the reaction. (2,5-dibromothiophen-3-yl)ethyl)-prop-1,2,3-triazol-4-yl-tetra-O-acetyl β-D-glucopyranoside (M4) (341.0mg, 0.49mmol) and 2,5-thiophenediboronic ester (M5) (123.5mg, 0.49mmol) were dissolved in 10mL degassed DMSO. The mixture was briefly subjected to high vacuum, then heated and stirred at 40°C. K_2CO_3 (340mg, 2.45mmol) was separately dissolved in 5mL dH_2O, and added to the reaction mixture. Then, $Pd(OAc)_2$ (5.5mg, 0.025mmol) was added. The reaction mixture was heated to 80°C overnight under nitrogen. The DMSO-water mixture was evaporated using vacuum distillation set-up under high vacuum. The dried reaction mixture was dissolved in minimum amount of water and Sephadex filtration was applied by loading sephadex gel, then the aqueous mixture. Dialysis was done for 2 days using 3000mpore dialysis bags. The dark brown eluent was dried under reduced pressure. Blackish shiny crystalline product was collected. Yield: 26.4mg, 9%. (See ^{1}H-NMR spectra Figure 3.9)

2.3.12. Synthesis of poly[(3- triazol-β-D-glucopyranosyl-thiophene)-co-(2,5-thiophene)] with Cucurbit[7]uril (P2)

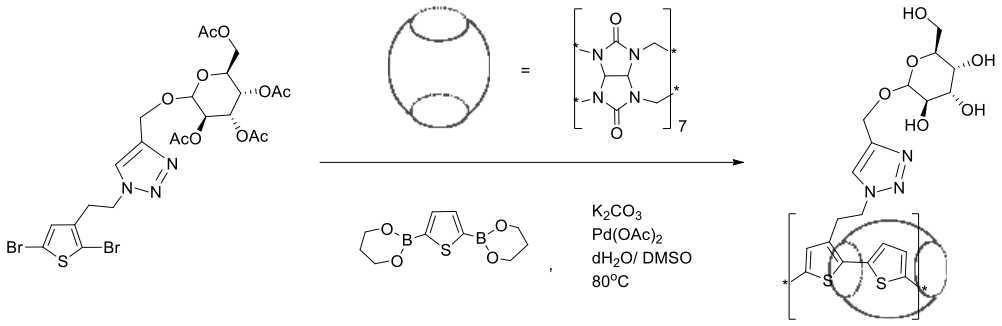

P2

2,5-thiophenediboronic ester (M5) (113.4mg, 0.45mmol) and cucurbit[7]uril (M6) (523.3mg, 0.45mmol) were initially dissolved in 20mL degassed dH_2O under nitrogen, and stirred at 50°C overnight for complexation. (2,5-dibromothiophen-3-yl)ethyl)-prop-1,2,3-triazol-4-yl-tetra-O-acetyl β-D-glucopyranoside (M4) (315.0mg, 0.45mmol) was added in 10mL of degassed DMSO. Freeze-pump-thaw was applied and nitrogen was fed. The reaction was heated back to 50°C and briefly sonicated. K_2CO_3 (311.0mg, 2.25mmol) was separately dissolved in 5mL dH_2O, and added to the reaction mixture. Then, $Pd(OAc)_2$ (5.1mg, 0.023mmol) was added. The reaction mixture was heated to 80°C under nitrogen for 6 days. The reaction mixture appeared creamy brown, with a yellowish glow. Creamy brown precipitation occured upon cooling. Yellowish supernatant was filtrated and solid was dried using vacuum. Dialysis was done for 2 days using 3000mpore dialysis bags. Reddish creamy brown product was collected NMR scale upon drying. (See ^{1}H-NMR spectra Figure 3.9)

2.3.13. Synthesis of 4,7-bis((E)-2-(9,9-bis(3- triazol- tetra-O-acetyl- α – D-mannopyranosyl)-9H-fluoren-2-yl)vinyl)benzo[c][1,2,5]thiadiazole (O1)

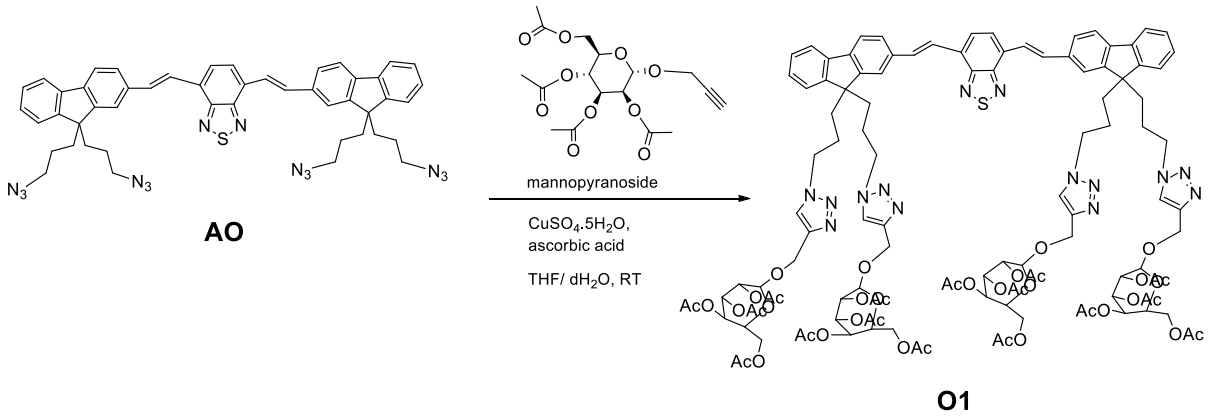

THF and ddH$_2$O were separately degassed before the reaction. 4,7-bis((E)-2-(9,9-bis(3-azidopropyl)-9H-fluoren-2-yl)vinyl)benzo[c][1,2,5]thiadiazole (AO) (52.0mg, 60.0µmol) and 2,3,4,6-Tetra-O-acetyl-O-prop-1-yl- α -D-mannopyranoside (S4) (92.7mg, 240µmol) was put in 7mL degassed THF into a 25mL round bottom flask and stirred for 10 min until completely dissolved. Aqueous solutions of $CuSO_4.5H_2O$ (6.00mg, 24.0 µmol) and sodium ascorbate (9.51mg, 48.0µmol) were prepared seperately using 1mL degassed ddH2O each. First the $CuSO_4$ solution, then ascorbate solution was added into the reaction mixture slowly with a pipette, while stirring. The reaction was stirred at 50°C for 2 days. The workup was done by first evaporating the solvent in a one neck round bottom flask under reduced pressure, washed with water by decanting, then drying again. One spot active both under UV light and *p*-Anisaldehyde staining was appearing on TLC. Pure red crystalline product was obtained. Yield= 94.8g, 66% ^{1}H-NMR (400 MHz, $CDCl_3$, δ): 8.17 -8.13 (dd, 4H), 7.82- 7.71 (m, 14H), 7.62- 7.54 (dd, 2H), 7.42- 7.37 (dd, 4H), 5.36 (dd, 4x1H) , 5.21(d, 4x1H), 4.92-4.89 (t, 4x1H), 4.81- 4.78 (dd, 4x2H), 4.64- 4.61(t, 4x1H), 4.37 (t, 4x2H), 4.31 (t, 4x2H), 3.77 (t, 1H), 3.02 (t, 1H), 2.52 (t, 1H), 2.19 (s, 4x3H), 2.15 (s, 4x3H), 2.07 (s, 4x3H), 2.04 (s, 4x3H), 1.64 (br, 4x2H), 1.28 (br, 4x2H) ppm.

2.3.14. Synthesis of 4,7-bis((E)-2-(9,9-bis(3- triazol- α – D- mannospyranosyl)-9H-fluoren-2-yl)vinyl)benzo[c][1,2,5]thiadiazole (O2)

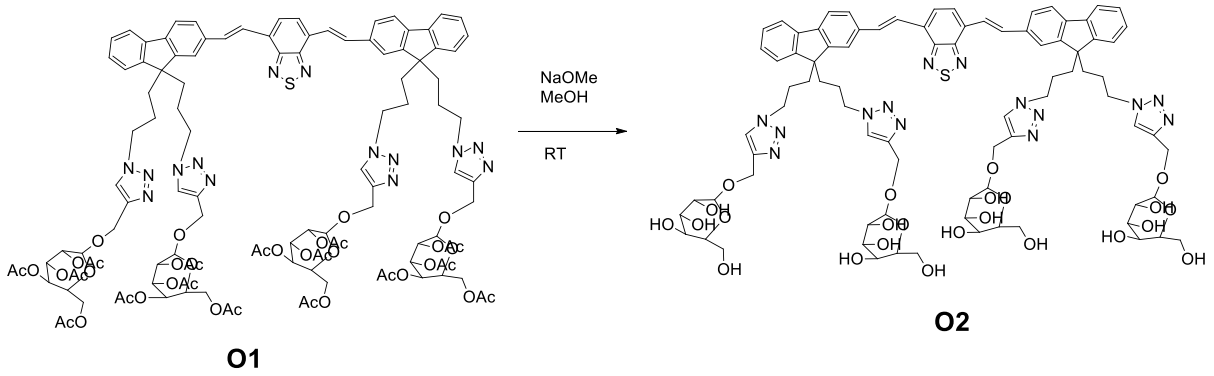

Synthesis 2.3.13 was repeated with 100mg 4,7-bis((E)-2-(9,9-bis(3-azidopropyl)-9H-fluoren-2-yl)vinyl)benzo[c][1,2,5]thiadiazole (AO) (118µmol), 2,3,4,6-Tetra-O-acetyl-O-prop-1-yl- α -D-mannopyranoside (S4) (182mg, 471µmol), $CuSO_4.5H_2O$ (12.4mg, 47.1 µmol) and sodium ascorbate (17.8mg, 94.2µmol). Zemplen deacetylation was applied: Dried Tetra- 2,3,4,6-tetra-O-acetyl- α – D- mannopyranosyl Red Oligomer (O1) was dissolved in 30mL MeOH. NaOMe (20.4mg, 378µmol) was added to the mixture with 1 mL of MeOH, and stirred for 2 hrs at 35°C. Yield= 198mg, 67% ^{1}H-NMR (400 MHz, d-DMSO, δ): 8.51 (s, 4H), 8.24-8.20 (dd, 4H), 8.02- 7.76 (m, 14H), 7.36 (d, 2H), 5.02 (m, 4x1H), 4.96 (dd, 4x1H), 4.81 (d, 4x1H), 4.70-4.58 (dd, 4x2H), 4.12 (d, 4x2H), 3.08 (d, 4x2H), 2.08- 1.91(br, residual -OAc), 1.24 (d, 4x2H), 1.08(br, 4x4H (OH)), 0.90(br, 4x2H) ppm.

2.3.15. Synthesis of 4,7-bis((E)-2-(9,9-bis(di-(3- triazol- tetra-O-acetyl- α – D-mannopyranosyl))- (di-(3-azidopropyl))-9H-fluoren-2-yl)vinyl)benzo[c][1,2,5]thiadiazole (O3)

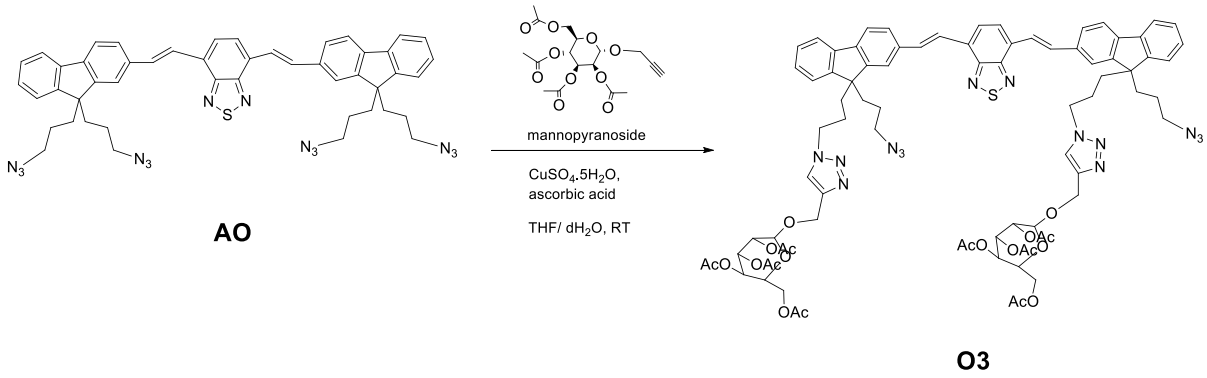

AO **O3**

Synthesis 2.3.13 was repeated with 100mg 4,7-bis((E)-2-(9,9-bis(3-azidopropyl)-9H-fluoren-2-yl)vinyl)benzo[c][1,2,5]thiadiazole (AO) (118µmol), 2,3,4,6-Tetra-O-acetyl-O-prop-1-yl- α -D-mannopyranoside (S4) (91.1mg, 236µmol), $CuSO_4.5H_2O$ (5.90mg, 23.6 µmol) and sodium ascorbate (9.35mg, 47.2µmol). Dried reaction mixture was dissolved in 6mL MeOH. NaOMe (10.2mg, 189µmol) was added to the mixture with 4 mL of MeOH, and stirred for 30min at RT. The mixture was centrifugated, supernatant was discarded. The mixture was treated with MeOH once again, centrifugated, and decanted. The dark red precipitate was collected and dried. Yield= 70mg, 34%. ^{1}H-NMR (400 MHz, $CDCl_3$, δ): 8.64 (d, 2H), 8.53 (dd, 2H), 8.22-7.98 (t, 2H), 7.78-7.42 (m, 14H), 5.31-5.23(dd, 2x1H), 4.93 (t, 2x1H), 4.79 (t, 2x1H), 4.65 (t, 2x1H), 4.30 (dd, 2x1H), 4.11 (dd, 2x2H), 3.07 (t, 2x2H), 2.19(s, 4x3H), 2.15(s, 4x3H), 2.11(s, 4x3H), 2.04(s, 4x3H), 1.69 (br, 4x2H), 1.33 (d, 2x2H), 1.12 (d, 2x2H), 0.90 (br, 2x2H) ppm. TOF-MS: $[M+H]^+$ m/z: 1621.62250

Chapter 3 RESULTS AND DISCUSSION

This chapter contains two parts. The first part (section 3.1) includes the synthesis and characterization of thiophene-based materials, namely thiophene and glucoside precursors, gluco-thiophene monomer, and the pre-functionalized polymer and polyrotaxane. The second part (section 3.2) includes the work done on the red-emitting oligomer, limited and full post-functionalizations using mannosides, and nanoparticle formation.

3.1 Section 1: Synthesis of Thiophene-based monomers, polymer and polyrotaxane

The aim of the project was to synthesize water soluble, CB-threaded thiophene-based conjugated polymers. Initially, we have attempted to synthesize the following cationic polymer and polyrotaxane (Figure 3.1a).

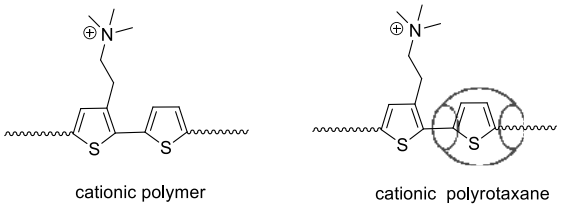

Figure 3.1a Initial design for water soluble, CB-threaded thiophene-based conjugated polymers.

The cationic group was eliminated in the Suzuki reaction conditions and an insoluble product (Figure 3.1b) was obtained instead.

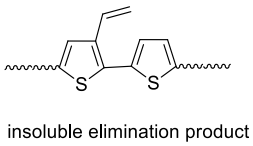

Figure 3.1b Elimination product in basic and heated Suzuki conditions.

The next attempt to prepare water soluble, CB-threaded thiophene-based conjugated polymers the following structures were designed (Figure 3.1c):

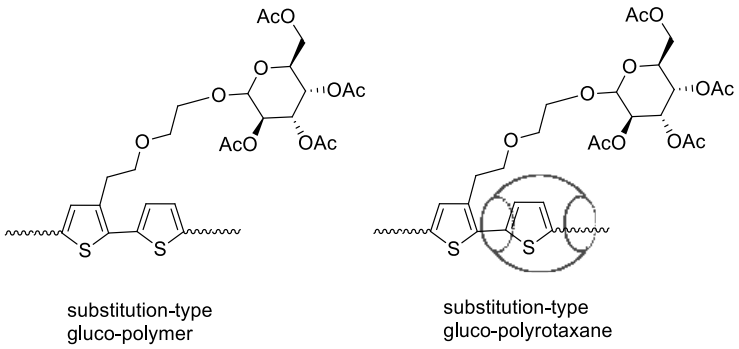

Figure 3.1c Initial design for the gluco-substituted alternative.

The monomer was designed to be obtained through S_N2 substitution reaction between a bromoethyl glucoside and hydroxyl-functional thiophene in basic conditions. However, the oxygen ended up attacking an acetyl group of the sugar, possibly from C2 position, to yield acetyl-functionalized thiophene (Figure 3.1d) instead of glucoside.

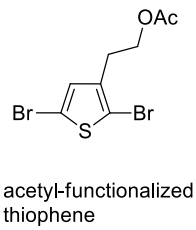

Figure 3.1d Acetylated product in S_N2 conditions.

In the last attempt, following structures (Figure 3.1e) were designed to use a milder chemistry, namely ‘click’, to obtain glucosides:

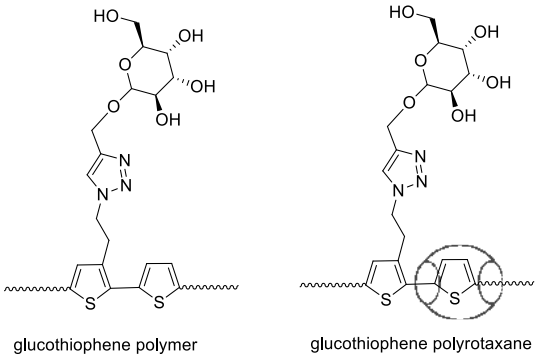

Figure 3.1e New design for the soluble CB-threaded polythiophenes using click chemistry.

In order to synthesize these target polymers and polyrotaxanes, first the required monomers were synthesized by following the reaction schemes (Scheme 3.1):

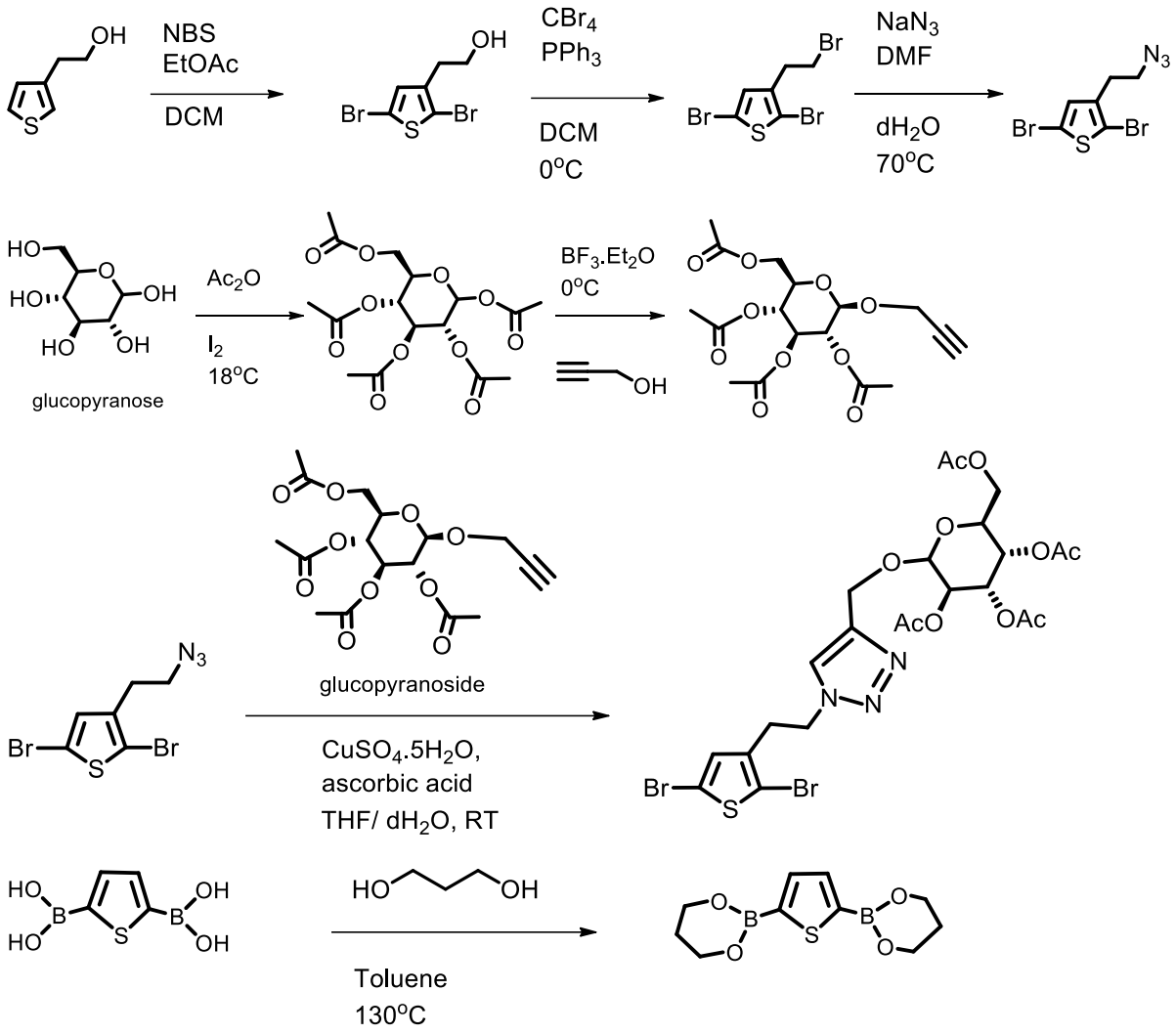

Scheme 3.1 Synthetic pathway of monomers.

After obtaining the functionalized monomer, pre-functionalized polyrotaxane can be carried out in aqueous conditions, allowing CB7 encapsulation (Scheme 3.3). To have a parallel assesment, the pre-functionalized polymer was synthesized similarly without CB7 (Scheme 3.2).

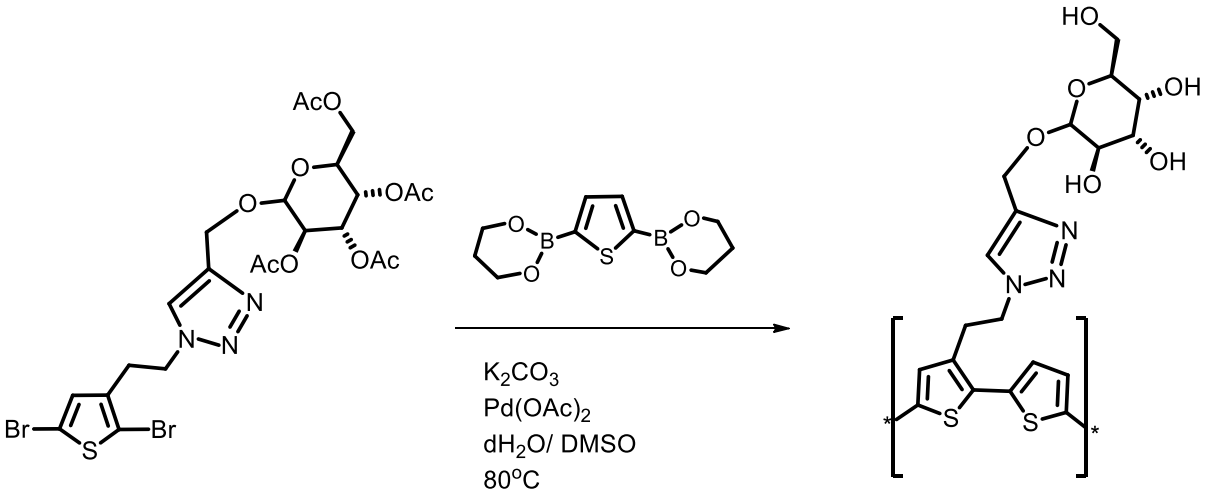

Scheme 3.2 Synthetic pathway of glucothiophene polymer.

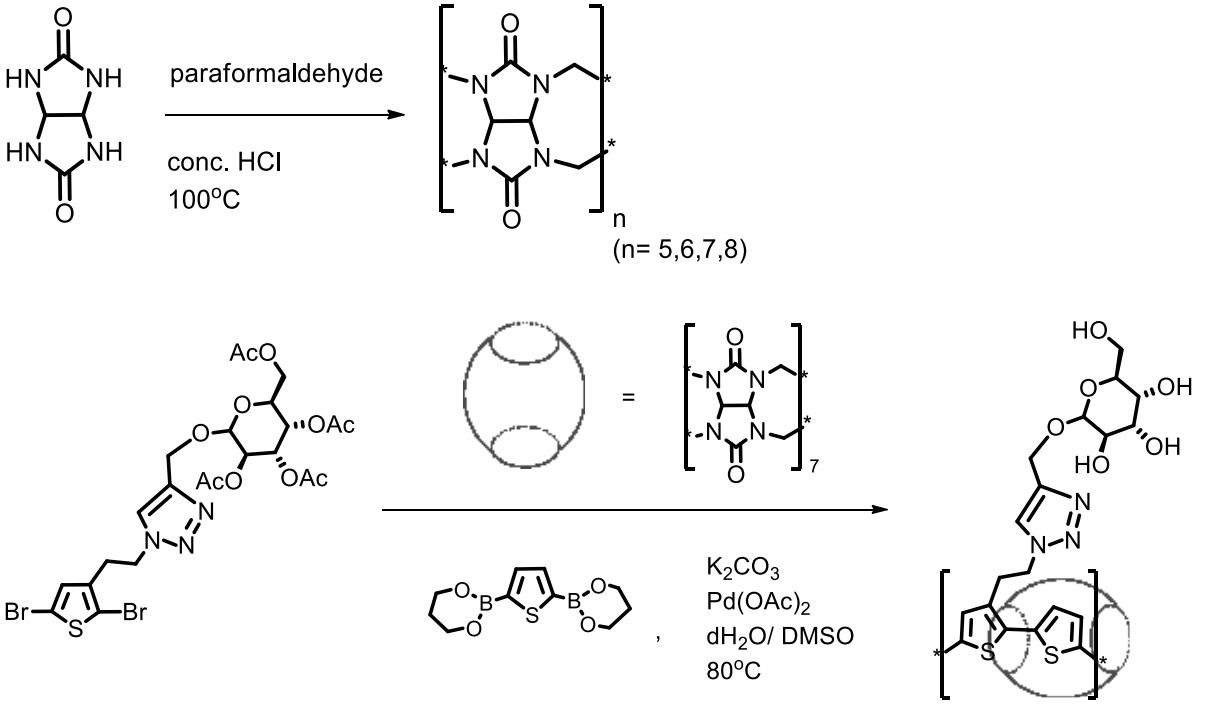

Scheme 3.3 Synthetic pathway of glucothiophene polyrotaxane.

3.1.1. Synthesis and Characterization of 2-(2,5-dibromothiophen-3-yl)ethanol (M1)

2-(2,5-dibromothiophen-3-yl)ethanol (M1) was synthesized from 2-(thiophene-3-yl)ethanol through electrophilic substitution using N-bromosuccinimide (NBS). The tendency for electrophilic substitutions to occur at the alpha-positions was previously discussed (section 1.1.1. Figure 1.5b).The mechanism of this reaction is shown in Scheme 3.4. M1 was characterized by ^{1}H-NMR spectroscopy (Figure 3.2a).

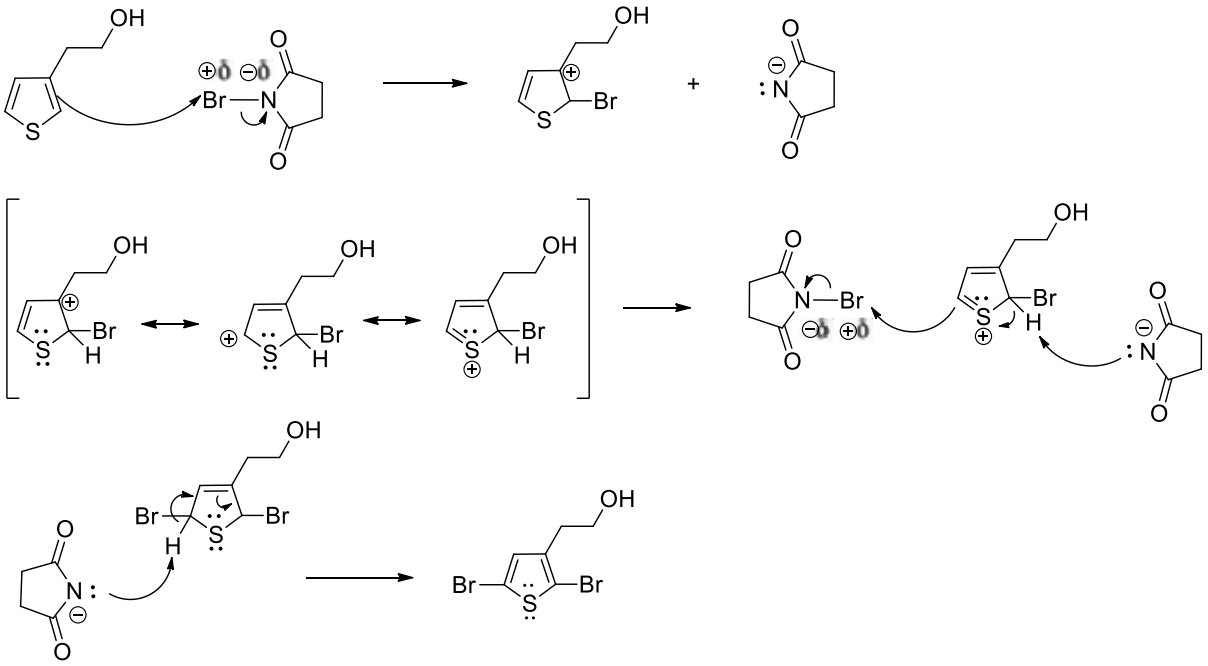

Scheme 3.4. Synthesis mechanism of M1.

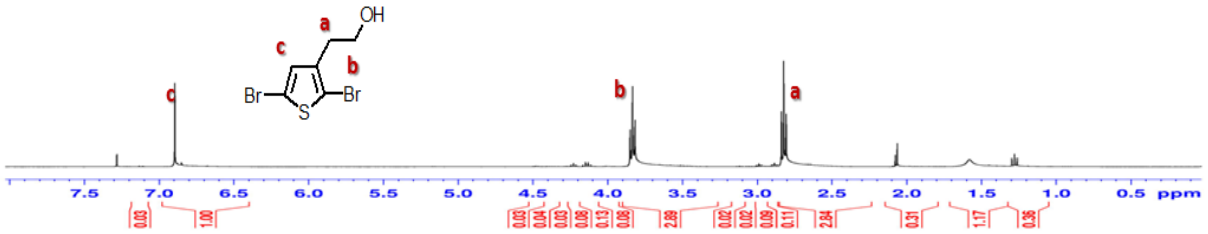

Figure 3.2a. ^{1}H-NMR (400Hz, $CDCl_3$, 25°C) spectrum of M1.

In the ^{1}H-NMR spectrum of M1, the triplet at at 3.84 ppm is due to the -CH_2 protons deshielded by the hydroxyl group, and the latter at 2.82 ppm belong to the adjacent –CH_2 protons. Singlet at 1.58 ppm is due to the hydroxyl proton, and the only proton on the aromatic thiophene signal comes as a singlet at 6.90 ppm. The hydroxyl functionality was confirmed using FT-IR with the characteristic broad O-H stretch around 3300 cm^{-1} (Figure 3.2b).

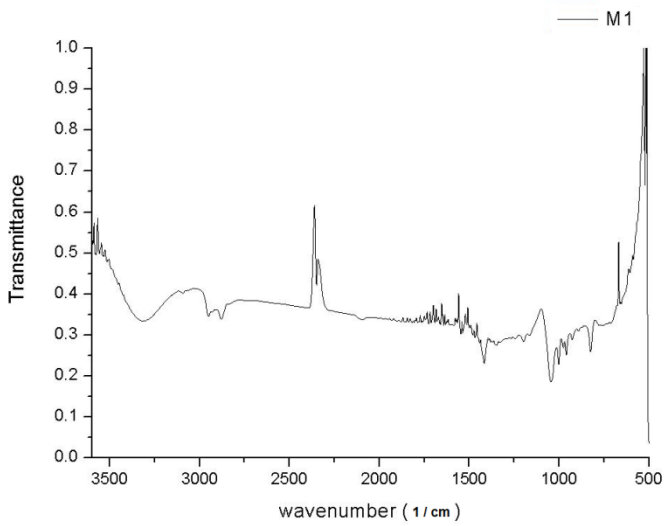

Figure 3.2b FT-IR spectrum of M1.

3.1.2. Synthesis and Characterization of 2,5-dibromo-3-(2-bromoethyl)thiophene (M2)

2,5-dibromo-3-(2-bromoethyl)thiophene (M2) was synthesized from 2-(2,5-dibromothiophen-3-yl)ethanol (M1) through Appel Reaction using carbontetrabromide as bromination source. The mechanism of this reaction is shown in Scheme 3.5. M2 was characterized by ^{1}H-NMR spectroscopy (Figure 3.3a).

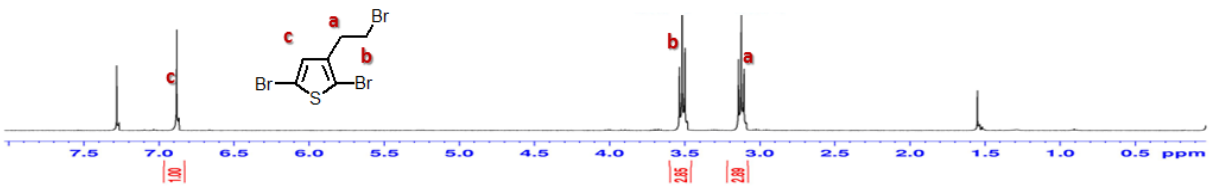

Figure 3.3a. ^{1}H-NMR (400Hz, $CDCl_3$, 25°C) spectrum of M2.

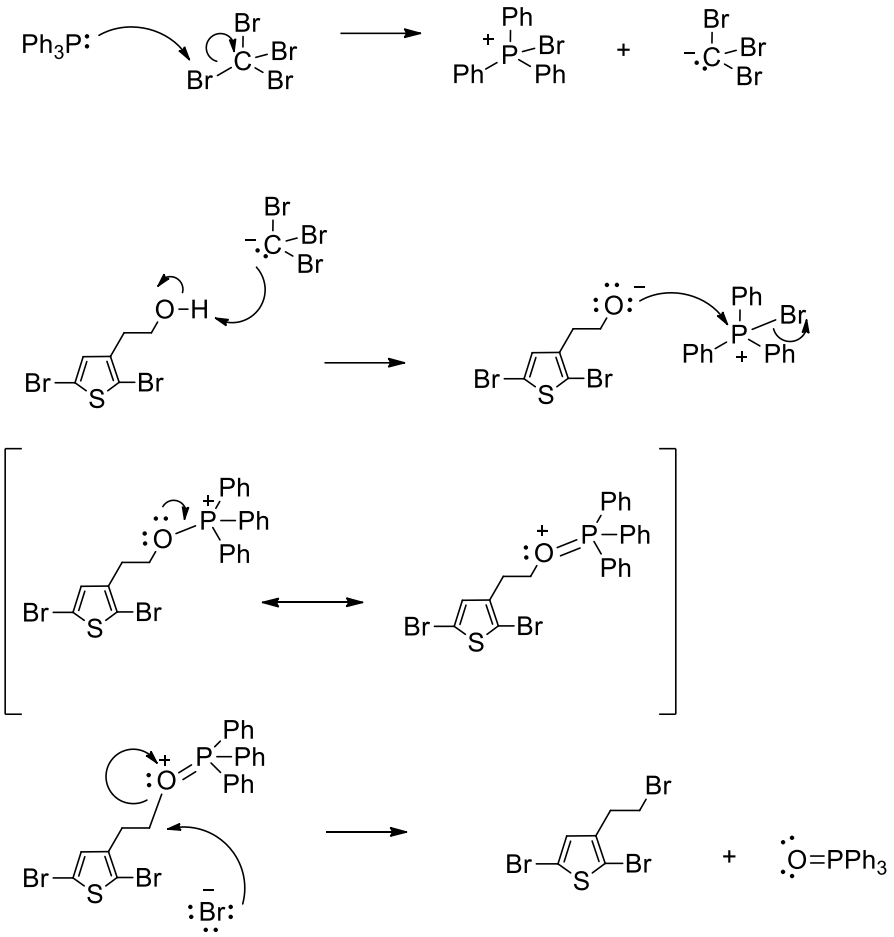

Scheme 3.5. Synthesis mechanism of M2.

In the ^{1}H-NMR spectrum of M2, the triplet at at 3.52 ppm is due to the -CH_2 protons deshielded by the bromide, and the latter at 3.12 ppm belong to the adjacent –CH_2 protons. The only proton on the aromatic thiophene signal comes as a singlet at 6.88 ppm. The residual peak around 1.5ppm doesn't reflect precursor M1 due to the lack of 3.84ppm triplet and is probably moisture-related. The FT-IR spectra of M2 confirms the disappearance of the precursor's strong and broad O-H stretch around 3300 cm^{-1} (Figure 3.2b).

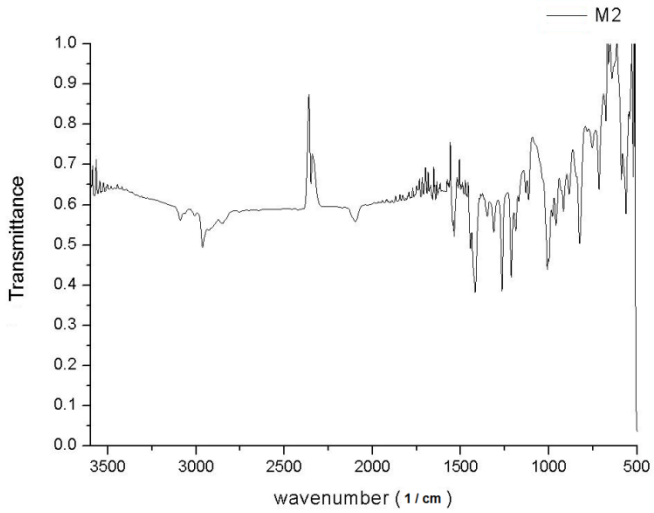

Figure 3.3b FT-IR spectrum of M2.

3.1.3. Synthesis and Characterization of 3-(2-azidoethyl)-2,5-dibromothiophene (M3)

3-(2-azidoethyl)-2,5-dibromothiophene (M3) was synthesized from 2,5-dibromo-3-(2-bromoethyl)thiophene (M2) through nucleophilic substitution with bromine leaving group. The mechanism of this reaction is shown in Scheme 3.6. M2 was characterized by ^{1}H-NMR spectroscopy (Figure 3.4a).

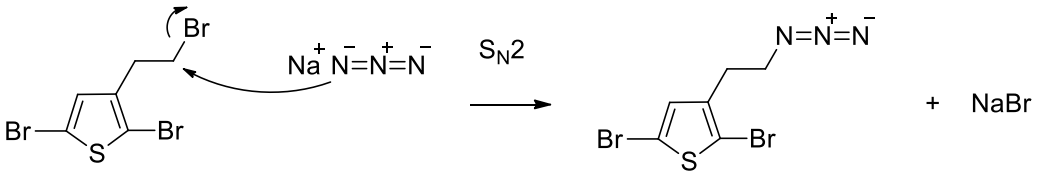

Scheme 3.6. Synthesis mechanism of M3.

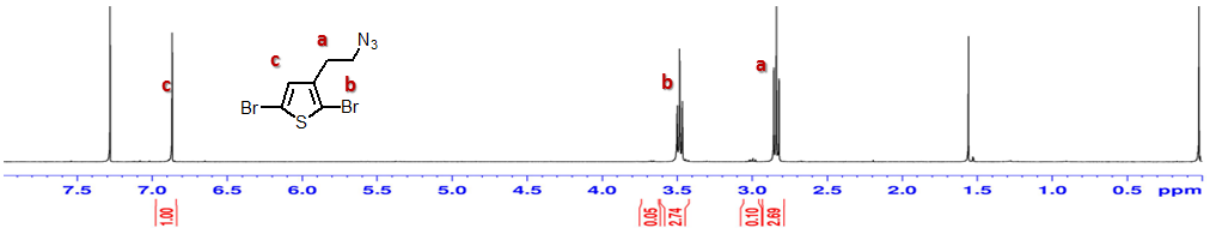

Figure 3.4a. ^{1}H-NMR (400Hz, $CDCl_3$, 25°C) spectrum of M3.

In the ^{1}H-NMR spectrum of M3, the triplet at at 3.78 ppm is due to the -CH_2 protons near azide, and the latter at 2.84 ppm belong to the adjacent –CH_2 protons. The only proton on the aromatic thiophene signal comes as a singlet at 6.87 ppm. The FT-IR spectra of M3 confirms azide functionality with signiture peak around 2100 cm^{-1} (Figure 3.3b).

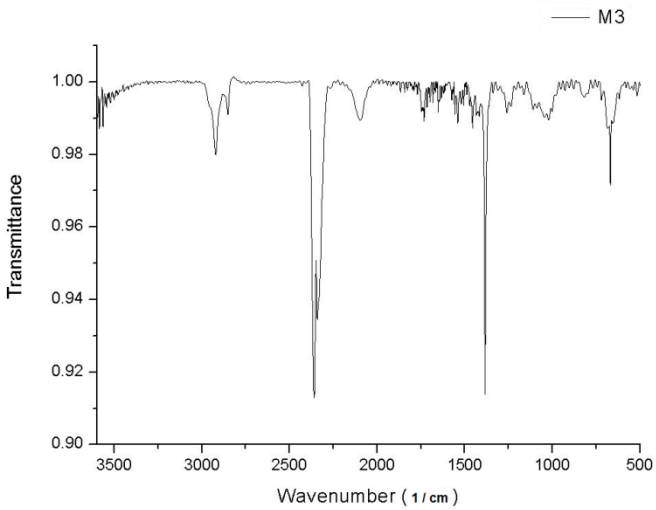

Figure 3.4b FT-IR spectrum of M3.

3.1.4. Synthesis and Characterization of 1,2,3,4,6-Penta-O-acetyl-D-glucopyranose (S1)

1,2,3,4,6-Penta-O-acetyl-D-glucopyranose (S1) was synthesized from D-glucopyranose through iodine-promoted acetylation with Ac_2O. A plausible mechanism for how iodine catalysis works is shown in Scheme 3.7. The iodine species were reduced using cold thiosulfate solution after the reaction, then evolving tetrathionate ions were converted presumably to bisulfate ions using bicarbonate, resulting in CO_2 bubbling off. S1 was characterized by ^{1}H-NMR spectroscopy (Figure 3.5a).

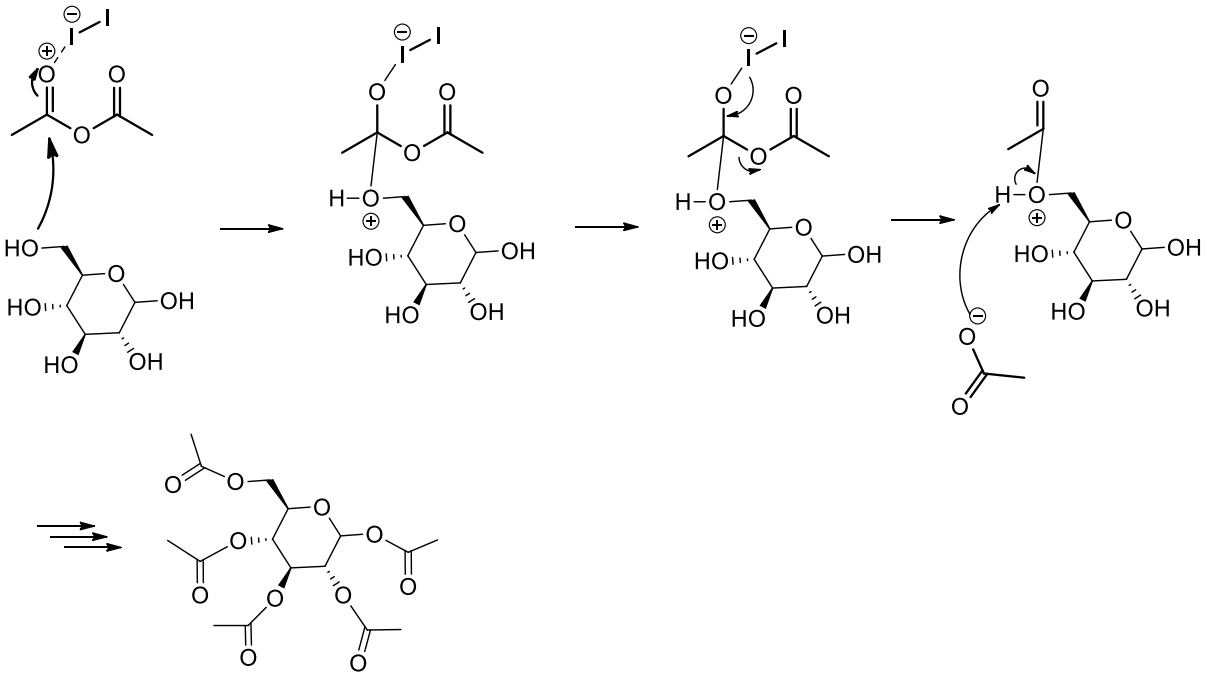

Scheme 3.7. Synthesis mechanism of S1.

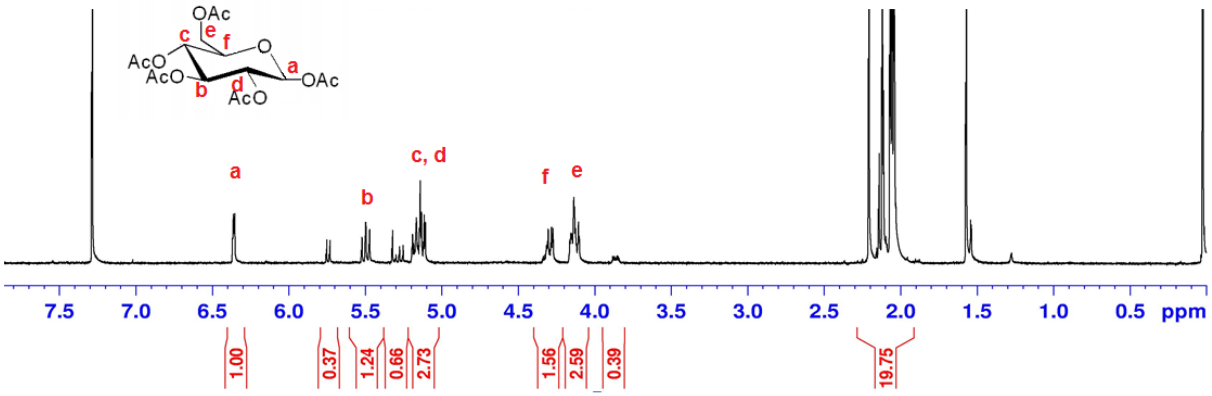

Figure 3.5a. ¹H-NMR (400Hz, $CDCl_3$, 25°C) spectrum of S1.

In the ¹H-NMR spectrum of S1, anomeric (acetal) hydrogen strongly deshielded comes at 6.36 ppm. The two seperate hydrogens (c,d) comes similar together almost like a multiplet around 5.19-5.11ppm due to the chair conformation of glucose providing them with similar environments, values agree with literature.[123] The hydrogens of acetyl groups comes as crowded group of singlets around 2ppm (section 2.3.4) The unlabeled residual peaks for α-glucopyranose all become β- upon functionalization (S2) as previously discussed (section 1.4.1.2. Figure 1.28). The FT-IR spectra of S1 confirms ester carbonyl stretches around 1750 cm^{-1} and C-O stretches around 1250 cm^{-1} (Figure 3.5b).

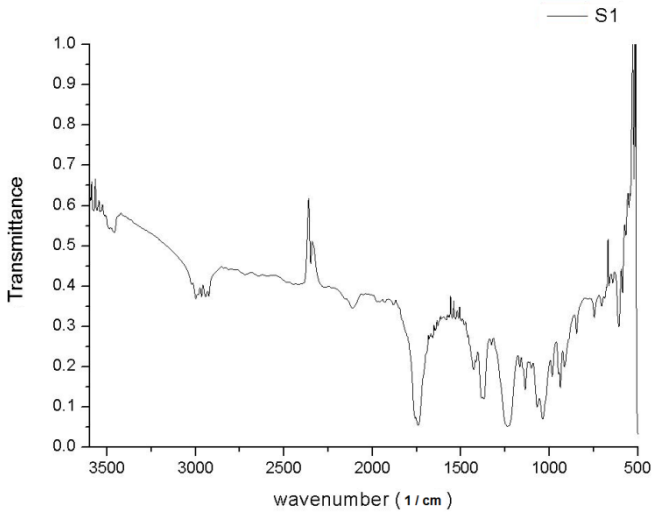

Figure 3.5b FT-IR spectrum of S1.

3.1.5. Synthesis and Characterization of 2,3,4,6-Tetra-O-acetyl-O-prop-1-yl-β- D-glucopyranoside (S2)

2,3,4,6-Tetra-O-acetyl-O-prop-1-yl-β- D-glucopyranoside (S2) was synthesized from 1,2,3,4,6-Penta-O-acetyl-D-glucopyranose (S1) through borontrifluoride-activated propargyl alcohol functionalization. The reaction mechanism of this activated glucoside synthesis was previously discussed (section 1.4.1.2. Figure 1.28). S2 was characterized by ^{1}H-NMR spectroscopy (Figure 3.6a).

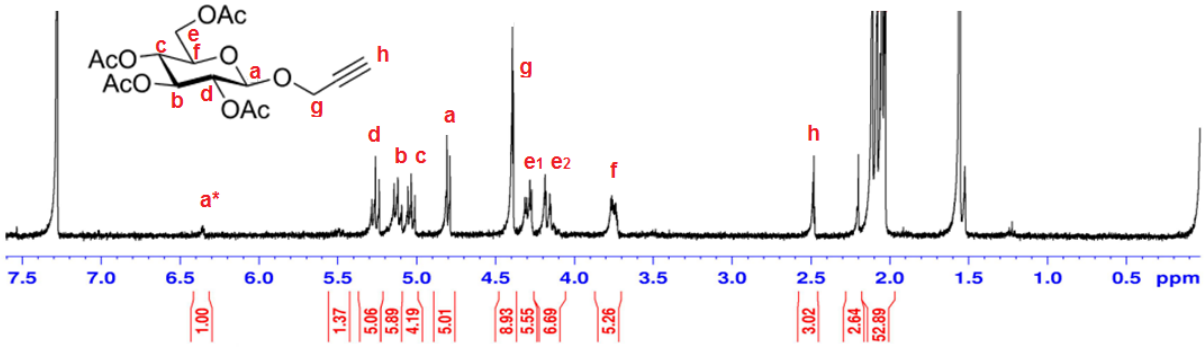

Figure 3.6a. ^{1}H-NMR (400Hz, $CDCl_3$, 25°C) spectrum of S2.

In the ^{1}H-NMR spectrum of S2, anomeric hydrogen comes at 4.81ppm showing a drastic upfield shift upon functionalization with propargyl group (compared to starting a*) values agree with literature [91 SI], replacing the highly electronegative acetyl group. The integrations show 1:5 impurity from starting material S1 upon crystallization. The FT-IR spectra of S2 confirms strong and narrow terminal alkyne hydrogen stretch around 3250 cm^{-1} (Figure 3.5b). For the synthesis of M4, S2 was thus used in excess.

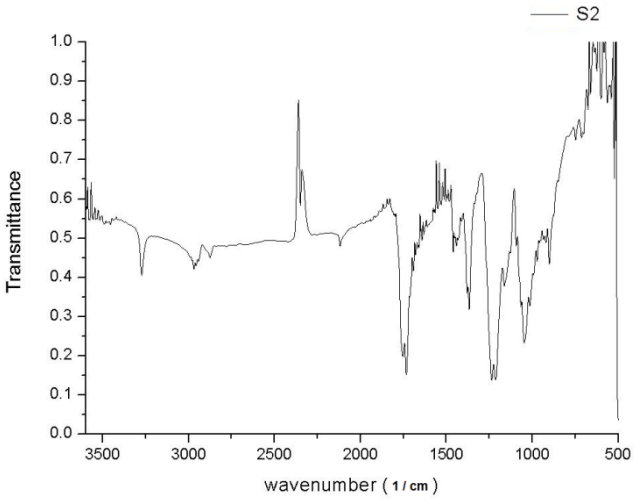

Figure 3.6b FT-IR spectrum of S2.

3.1.6. Synthesis and Characterization of (2,5-dibromothiophen-3-yl)ethyl)-prop-1,2,3-triazol-4-yl-tetra-O-acetyl β-D-glucopyranoside (M4)

(2,5-dibromothiophen-3-yl)ethyl)-prop-1,2,3-triazol-4-yl-tetra-O-acetyl β-D-glucopyranoside (M4) was synthesized by 1,4-disubstituted cycloaddition through directing Cu(I) catalysis between the azide group of 3-(2-azidoethyl)-2,5-dibromothiophene (M3) and the alkyne group of 2,3,4,6-Tetra-O-acetyl-O-prop-1-yl-β-D-glucopyranoside (S2), as previously described in (section 1.1.1. Fig 1.7). Detailed mechanism is given in Scheme 3.8. Cu(I) is generated using $CuSO_4.5H_2O$ and sodium ascorbate as reducing agent. . M4 was characterized by ^{1}H-NMR spectroscopy (Figure 3.7a) and ^{13}C-NMR (Figure 3.7b).

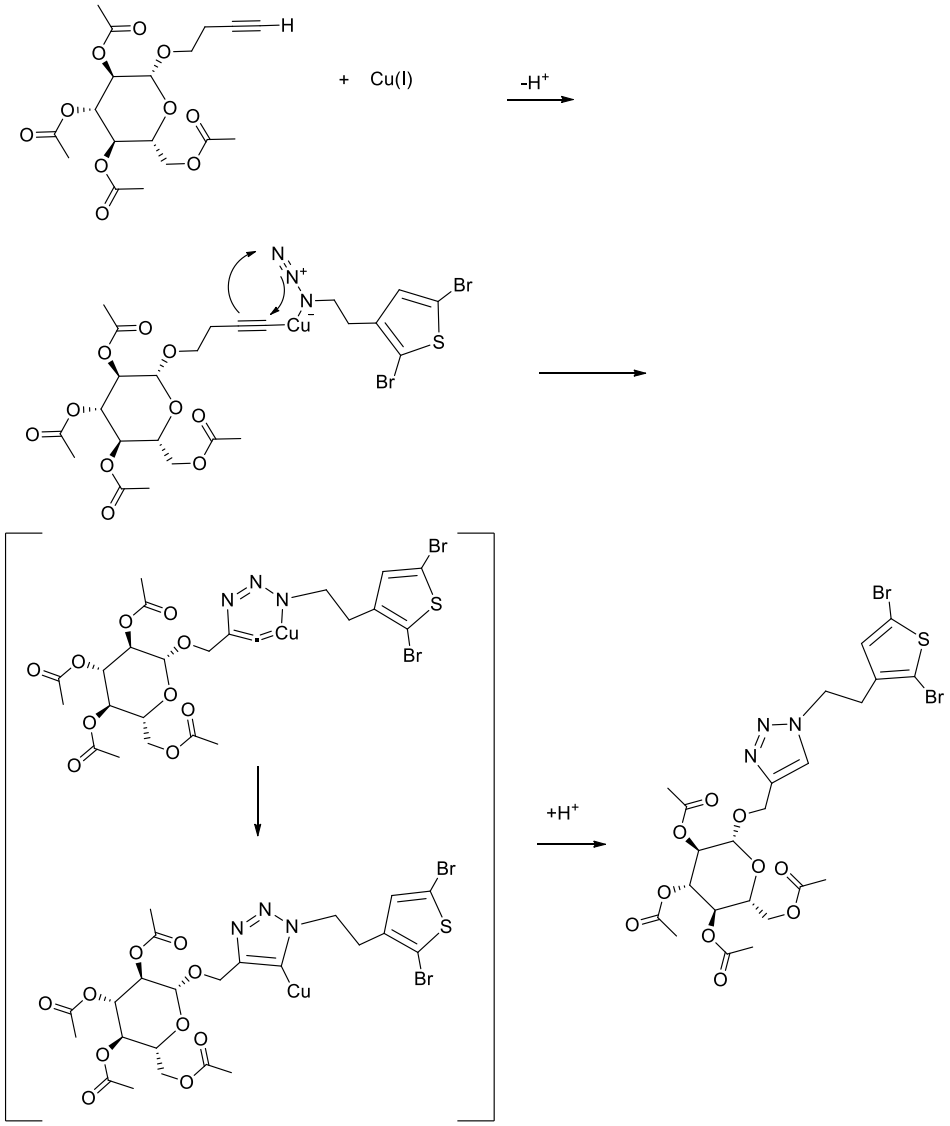

Scheme 3.8. Synthesis mechanism of M4.

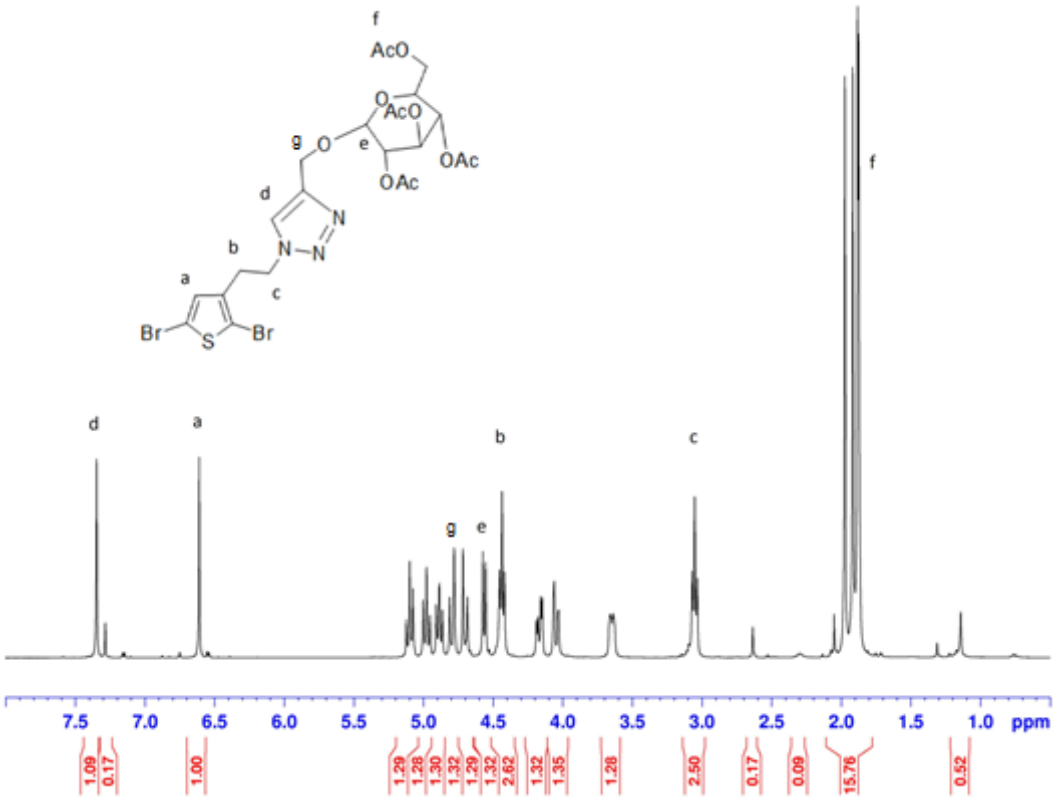

Figure 3.7a. ^{1}H-NMR (400Hz, $CDCl_3$, 25°C) spectrum of M4.

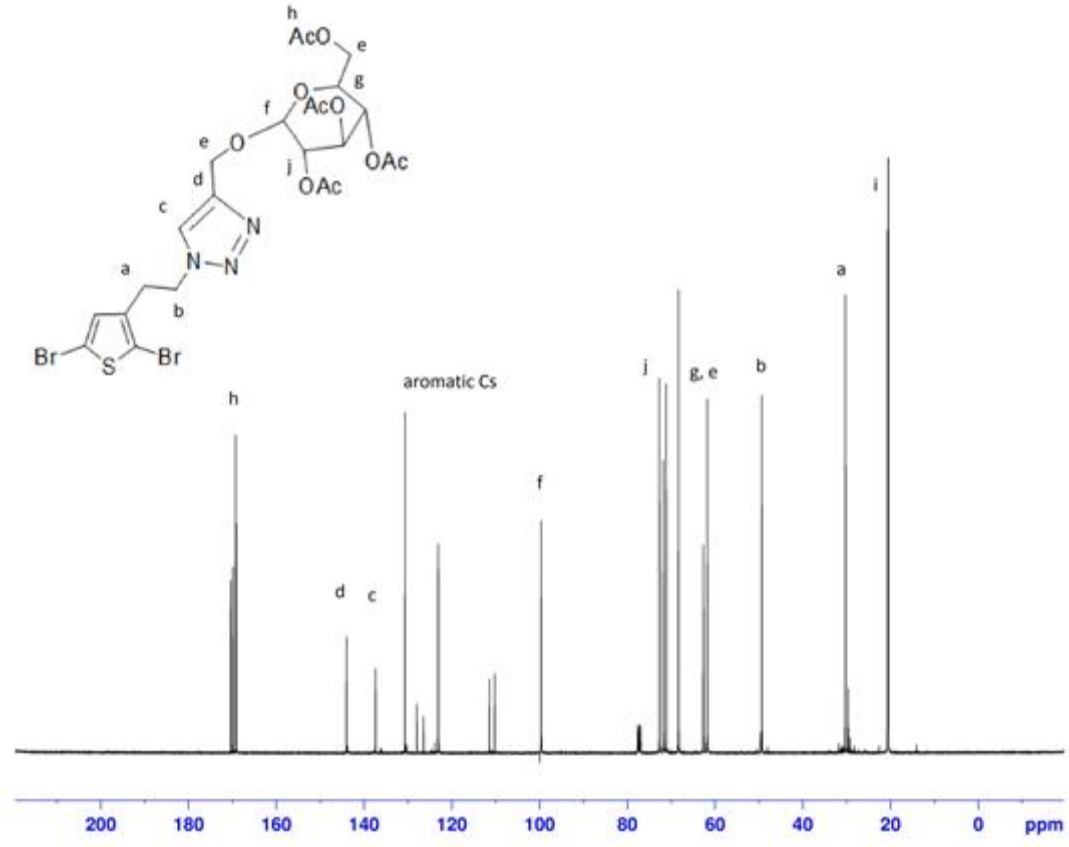

Figure 3.7b ^{13}C-NMR (100Hz, $CDCl_3$, 25°C) spectrum of M4.

3.1.7. Synthesis and Characterization of 2,5-thiophenediboronic ester (M5)

2,5-thiophenediboronic ester (M5) was synthesized from 2,5-thiophenebiboronic acid to further use in Suzuki coupling. Nucleophilic substitution was carried out using excess propylene glycol, with water leaving groups. The mechanism of formation of ester involves the oxygen lone pairs in the glycol hydroxyls to attack boronic acid to abstract its hydrogens, followed by the resulting nucleophilic oxygen to attack glycol back with the leaving groups of water [124b]. The excess glycol was extensively washed after the reaction as described in section 2.3.9. As previously discussed (section 1.1 Figure 1.4) Suzuki coupling is tolerant to boronic acid or ester species. For our purpose of encapsulation trial for the synthesis of P2, and to hinder strong hydrogen bonding interactions with deacetylated monosaccharides and CB portals, esterification reaction was carried out for 2,5-thiophenebiboronic acid. M5 was characterized by ^{1}H-NMR spectroscopy (Figure 3.8a) and ^{13}C-NMR (Figure 3.8b). The accurate ratio of integrations in ^{1}H-NMR spectrum of M5 shows efficient functionalization of the boronic acid and that the residual OH peak is solvent related.

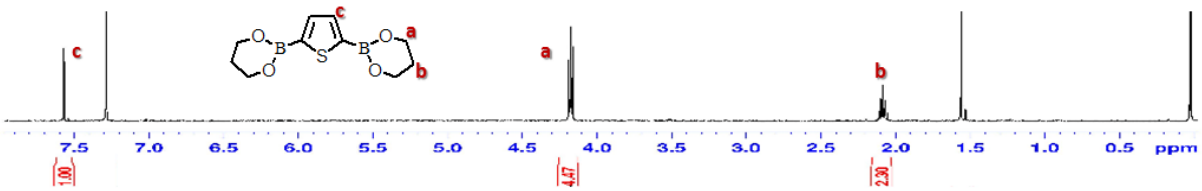

Figure 3.8a ^{1}H-NMR (400Hz, $CDCl_3$, 25°C) spectrum of M5.

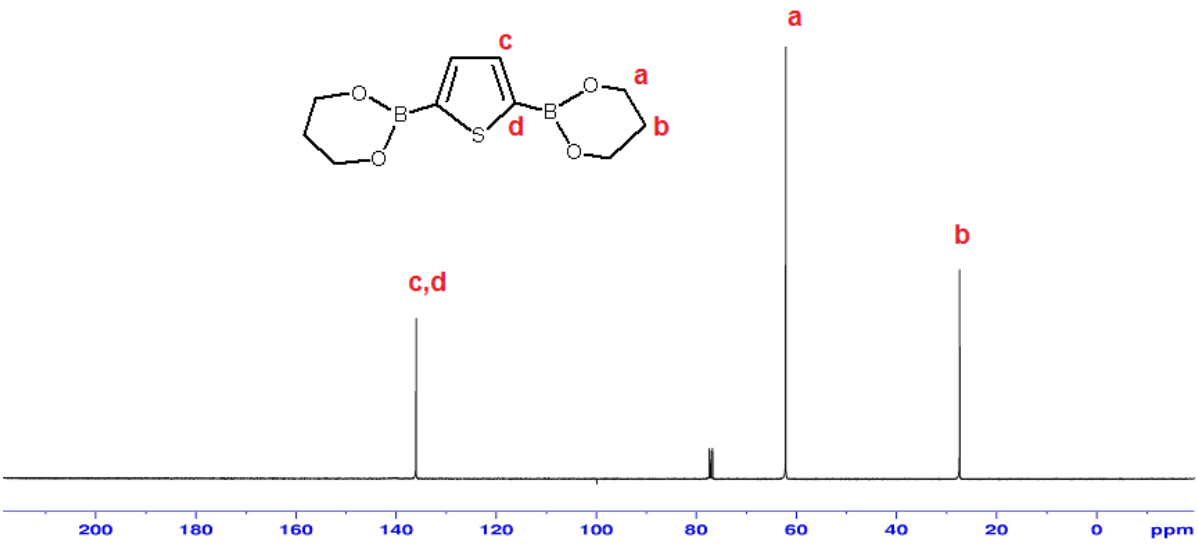

Figure 3.8b ^{13}C-NMR (100Hz, $CDCl_3$, 25°C) spectrum of M5.

3.1.8. Synthesis and Characterization of Cucurbit[7]uril (M6)

Cucurbit[7]uril (M6) was isolated from CBn s synthesized through acid catalysed condensation polymerization of glycoluril and formaldehyde. Paraformaldehyde was used to generate formaldehyde since paraformaldehyde provides better reagent in terms of safety and stability. Cucurbituril species were synthesized by series of glycoluril nitrogen attacks to formaldehyde carbonyl sites [124b]. The isolation was done according to different properties of CBs described in section 1.2, through a method described in section 2.3.10. M6 was characterized by ^{1}H-NMR spectroscopy (Figure 3.9).

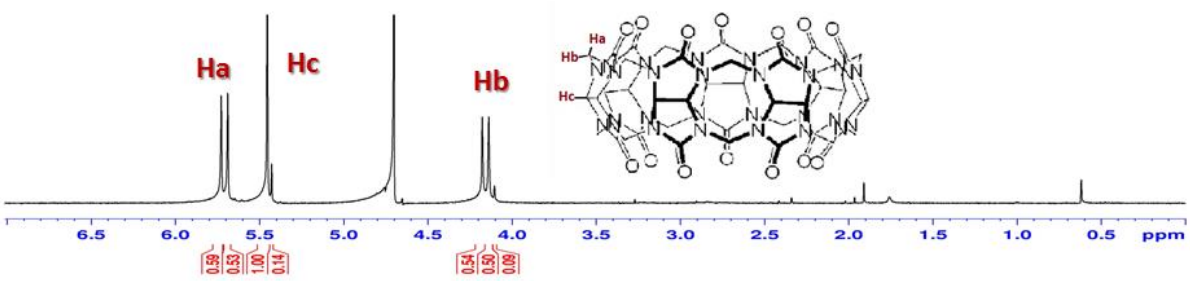

Figure 3.9 ^{1}H-NMR (400Hz, D_2O, 25°C) of M6.

The ^{1}H-NMR spectrum of M6 shows pure CB7 hydrogen environment signals of 5.73 (Ha), 5.45 (Hc), and 4.18 ppm (Hb). The hydrogens of the methylene bridge (Ha, Hb) give different doublets due to the strong influence of the carbonyl portals to their electronic environment. The Ha hydrogen comes strongly downfield shifted due to deshielding positioning to the carbonyl groups, as briefly described in Scheme 3.9.

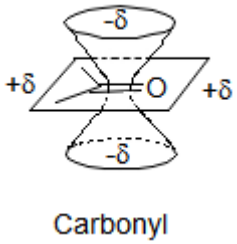

Scheme 3.9 Magnetic anisotropy shielding/deshielding cones of a carbonyl group [125].

The shifting of these hydrogen environments differ among the CBn species due to their structural differences (see Table 1.1) that determine the extend of the prominent deshielding/shielding effects of the carbonyl portals [40-43].

3.1.9. Synthesis and Characterization of poly[(3- triazol-β-D-glucopyranosyl-thiophene)-co-(2,5-thiophene)] (P1) and poly[(3- triazol-β-D-glucopyranosyl-thiophene)-co-(2,5-thiophene)] with Cucurbit[7]uril (P2)

P1 and P2 were synthesized through Suzuki Coupling between M4 and M5(with M6 for P2) by $Pd(OAc)_2$ catalysis and nucleophilic mild base K_2CO_3 (section 1.1. Figure 1.4). For P2, *in situ* complexation between M5 and M6 was forced before the reaction, and was expected to stay on polythiophene backbone being formed to some extend in aqueous media. The driving force for this encapsulation is the hydrophobic interaction between the CB cavity and the thiophene.

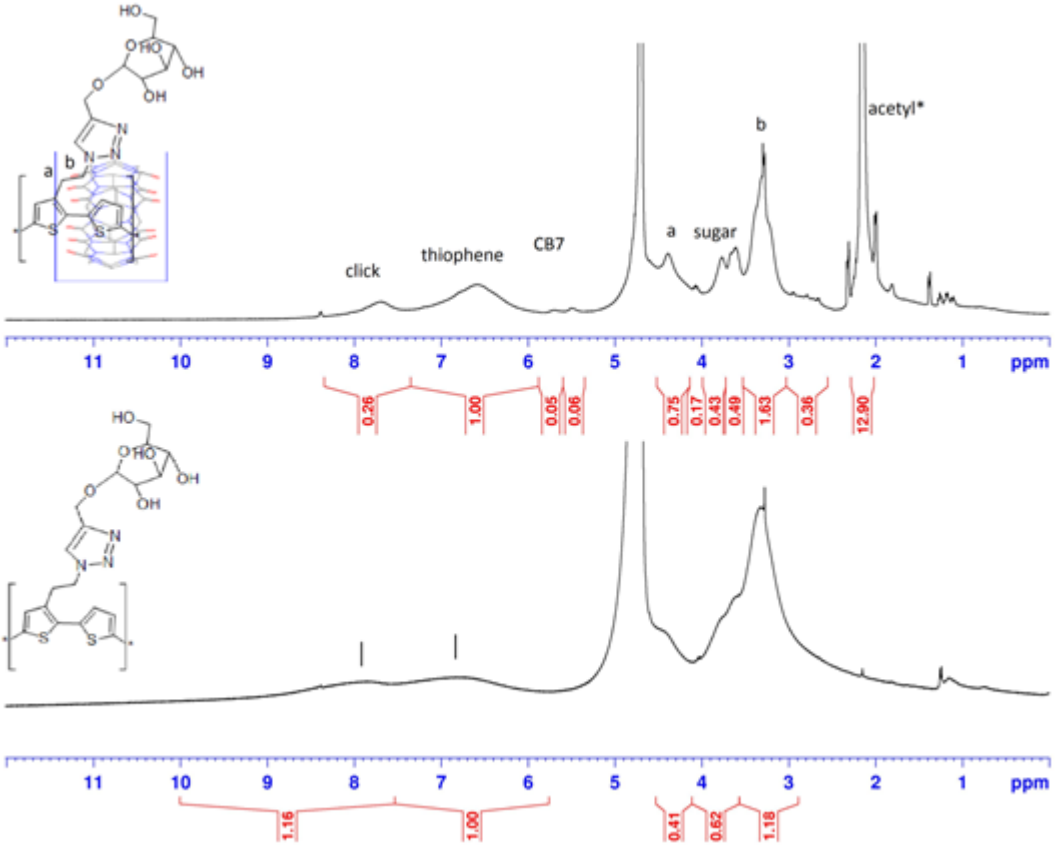

Figure 3.10 ^{1}H-NMR (400Hz, D_2O, 25°C) of P2 and P1, overlayed.

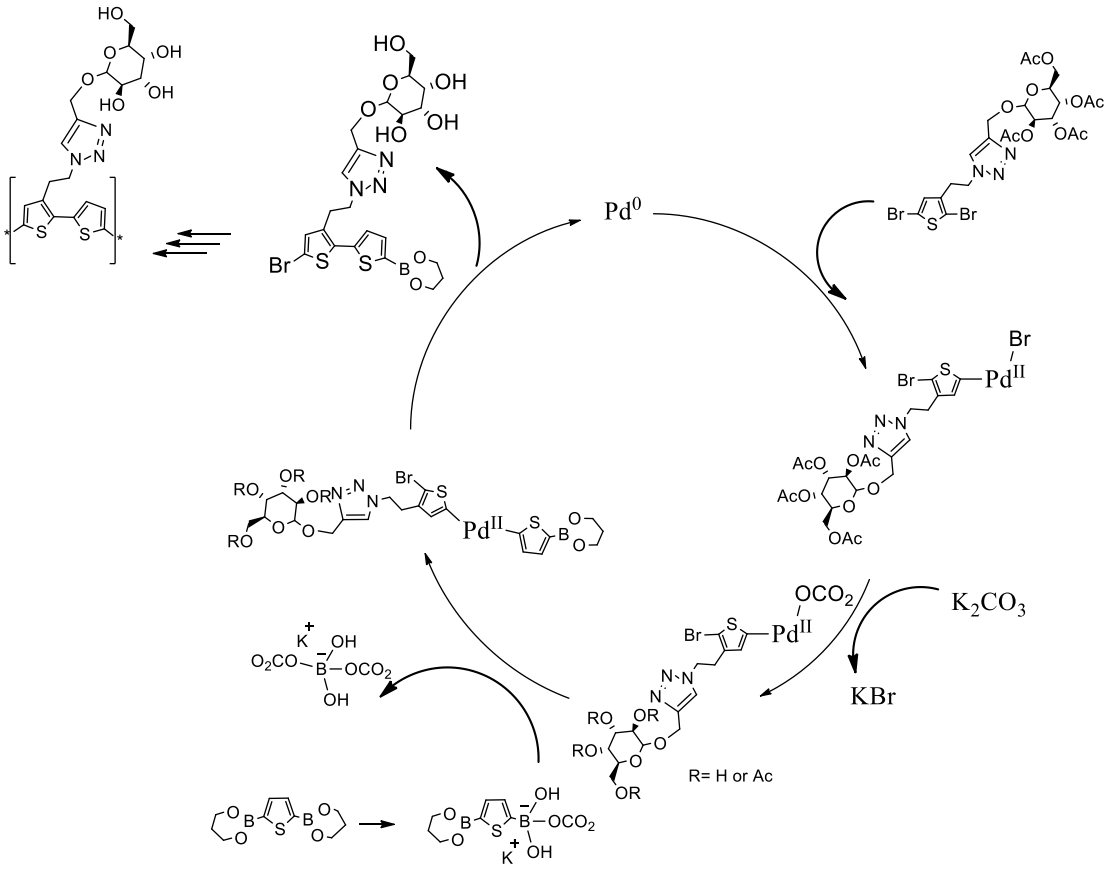

Scheme 3.10 Suzuki coupling reaction between M4 and M5 to yield P1.

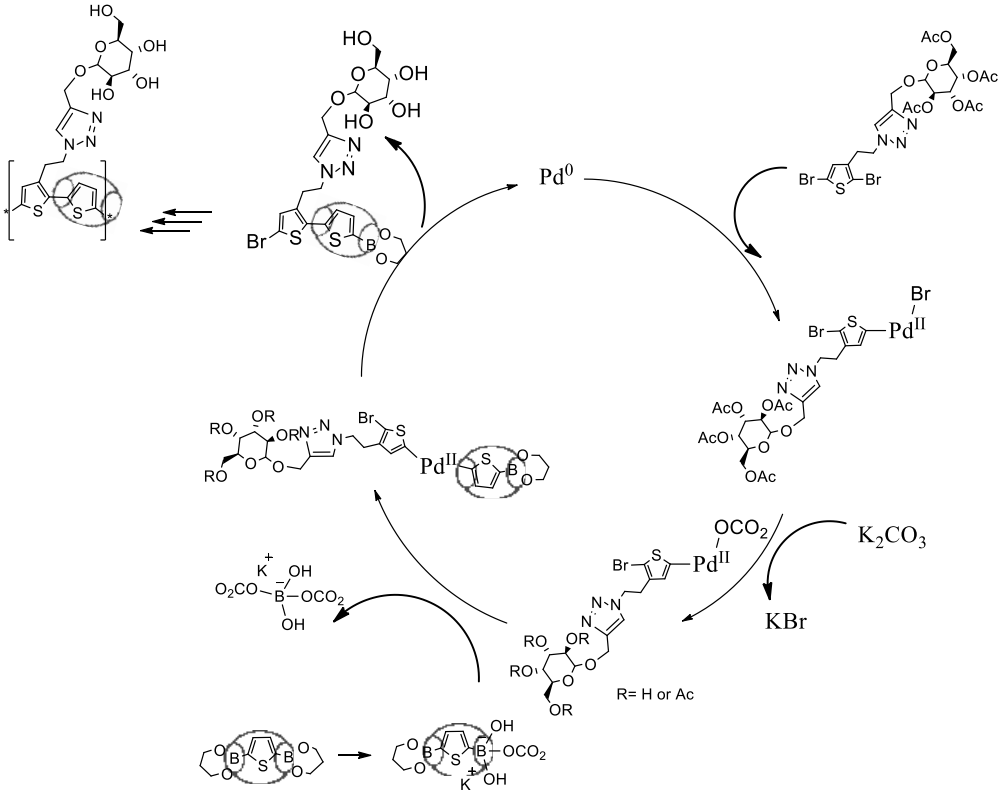

Scheme 3.11 Suzuki coupling reaction between M4 and M5 with M6, to yield P2.

Figure 3.10 shows the ^{1}H-NMR spectra of P1 and P2. The ^{1}H-NMR shows severe peak broadening even compared to typical polymer spectra, due to the fact that the concentration of the NMR sample should be optimized to overcome high hydrogen bonding interactions of the glycoside groups and aggregation issues together considered for such polymer. As can be seen, after removing free oligomeric and monomeric species with dialysis workup (section 2.3.11 and 2.3.12), only very little CB7 was left on the backbone to form a insulated molecular wire. As previously shown in Figure 1.16, a new encapsulation was done using bithiophene, *and* was forced by drying and using polar organic solvents for further reactions instead of aqueous as reported in their procedure [57]. The cavity size of water soluble CB7 was argued to be too large for efficient hydrophobic interactions with the mono-thiophene body. There are several other factors to consider for the efficiency of the polymerization, with the yields being low.

It is fairly important to consider the boronic species that evolve during the reaction since there is monosaccharide functionality present. It is discussed [126] that B-O bond in boronic esters exhibit greater chemical stability than their corresponding boronic acids, since the lone pairs of oxygen in boronic esters having s-donating carbons are more readily conjugated into the electron deficient boron centre. For Suzuki coupling transmetalation, it is not certain what species is the active transmetalating species is during the coupling, due to the existance of successful couplings using boronic esters without added water in the literature [127]. However is highly suggested that it undergoes complete or partial hydrolysis in aqueous, especially basic systems and boronic acid comes out to be the most reactive boronic species overall, which is in favor of the coupling. Scheme 3.10 and Scheme 3.11 shows the similar catalytic cycle for P1 and P2 reagents, respectively.

3.1.10 Photophysical properties of P1 and P2

Figure 3.11a and b shows the photoluminescence properties of P1 and P2. The spectra were taken after the dialysis workup, which cleared and sharpen the peaks by obtaining only the polymeric species. They both exhibit absorbance at 374nm and initial emission peak at 476nm, where the maxima is both slightly red-shifted towards 500nm. The red-shifted broadening makes a shoulder for P2 at around 570nm. This correlates with their appearing color (Figure 3.11c).

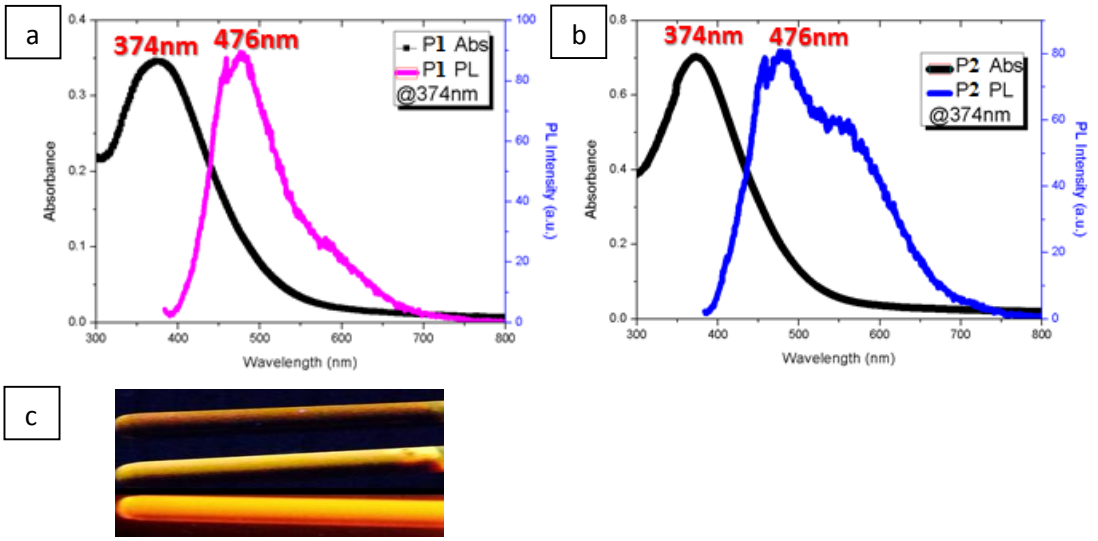

Figure 3.11 a. UV-Vis and Fluorescence spectra of P1 **b.** UV-Vis and Fluorescence spectra of P2 (λ_{abs}= λ_{excit}= 374 nm, λ_{emm}= 476nm in water). **c.** Fluorescent appearance of synthesized conjugated materials under longwave UV light (up to down: P1, P2 in D_2O, O1 in d-DMSO).

For photoluminescence properties, solvent effects acting on backbone strain thus the absorbance is important to consider for this water-soluble co-polythiophene, as previously mentioned in section 1.1.1 figure 1.9. The P2 emission shoulder suggests minor contribution of the CB7 on the backbone for such 'insulated molecular wire effect' (see section 1.2), enhancing conjugation, thus causing PL red-shift. This effect however is not so prominent since the encapsulation takes place only in small population of molecules and not abundant in repeating units within molecules, as the ^{1}H-NMR suggests. The ^{1}H-NMR and PL results, however, show that the coupling takes place despite all the risk factors discussed in section 3.1.9, although not efficient in terms of yield.

3.2 Section 2: Functionalization and Nanoparticle formation of Red-emitting oligomers

Azide functionalized red oligomers were functionalized with mannosides using similar click chemistry. Mannosides were made water-soluble after the functionalization (Scheme 3.12). Mannosides were prepared with similar method as glucosides having alkyne functionalities (see section 2.3.7).

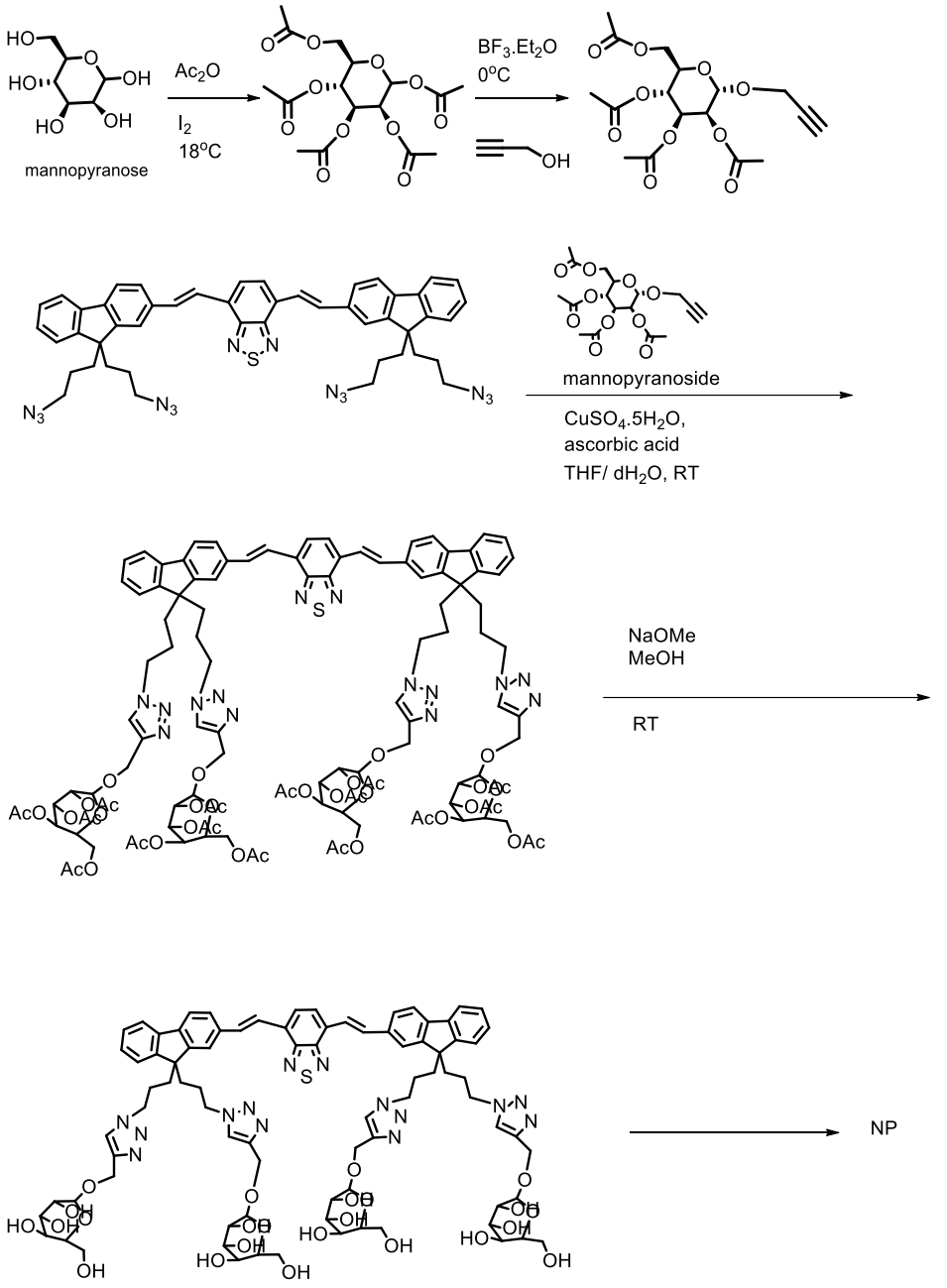

Scheme 3.12 Red-oligomer functionalization pathway to respectively yield O1 and O2.

A limitedly functionalized oligomer trial was also done to obtain an initial nanoparticle that would then be open to further post-functionalizations available through the free azide groups (Scheme 3.13).

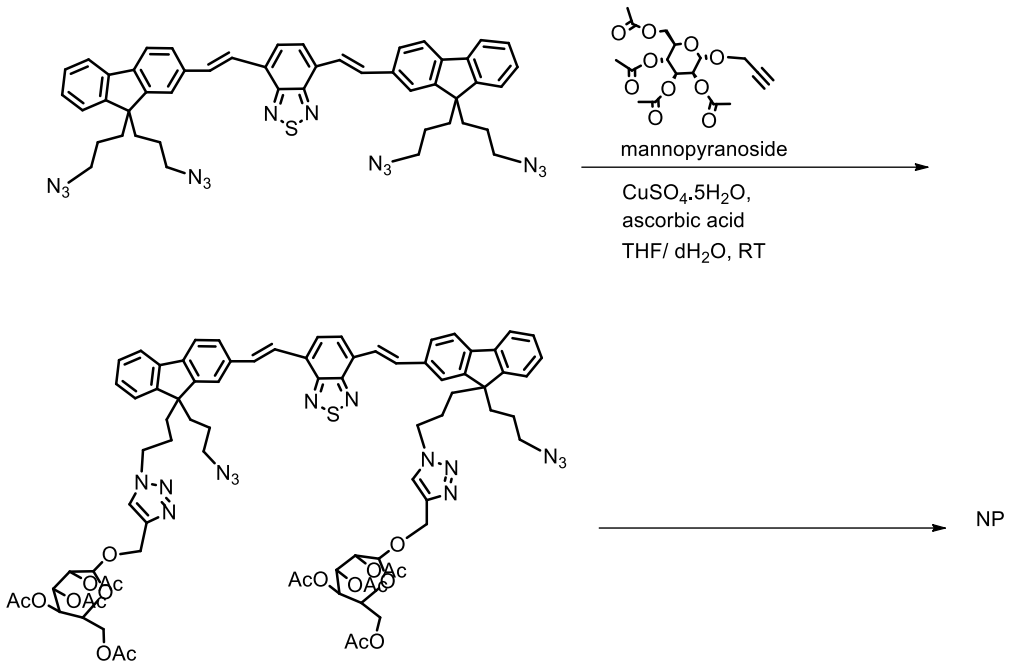

Scheme 3.13 Partial functionalization pathway for red-oligomer to yield O3.

3.2.1. Synthesis and Characterization of 1,2,3,4,6-Penta-O-acetyl-D-mannopyranose (S3)

1,2,3,4,6-Penta-O-acetyl-D-mannopyranose (S3) was synthesized from D-mannose according to the same principles discussed for its stereoisomer 1,2,3,4,6-Penta-O-acetyl-D-glucopyranose (S1) (section 3.1.4.) with same mechanism in action discussed in Scheme 3.7. S3 was characterized by 1H-NMR spectroscopy (Figure 3.12).

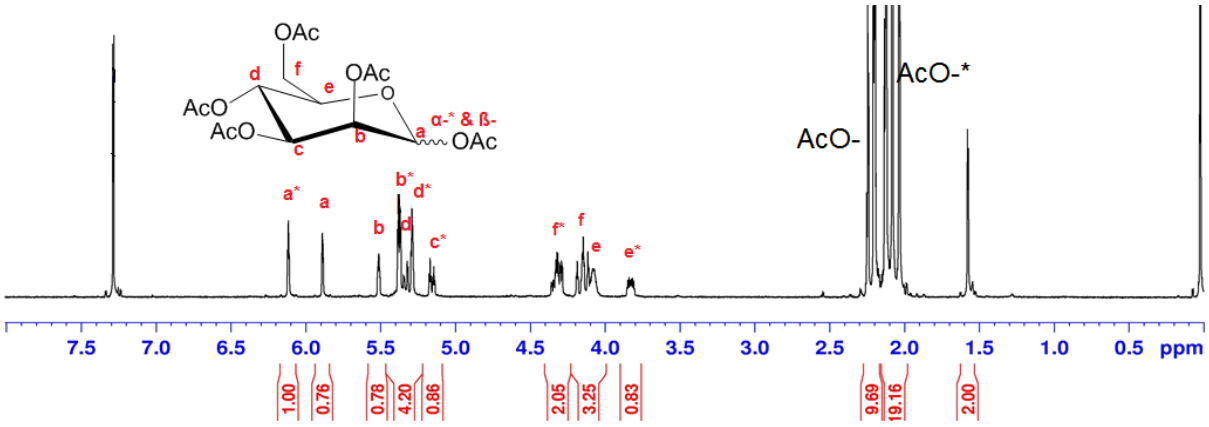

Figure 3.12 ^{1}H-NMR (400Hz, $CDCl_3$, 25°C) spectrum of S2.

The ¹H-NMR spectrum of S3 shows an anomeric mixture of α- and β- products with distinct peaks. The of α- mannopyranose anomeric hydrogen signal comes at 6.11ppm whereas the one of β- is at 5.89ppm, values agree with literature [124]. All other hydrogen environments are seperately identified as well (Figure 3.12) with numeric values (section 2.3.6.) As can be seen, compared to its stereoisomer S1 (section 3.1.4.) which has equatorial acetyl group on C2 results in abundant β- product whereas axial acetyl on C2 does not have such prominent effect.

3.2.2. Synthesis and Characterization of 2,3,4,6-Tetra-O-acetyl-O-prop-1-yl- α - D-mannopyranoside (S4)

2,3,4,6-Tetra-O-acetyl-O-prop-1-yl- α - D-mannopyranoside (S4) was synthesized from 1,2,3,4,6-Penta-O-acetyl-D-mannopyranose (S3) through the same borontrifluoride-activated propargyl alcohol functionalization as its stereoisomer S2 (section 3.1.5). Both precursor stereoisomers of α- and β- (S3) are restricted to become α- upon functionalization as previously discussed (section 1.4.1.2. Figure 1.28). S4 was characterized by ¹H-NMR spectroscopy (Figure 3.13).

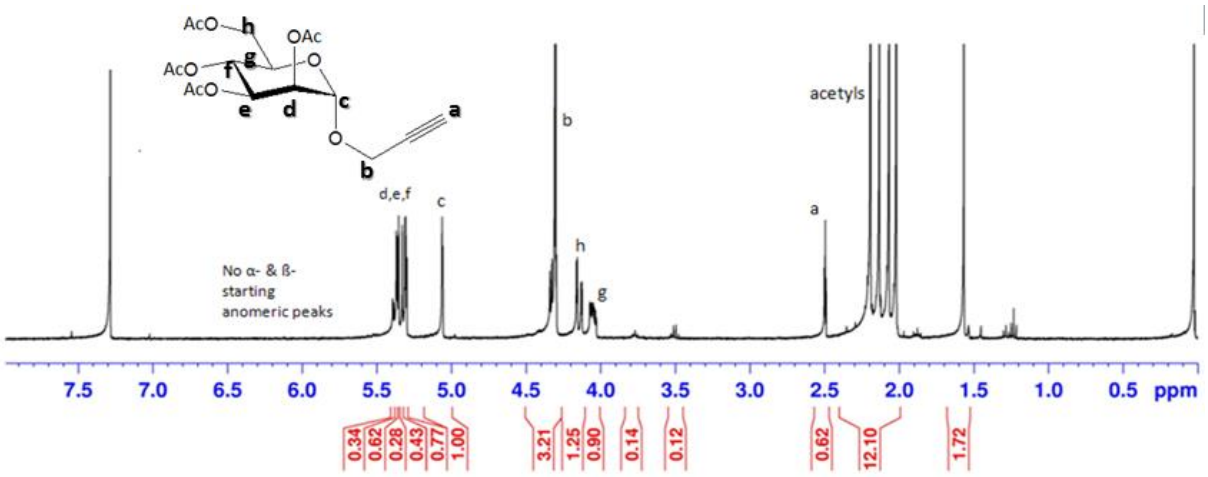

Figure 3.13 ¹H-NMR (400Hz, $CDCl_3$, 25°C) spectrum of S4.

The ¹H-NMR spectrum of S4, values agree with literature [91 SI]. The anomeric hydrogen comes at 5.05ppm showing a drastic upfield shift upon functionalization with propargyl group (compared to S3), as in the case with S2. The simple method for crystallization trial using diethyl ether was suggested by Dr. Rehan Khan. The integrations show pure crystallization with total yield of 70%, highest value reported to our knowledge, 2-3 times more efficient than the values reported in literature, which report columns for almost inseperably close Rfs.

Compared to S2 where the same method was applied with lower efficacy, S4 stereoisomer apparently shows solubility properties similar initially when heated, but lower solubility upon cooling and thus higher crystallization properties compared to its own precursor S3 in mixture. Pure S4 was used for the synthesis of click-oligomers O1, O2, O3.

3.2.3. Synthesis and characterization of 4,7-bis((E)-2-(9,9-bis(3- triazol- tetra-O-acetyl- α – D- mannopyranosyl)-9H-fluoren-2-yl)vinyl)benzo[c][1,2,5]thiadiazole (O1)

4,7-bis((E)-2-(9,9-bis(3- triazol- tetra-O-acetyl- α – D- mannopyranosyl)-9H-fluoren-2-yl)vinyl)benzo[c][1,2,5]thiadiazole (O1) was synthesized by 1,4-disubstituted cycloaddition through directing Cu(I) catalysis between the four azide groups of 4,7-bis((E)-2-(9,9-bis(3-azidopropyl)-9H-fluoren-2-yl)vinyl)benzo[c][1,2,5]thiadiazole (AO) and the alkyne groups of 2,3,4,6-Tetra-O-acetyl-O-prop-1-yl- α - D-mannopyranosides (S4), with the same click chem istry discussed for M4 (Scheme 3.8). 4 equivalent of mannoside was used. O1 was characterized by ^{1}H-NMR spectroscopy (Figure 3.14). The spectrum shows aromatic peaks of the red oligomer backbone between 8.2-7.7ppm, and the crowded peaks of mannopyranoside hydrogens between 5.5-4 ppm. The peaks labeled g* and * shows residual free S4.

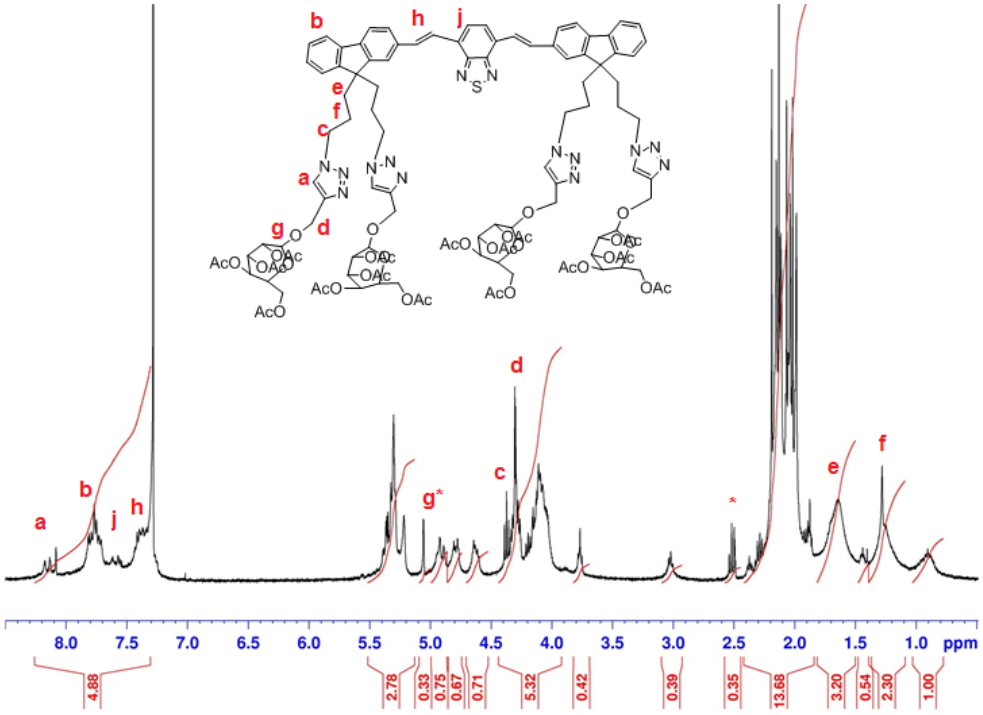

Figure 3.14 ^{1}H-NMR (400Hz, $CDCl_3$, 25°C) spectrum of O1.

3.2.4. Synthesis and characterization of 4,7-bis((E)-2-(9,9-bis(3- triazol- α – D-mannospyranosyl)-9H-fluoren-2-yl)vinyl)benzo[c][1,2,5]thiadiazole (O2)

4,7-bis((E)-2-(9,9-bis(3- triazol- α – D- mannospyranosyl)-9H-fluoren-2-yl)vinyl)benzo[c][1,2,5]thiadiazole (O2) was synthesized by applying Zemplen deacetylation to synthesized 4,7-bis((E)-2-(9,9-bis(3- triazol- tetra-O-acetyl- α – D- mannopyranosyl)-9H-fluoren-2-yl)vinyl)benzo[c][1,2,5]thiadiazole (O1). O2 was characterized by ^{1}H-NMR spectroscopy (Figure 3.15). The spectrum shows upfield shift of mannopyranoside peaks upon deacetylation starting from 5.0ppm rather than the acetyl precursor where the crowded hydrogen peaks were starting from 5.5ppm (Figure 3.14). The peaks labeled g* and * shows residual free S4. In Zemplen deacetylation, methoxide is generated by dissolving sodium methoxide in methanol, which attacks the acetyl groups, with plausibly methyl acetate leaving group [128]. 2 times excess NaOMe was used in our procedure for 16 acetyl groups since the traditional procedure with readily MeOH soluble species indicated 0.1eq per acetyl group (3.2eq). Still, residual acetyl hydrogen peaks show up at around 2ppm.

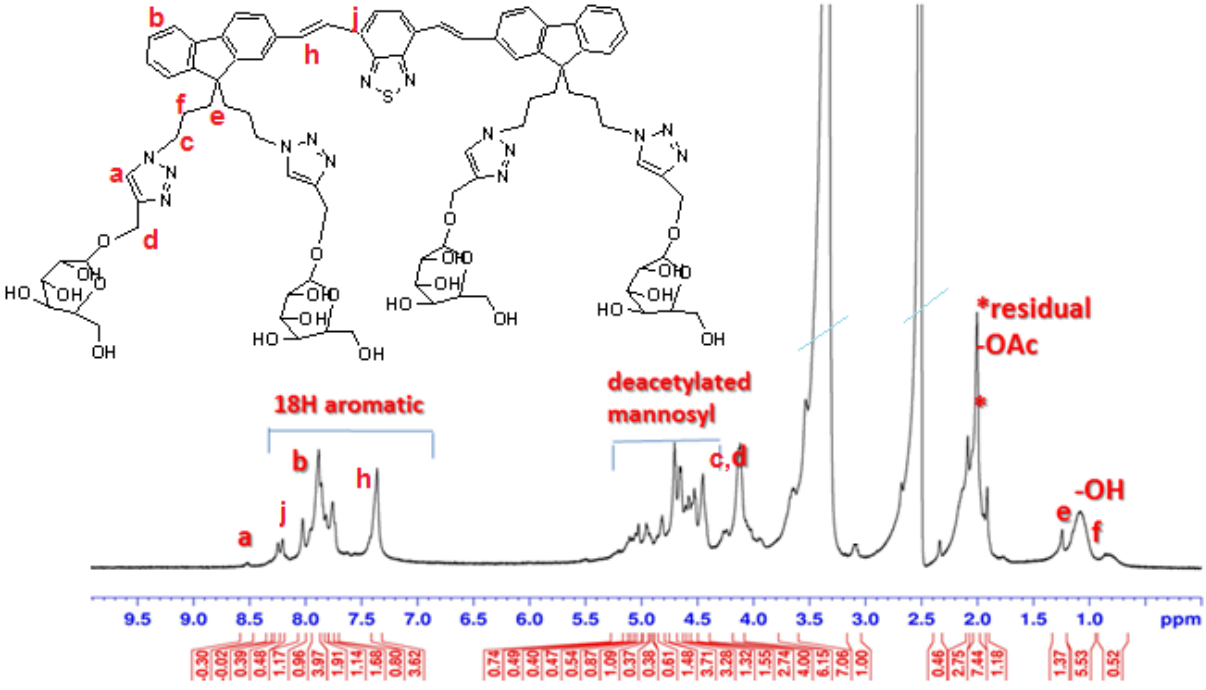

Figure 3.15 ^{1}H-NMR (400Hz, d-DMSO, 25°C) spectrum of O2.

3.2.5. Synthesis and characterization of 4,7-bis((E)-2-(9,9-bis(di-(3- triazol- tetra-O-acetyl- α – D- mannopyranosyl))- (di-(3-azidopropyl))-9H-fluoren-2-yl)vinyl)benzo[c][1,2,5]thiadiazole (O3)

4,7-bis((E)-2-(9,9-bis(di-(3- triazol- tetra-O-acetyl- α – D- mannopyranosyl))- (di-(3-azidopropyl))-9H-fluoren-2-yl)vinyl)benzo[c][1,2,5]thiadiazole (O3) was synthesized by similar fashion as O1, using 'click reaction' between two of the azide groups of 4,7-bis((E)-2-(9,9-bis(3-azidopropyl)-9H-fluoren-2-yl)vinyl)benzo[c][1,2,5]thiadiazole (AO). 2 equivalent of mannoside was used for limited reaction. O3 was characterized by ^{1}H-NMR spectroscopy (Figure 3.16). Equally prominent peaks of **c,f** and **g,h** strongly suggest equal amount of azide and mannoside functionalities on the oligomers, which was validated through HRMS-TOF spectroscopy (Figure 3.17). The peaks labeled * shows residual, partially deacetylated mannoside hydrogen shifts during the workup (section 2.3.15).

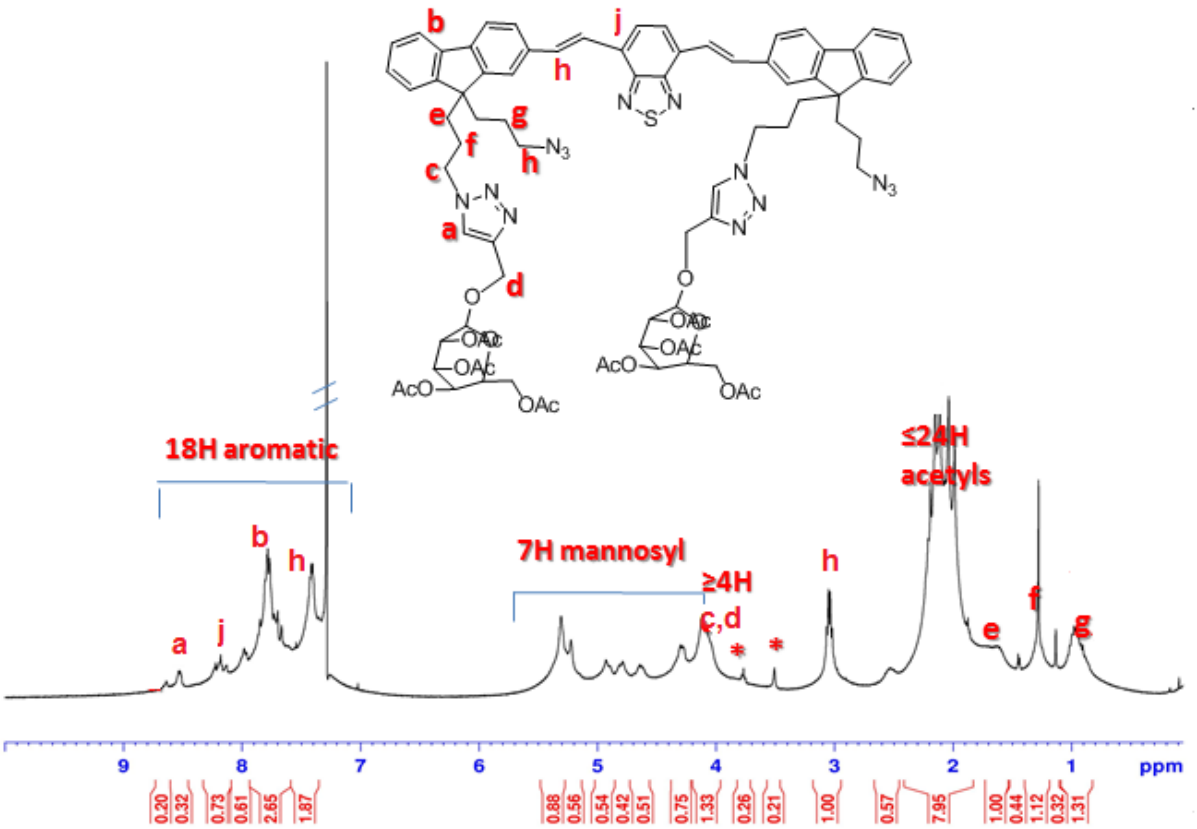

Figure 3.16 ^{1}H-NMR (400Hz, $CDCl_3$, 25°C) spectrum of O3.

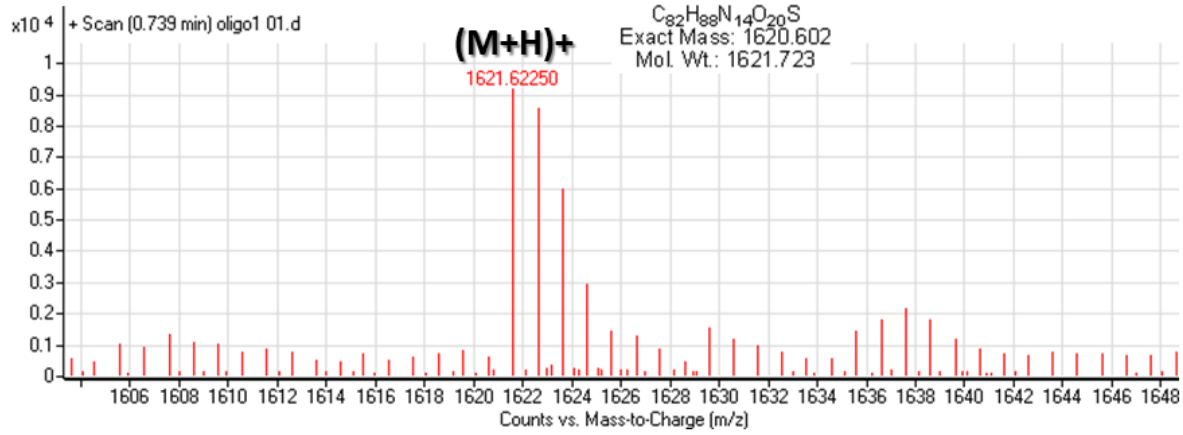

Figure 3.17 HRMS-TOF (+ , 4500V, MeOH sample, MeCN eluent) spectrum of O3.

The HRMS-TOF spectrum of O3 shows the $[M+H]^+$ m/z: 1621.62250 peak with great accuracy, the theoretical M being 1620.602 (Figure 3.17). This oligomer is important for multifunctional or cross-linking designs for particle preparation.

3.2.6. Photophysical properties of oligomers

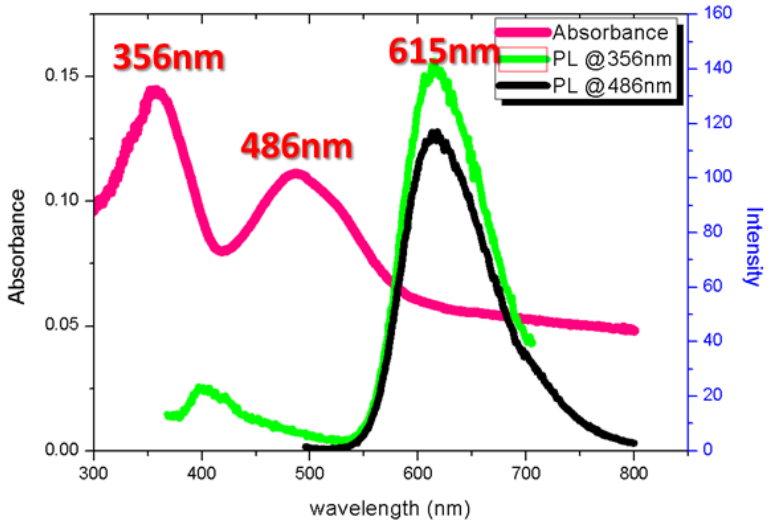

Figure 3.18 UV-Vis and Fluorescence spectra of O2 (λ_{abs}= 356 nm and 486 nm, λ_{emm}= 615nm in water)

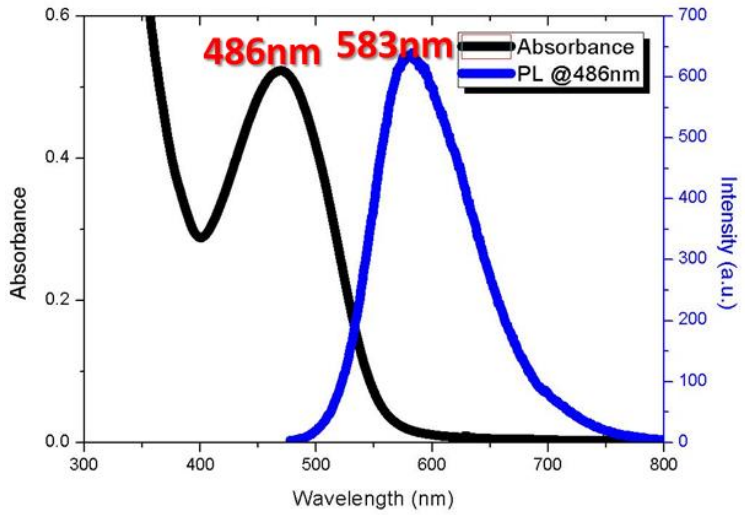

Figure 3. 19 UV-Vis and Fluorescence spectra of O3 (λ_{abs}= 486 nm, λ_{emm}= 583nm in $CHCl_3$)

Figures 3.18 and 3.19 show the photoluminescence properties of oligomers O2 and O3, respectively in water and in chloroform. O2 in water shows two absorbance peaks of 356 nm and 486 nm, and emission at 615nm. The early, blue-shifted absorbance is expectable for such polar solution and amphiphilic large molecule, whereas the red emission at 615nm, same for both excitation wavelengths is a very desirable for biological applications. O3 in chloroform shows absorbance peak at only 486 nm possibly due to non-straining solvent environment, and emission at 583nm. The oligomers O1, O2 and O3 similarly appear intensely transparent dark orange. Figure 3.11c shows appearance of O1 in d-DMSO under longwave UV light.

3.2.7. Morphological properties of oligomer nanoparticles

Particles were prepared from O2 and O3 using 1. 5mg of oligomer dissolved in 1mL DMF. 5mL dH_2O was added in a flow rate of 0.5mL/h using flow-syringe pump (section 2.2.5) and constantly stirred. After complete addition the mixture was put for dialysis in 3000mpore dialysis bags for a day to diffuse out DMF without disrupting particle properties, with frequent water bath change. Particles were confirmed through DLS particle size measurements and SEM images.

Z-Average (d.nm):	127.3	Peak 1:	34.41	100.0	13.38
PdI:	0.280	Peak 2:	0.000	0.0	0.000
Intercept:	0.934	Peak 3:	0.000	0.0	0.000
Result quality :	Good				

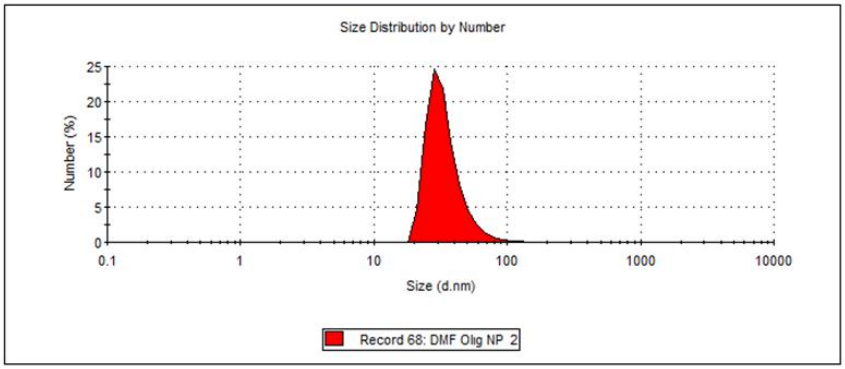

Figure 3.20 DLS measurement of O2 nanoparticles, size distribution of by number

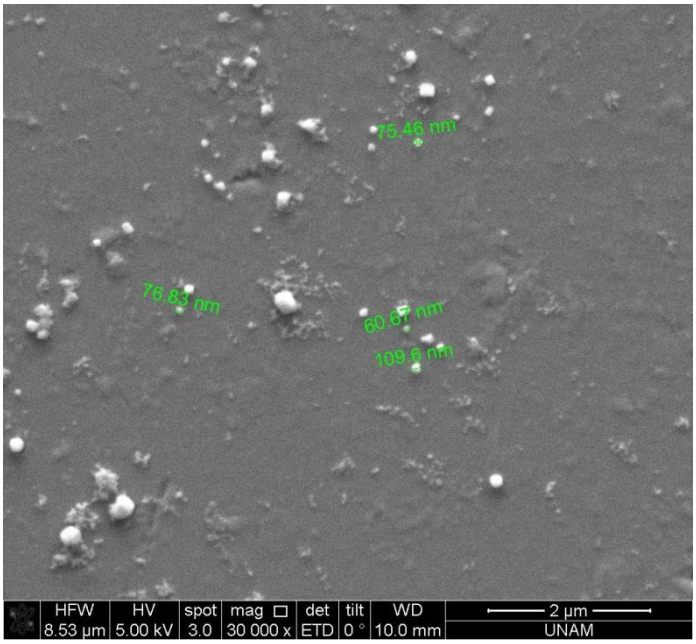

Figure 3.21 SEM image of O2 nanoparticles, DLS dilution.

Figure 3.20 and 3.21 shows the particles prepared using O2. “Dynamic light scattering” measurements to determine size distribution of particles by number were taken and software-calculated as described in section 2.2.7. O2 shows peak maximum value at 34nm, which means the most particle population is near this value with a narrow distribution, the average being 127nm, with distribution index (PDI) of 0.28. The SEM image with 80,000x magnification shows particles around 75nm diameter. However, the particles were observed to be not stable. Figure 3.22 shows O2 particles swell and aggregate to form two populations

of maxima 107 and 539nm after 3 days. The multiple OH groups of monosaccharides surrounding the particles formed by nanoaggragates in aqueous environment are suspected to strongly interact with each other through hydrogen bonding.

		Diam. (nm)	% Number	Width (nm)
Z-Average (d.nm): 466,0	Peak 1:	107,9	92,0	30,84
PdI: 0,400	Peak 2:	539,8	8,0	267,0
Intercept: 0,867	Peak 3:	0,000	0,0	0,000
Result quality : Good				

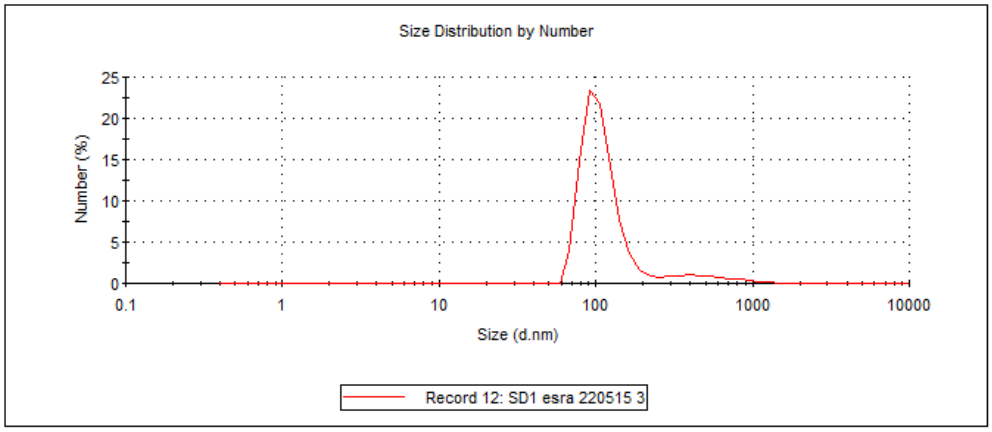

Figure 3.22 DLS measurement of O2 nanoparticles after 3days, size distribution of by number.

Figure 3.23 shows the particles prepared using O3. O3 particles peak maximum value at 74nm, the overall average being 138nm, with distribution index (PDI) of 0.237. These similar values for the hydrophilic (O2) and non-hydrophilic cross-linkable particles (O3) with small diameters show promising results for further investigation.

		Diam. (nm)	% Number	Width (nm)
Z-Average (d.nm): 138,8	Peak 1:	74,33	100,0	26,76
PdI: 0,237	Peak 2:	0,000	0,0	0,000
Intercept: 0,930	Peak 3:	0,000	0,0	0,000

Result quality : Good

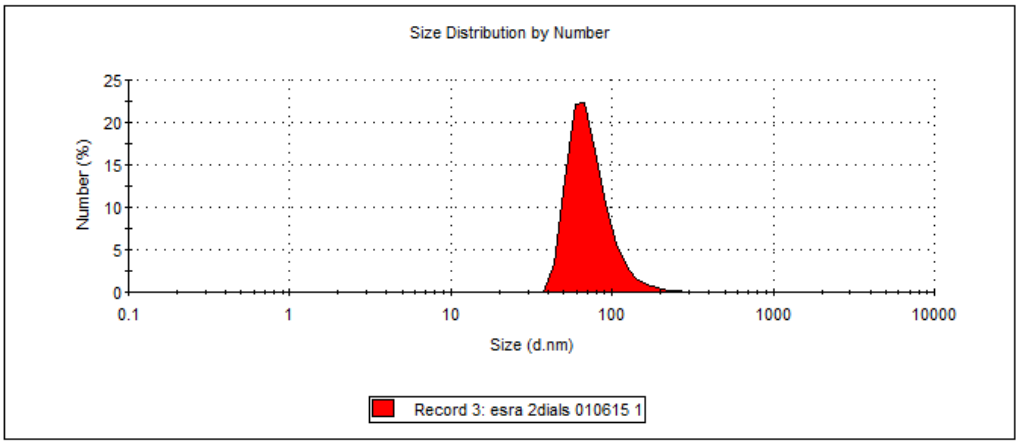

Figure 3.23 DLS measurement of O3 nanoparticles, size distribution of by number

CONCLUSION

In this work, polymers and oligomers were made water soluble by functionalizing them with monosaccharides. Co-polymer and analogous polyrotaxane of two thiophene monomers were synthesized through pre-functionalized glucoside design and Suzuki coupling. *In situ* complexation trial was made to produce CB7 threaded novel glycopolythiophenerotaxane. Post-functionalization was applied to oligomers to produce mannoside. Structural and photophysical properties were shown through ^{1}H-NMR, UV-VIS, and Fluorescence Spectroscopy.

The pre-functionalized glucopolythiophene and its polyrotaxane showed 476nm emission in water when excited with 374 nm light. The post-functionalized oligomers showed 615nm (O2 in water) and 583nm (O3 in chloroform) excited with 486 nm light.

Particles from oligomers were formed through flow-syringe method and the sizes were shown through DLS measurements. Mannoside red oligomer O2 formed particles around 34nm and O3 around 74nm.

These fluorescent, water-soluble, multivalent glycoconjugate designs are candidates for active-targetted cellular theranostics because their ability for receptor-mediated endocytosis. Polyrotaxane design may be further persued using CB6, and optimization in terms of synthesis. O3 can be further functionalized by a bio-active cross-linker to make functional particles.

REFERENCES

[1] Chiang, C.K.; Fincher, C. R.; Park, Y. W.; Heeger, A. J.; Shirakawa, H.; Louis, E. J.; Gau, S. C.; MacDiarmid; A. G. *Phys. Rev. Lett.*, **1977**. *39*, 1098–1101.

[2] *"The Nobel Prize in Chemistry 2000"*. Nobelprize.org. Nobel Media AB **2014**. Web. 30 Jun 2015. http://www.nobelprize.org/nobel_prizes/chemistry/laureates/2000/

[3] Skotheim, T. A.; Reynolds, T. A., Eds., *Handbook of Conducting Polymers*, 3rd ed., CRC Press, Boca Raton, **2007**.

[4] Grimsdale, A. C.; Chan, K. L.; Martin, R. E.; Jokisz, P. G.; Holmes, A. B. *Chem. Rev.* **2009**, 109, 897–1091.

[5] Günes, S.; Neugebauer, H.; Sariciftci, N. S. *Chem. Rev*., **2007**, *107*, 4, 1324–1338.

[6] Ho, P.K.H., D.S. Thomas, R.H. Friend, and N. Tessler. *Science*, **1999**, *285*, 233.

[7] Thomas, S. W.; Joly, G. D.; Swager, T. M. *Chem. Rev.*, **2007**, *107*, 1339-1386 .

[8] Feng, X.; Liu, L.; Wang, S.; Zhu, D. *Chem. Soc. Rev*., **2010**, *39*, 2411-2419.

[9] Zhu, C.; Liu, L.; Yang, Q.; Lv, F.; Wang, S. *Chem. Rev*., **2012**, *112*, 4687−4735.

[10] Kim, S.; Lim, C.; Na, J.; Lee, Y.; Kim, K.; Choi, K.; Learyb, J. F.; Kwona, I. C. *Chem. Commun.*, **2010**, *46*, 1617–1619.

[11] Imamura, A.; Aoki, Y., *Int. J. Quantum Chem.*, **2006**, *106*, 8, 1924-1933.

[12] Salzner, U.; Lagowski, J.B.; Pickup, P.G.; Poirier, P.A. *Synth. Met*., **1998**, *96*, 177.

[13] Pu, K.; Cai, L.; Liu, B. *Macromolecules*, **2009**, *42*, 5933–5940.

[14] Liu, B.; Yu, W.; Lai, Y.; Huang, W. *Macromolecules*, **2002**, *35*, 4975 –4982.

[15] Abbel, R.; Schenning, A. J.; Meijer, E. W. *J. of Polym. Sci: A: Polym. Chem.*, **2009**, *47*, 4215–4233.

[16] Mei, J.; Bao, Z. *Chem. Mater.*, **2014**, *26*, 604−615

[17] "*The Nobel Prize in Chemistry 2010*". Nobelprize.org. Nobel Media AB **2014**. Web. 13 Jul 2015. http://www.nobelprize.org/nobel_prizes/chemistry/laureates/2010/

[18] Negishi, E. *Handbook of Organopalladium Chemistry for Organic Synthesis*, p3-5, John Wiley & Sons, **2003**.

[19] Torborga, C.; Beller, M. *Adv. Synth. Catal*., **2009**, 351, 3027 – 3043.

[20] Suzuki, A., Miyaura, N. *Chem. Rev*., **1995**, *95*, 2457-2483.

[21] a) McCullough, Richard D. *Adv. Mat*., **1998**, *10*, 2, 93. b) Osaka, I.; McCullough, R. D. *Acc. of Chem. Res*. **2008**, *41*, 9, 1202-1214.

[22] Perepichka, Igor F., Eds., *Handbook of thiophene-based materials*. 577-828, John Wiley & Sons Ltd, **2009**.

[23] Guo, B.; Glavasa, L.; Albertssona, A. *Progress in Polymer Science*, **2013**, *38*, 1263–1286

[24] Wang, B.; Yuan, H.; Zhu, C.; Yang, Q.; Lv, F.; Liu, L.; Wang, S. *Nature Sci. Rep*., **2012**, 2, 766.

[25] Lukkari, J.; Saloma1ki, M.; Viinikanoja, A.; Aaritalo, T.; Paukkunen, J.; Kocharova, N.; Kankare, J. *J. Am. Chem. Soc.*, **2001**, 123, 25.

[26] Matthews, J. R.; Goldoni, F.; Schenning, A.; Meijer, E. W. *Chem. Commun*., **2005**, 5503–5505.

[27] Englebienne, P.; Weiland, M. *Chem. Comm*., **1996** , 14, 1651.

[28] Andersson, M.; Ekeblad, P. O.; Hjertberg, T.; Wennerström, O.; Inganäs, O. *Polym. Commun*., **1991**, 32, 546–548.

[29] Patil, A. O.; Basescu, Y.; Colaneri, N.; Chen, J.; Wudl, F.; Heeger, A. *J. Synth. Met*., **1987**, 20, 151–159.

[30] Liu, J.; Feng, G.; Geng, J.; Liu, B. *ACS Appl. Mater. Interfaces*, **2013**, 5, 4511−4515.

[31] Zhou, L.; Geng, J.; Wang, G.; Liu, J.; Liu, B. *ACS Macro Lett*., **2012**, 1, 927−932.

[32] Mohamed, M. G.; Cheng, C.; Lin, Y.; Huang, C.; Lu, F.; Changa, F.; Kuo, S. *RSC Adv.*, **2014**, 4, 21830.

[33a] Ho, H.-A.; Bera-Aberem, M.; Leclerc, M. *Chem.Eur. J.*, **2005**, 11, 1718.

[33b] F. Stabo-Eeg et al. *Chemical Physics*, **2007**, 336, 121–126.

[33c] Ho, H.; Najari, A.; Leclerc, M. *Acc. of Chem. Res.*, **2008**, *41*, 2, 168-178.

[34] Martin, R. E.; Diederich, F. *Angew. Chem. Int. Ed.*, **1999**, 38, 1350 – 1377.

[35] Zhang, F.; Wu, D.; Xua, D.; Feng, X. *J. Mater. Chem.*, **2011**, 21, 17590.

[36] Stalder, R.; Xie, D.; Islam, A.; Han, L.; Reynolds, J. R.; Schanze, K. S. *ACS Appl. Mater. Interfaces*, **2014**, 6, 8715−8722.

[37] Abbel, R.; Weegen, R.; Meijer, E. W.; Schenning, A. J. *Chem. Commun.*, **2009**, 1697–1699.

[38] Reynolds, J. R. et al. *Chem. Mater.*, **2011**, 23, 3805–3817.

[39] Daniel T. Chiu et al. *J. Am. Chem. Soc.*, **2015**, 137, 173-178

[40] Kim, J.; Jung, S.; Kim, Y.; Lee, E.; Kang, J.; Sakamato, S.; Yamaguchi, K.; Kim, K. *J. Am. Chem. Soc.*, **2000**, 122, 540-541.

[41a] https://chem10076.files.wordpress.com/2010/07/graphic1.jpg?w=470 Web. 16 Jul 2015.

[41b] Assaf, K.; Nau, W. M. *Chem. Soc. Rev*., **2015**, 44, 394-418.

[42] Kim, K. et al. *J. Am. Chem. Soc*., **2005**, 127, 12984-12989.

[43] Masson, E.; Ling, X.; Joseph, R.; Mensah, L.; Lu, X. *RSC Adv.*, **2012**, 2, 1213-1247.

[44] Uzunova, V. D.; Cullinane, C.; Brix, K.; Nau, W. M.; Day, A. I. *Org. Biomol. Chem.*, **2010**, 8, 2037.

[45] Huang, Z.; Yang, L.; Liu, Y.; Wang, Z.; Scherman, O.; Zhang, X. *Angew. Chem.*, **2014**, 126, 5455 –5459.

[46] S. T. Jones, J. M. Zayed and O. A. Scherman, *Nanoscale*, **2013**, 5, 5299–5302.

[47] Tuncel, D.; Ozsar, O.; Tiftik, H.; Salih, B. *Chem. Commun*., **2007**, 1369.

[48] Saleh, N.; Koner, A. L.; Nau, W. M. *Angew. Chem.*, **2008**, *120*, 5478 –5481.

[49] Tuncel, D.; Ünal, Ö.; Artar, M. *Isr. J. Chem*., **2011**, 51, 525 – 532.

[50] Lee, T.-C.; Scherman, O. A. *Chem. Commun.*, **2010**, 46, 2438–2440.

[51] Tian, F.; Cheng, N.; Nouvel, N.; Geng, J.; Scherman, O. A. *Langmuir*, **2010**, 26, 5323–5328.

[52] Kim, K. et al. *J of Incl. Phenom. Macrocyclic Chem*., **2004**, 50, 31–36.

[53] Ooya, T. et al. *Org. Lett*., **2006**, *8*, 15, 3159–3162.

[54] Sun, R.; Ma, X. *Tetrahedron* , **2013**, 69, 1069-1073.

[55] Michels, J. J.; O'Connell, M. J.; Taylor, P. N.; Wilson, J. S.; Cacialli, F.; Anderson, H. L. *Chem. Eur. J.*, **2003**, 9, 6167 – 6176.

[56] Yamaguchi, I.; Kashiwagi, K.; Yamamoto, T. *Macromol. Rapid Commun*., **2004**, 25, 1163–1166.

[57] A. Farcas et al. *European Polymer Journal*, **2015**, 62, 124–129.

[58] Frampton, M. J.; Anderson, H. L. *Angew. Chem. Int. Ed.*, **2007**, 46, 1028 – 1064.

[59] Arunachalam, M.; Gibson, H. W. *Progress in Polymer Science*, **2014**, 39, 1043–1073.

[60] Pennakalathil, J.; Jahja, E.; Özdemir, E. S.; Konu, Ö.; Tuncel, D. *Biomacromolecules*, **2014**, 15, 3366−3374.

[61] Pu, K-Y.; Liu, B. *Adv. Funct. Mater*., **2011**, 21, 3408–3423

[62] Feng, L.; Zhu, C.; Yuan, H.; Liu, L.; Lv, F.; Wang, S. *Chem. Soc. Rev*., **2013**, 42, 6620-6633.

[63] Tuncel, D.; Demir, H. V. *Nanoscale*, **2010**, 2, 6633, 484–494.

[64] Guoa, B.; Glavasa, L.; Albertsson, A-C. *Prog in Polym Sci*., **2013**, 38, 1263– 1286.

[65] Peng, H-S.; Chiu, D. T. *Chem. Soc. Rev*., **2015**, 44, 4699-4722.

[66] Wu, C.; Chiu, D. T. *Angew. Chem. Int. Ed.*, **2013**, 52, 3086 – 3109.

[67] Yang, G.; Lv, F.; Wang, B.; Liu, L.; Yang, Q.; Wang, S. *Macromol. Biosci.*, **2012**, 12, 1600–1614.

[68] Li, C.; Shi, G. *ACS Appl. Mater. Interfaces*, **2013**, 5, 4503−4510.

[69] Duan, X.; Liu, L.; Feng, F.; Wang, S. *Acc. Chem. Res*., **2010**, 43, 260–270.

[70] Wang, F.; Li, M.; Wang, B.; Zhang, J.; Cheng, Y.; Liu, L.; Lv. F.; Wang, S. *Sci. Rep.*, **2015**, 5, 7617.

[71] Stabo-Eeg, F.; Lindgren, M.; Nilsson, P.; Inganas, O.; Hammarstrom, P. *Chemical Physics*, **2007**, 336, 121–126.

[72] Zhu, C.; Yang, Q.; Liu, L.; Wang, S. *Chem. Commun*., **2011**, 47, 5524–5526.

[73] Kamaly, N.; Xiao, Z.; Valencia, P. M.; Radovic-Morenob, A. F.; Farokhzad, O. C. *Chem. Soc. Rev*., **2012**, 41, 2971–3010.

[74] M. Kanapathipillai et al. *Adv. Drug Delivery Rev.*, **2014**, 79, 107–118.

[75] Yuan, H.; Wang, B.; Lv, F.; Liu, L.; Wang, S. *Adv. Mater.*, **2014**, 26, 6978–6982.

[76] Wang, X.; He, F.; Li, L.; Wang, H.; Yan, R.; Li, L. *ACS Appl. Mater. Interfaces*, **2013**, 5, 5700−5708.

[77] H. Ringsdorf, *J. Polym. Sci. Polym. Symp*., **1975**, 51, 135-153.

[78] Kim, I-B.; Shin, H.; Garcia, A. J.; Bunz, U. *Bioconjugate Chem.*, **2007**, *18*, 3, 815–820.

[79] Pu, K-Y.;Li, K.; Liu, B. *Chem. Mater.* **2010**, 22, 6736–674.

[80] Dhara, S.; Gub, F. X.; Langer, R.; Farokhzad, O. C.; Lippard, S. J. *PNAS*, **2008**, *105*, 45, 17356 –17361.

[81] David, A. *Isr. J. Chem.* **2010**, 50, 204 – 219.

[82] Marradi, M.; Chiodo, F.; Garcia, I.; Penades, S. *Chem. Soc. Rev*., **2013**, 42, 4728.

[83] Chabre, Y. M.; Roy, R. *Chem. Soc. Rev*., **2013**, 42, 4657-4708.

[84] Sunasee, R.; Narain, R. *Macromol. Biosci*. **2013**, 13, 9–27.

[85] http://www.nature.com/nchembio/journal/v1/n5/images/nchembio730-F1.jpg. Web. 29 Jul 2015.

[86] Whitesides, G. M. et al. *Angew. Chem. Int. Ed.*, **1998**, 37, 2754 – 2794.

[87] G. Parut and F. M . Veronese, *Prog. Polym. Sci*., **2007**, 32, 933-961.

[88] Alexei V. Demchenko. *Handbook of Chemical Glycosylation: Advances in Stereoselectivity and Therapeutic Relevance. "General Aspects of the Glycosidic Bond Formation"*, p1-27, John Wiley & Sons, **2008**.

[89] Miura, Y. *Polymer Journal*, **2012**, *44*, 679–689.

[90] Lai, C.-H.; Lin, C.-Y. ; Wu, H.-T.; Chan, H.-S. ; Chuang, Y.-J.; Chen , C.-T.; Lin, C.-C. *Adv. Funct. Mater*., **2010**, 20, 3948.

[91] Basuki, J. S.; Esser, L.; Duong, H. T. T.; Zhang, Q.; Wilson, P.; Whittaker, M. R.; Haddleton, D. M.; Boyer , C.; Davis, T. P. *Chem. Sci*., **2014**, 5, 715–726.

[92] Jiawei Lu et al. *Macromol. Biosci*., **2014**, 14, 340–346.

[93] Fabian Suriano et al. *Biomaterials*, **2010**, 31, 2637–2645.

[94] Yih-Shyan Lin et al. *J. Med. Chem*., **2008**, 51, 7428–7441.

[95] Sang-Heon Kim et al. *Biotechnology Letters*, **2000**, 22, 1049–1057.

[96] Hashida, M. ; Nishikawa, M.; Yamashita, F. ; Takakura, Y. *Adv. Drug Delivery Rev*., **2001**, 52, 187–196.

[97] Li, X.; Zhou, H.; Yang, L.; Du, G.; Pai-Panandiker, A. S.; Huang, X.; Yan, B. *Biomaterials*, **2011**, 32, 2540–2545.

[98] Bergen, J. M.; von Recum, H. A.; Goodman, T. T.; Massey, A. P.; Pun, S. H. *Macromol. Biosci*., **2006**, 6, 506–516.

[99] Moros, M.; Hernaez, B.; Garet, E.; Dias, J. T.; Saez, B.; Grazu, V.; Gonzalez-Fernandez, A.; Alonso, C.; de la Fuente, J. M. *ACS Nano*, **2012**, 6, 1565–1577.

[100] Wang, G.; Pu, K-Y; Zhang, X.; Li, K.; Wang, L.; Cai, L.; Ding, D.; Lai Y.-H.;. Liu, B. *Chem. Mater*., **2011**, 23, 4428–4434.

[101] Rajakumar, R.; Anandhan, P. *Eur. J. Med. Chem.*, **2011**, 46, 4687–4695.

[102] Cecioni, S.; Oerthel, V.; Iehl, J.; Holler, M.; Goyard, D.; Praly, J.-P.; Imberty, A.; Nierengarten, J.-F.; Vidal, S. *Chem.–Eur. J.*, **2011**, 17, 3252–3261.

[103] N. Sharon, *Trends Biochem. Sci.*, **1993**, 18, 221–226.

[104] Wu, S.; Huang, X.; Du, X. *Angew. Chem. Int. Ed*., **2013**, 52, 5580–5584.

[105] Manel N; Kim FJ; Kinet S; Taylor N; Sitbon M; Battini JL. *Cell*, **2003**, 115, 4, 449–59.

[106] Carvalho et al. *Clinics*, **2011**, 66, 6, 965-972.

[107] Shi, J.; Cai, L.; Pu, K-Y.; Liu, B. *Chem. Asian J*., **2010**, 5, 301 – 308.

[108] Schmid, S.; Mishra, A.; Wunderlin, M.; Bäuerle, P. *Org. Biomol. Chem*., **2013**, 11, 5656.

[109] Pu, K-Y.; Shi, J.; Wang, L.; Cai, L.; Wang,G.; Liu, B. *Macromolecules*, **2010**, 43, 9690–9697.

[110] Xue, C.; Luo, F-T.; Liu, H. *Macromolecules*, **2007**, 40, 6863-6870.

[111] Ting, S. R. S.; Chen, G.; Stenzel, M. H. *Polym. Chem*., **2010**, 1, 1392–1412.

[112] Disney, M.D.; Zheng, J.; Swager,T.M.; Seeberger, P.H. *JACS*, **2004**, 126, 13343-13346.

[113] Baek, M-G.; Stevens, R. C.; Charych, D. H. *Bioconjugate Chem*., **2000**, 11, 777-788.

[114] Xue, C.; Velayudham, S.; Johnson, S.; Saha, R.; Smith, A.; Brewer, W.; Murthy, P.; Bagley, S.T.; Liu, H. *Chem. Eur. J.*, **2009**, 15, 2289 – 2295.

[115] Yin, L.; Chen, Y.; Zhang, Z.; Yin, Q.; Zheng, N.; Cheng, J. *Macromol. Rapid Commun*., **2015**, 36, 483−489.

[116] He, L. Z.; Crocker, A.; Lee, J.; Mendoza-Ramirez, J. Wang, X. T.; Vitale, L. A.; O'Neill, T.; Petromilli, C.; Zhang, H.F.; Lopez, J.; Rohrer, D.; Keler, T.; Clynes, R. *J. Immunol*., **2007**, 178, 6259–6267.

[117] Joshi, M.D.; Unger, W. J.; Storm, G.; van Kooyk, Y.; Mastrobattista, E. *J. Control. Release*, **2012**, 161, 25–37.

[118] Jain, K.; Kesharwani, P.; Gupta, U.; Jain, N. K. *Biomaterials*, **2012**, 33, 4166-4186.

[119] Spaina, S. G.; Cameron, N. R. *Polym. Chem*., **2011**, 2, 60.

[120] Pawar PV, Gohil SV, Jain JP, Kumar N. *Polymer Chemistry*, **2013**, 4, 3160–76.

[121] Wang, L. H.; Pu, K. Y.; Li, J.; Qi, X. Y.; Li, H.; Zhang, H.; Fan, C. H.; Liu, B. *Adv. Mater.*, **2011**, 23, 4386.

[122] Chen, Q.; Cui, Y.; Zhang, T-L.; Cao, J.; Han, B-H. *Biomacromolecules,* **2010**, 11, 13–19.

[123] Pearson, S.; Scarano, W.; Stenzel, M. H. *Chem. Commun.*, **2012,** 48, 4695–4697, SI

[124a] Mahrova, M. *1, 3, 4, 6-Tetra-O-acetyl-2-O-trifluoromethanesulfonyl-β-mannopyranose as FDG precursor*. MSc. Thesis, Appendix 1, University of Tartu, **2009.**

[124b] Idris, M. *Synthesis of Oligomers, Polymers and Cucurbituril Based Polyrotaxanes Towards Polymer Light Emitting Diode and Photodynamic Therapy Application.* MSc. Thesis, p61-64, Bilkent University, **2014.**

[125] http://www.chem.wisc.edu/areas/reich/nmr/05-hmr-02-delta.htm Web. 10 Aug 2015.

[126] Lennox, A. J. J.; Lloyd-Jones, G. C. *Chem. Soc. Rev*., **2014**, 43, 412.

[127] Fujii, S.;Chang, S. Y.; Burke, M.D. *Angew. Chem.* Int. Ed., **2011**, 50, 7862–7864.

[128] Ren, B.; Wang, M.; Liu, J.; Ge, J.; Zhanga, X.; Dong, H. *Green Chem.*, **2015**, 17, 1390.